UNIONE EUROPEA Fondo Sociale Europeo

REPUBBLICA ITALIANA

REGIONE CALABRIA
Assessorato Cultura, Istruzione e Ricerca
Dipartimento 11

UNIVERSITÀ DELLA CALABRIA

Università della Calabria

DIPARTIMENTO DI INGEGNERIA PER L'AMBIENTE E IL TERRITORIO E INGEGNERIA CHIMICA

Dottorato di Ricerca in Ingegneria Chimica e dei Materiali

SCUOLA DI DOTTORATO " PITAGORA " IN SCIENZE INGEGNERISTICHE

Ciclo XXVI

Tesi

An insight on pharmaceutical crystallization process by using membrane technology:

PVDF-based mixed matrix membranes and PP grafted membranes as new tools for controlling the supersaturation rate and the heterogeneous nucleation mechanism.

Settore Scientifico Disciplinare CHIM/07 – Fondamenti Chimici delle Tecnologie

Supervisori

Ch.mo Prof. Enrico Drioli

Dr. Gianluca Di Profio

Candidato

Antonella Caridi

Coordinatore del Corso di Dottorato

Ch.mo Prof. Raffaele Molinari

AA 2013/2014

UNIONE EUROPEA
Fondo Sociale Europeo

REPUBBLICA
ITALIANA

REGIONE
CALABRIA
Assessorato Cultura,
Istruzione e Ricerca
Dipartimento 11

UNIVERSITÀ DELLA CALABRIA

Università della Calabria

DIPARTIMENTO DI INGEGNERIA PER L'AMBIENTE E IL TERRITORIO E INGEGNERIA CHIMICA

Dottorato di Ricerca in Ingegneria Chimica e dei Materiali

SCUOLA DI DOTTORATO " PITAGORA " IN SCIENZE INGEGNERISTICHE

Ciclo XXVI

Tesi

An insight on pharmaceutical crystallization process by using membrane technology:

PVDF-based mixed matrix membranes and PP grafted membranes as new tools for controlling the supersaturation rate and the heterogeneous nucleation mechanism.

Settore Scientifico Disciplinare CHIM/07 – Fondamenti Chimici delle Tecnologie

Supervisori
Ch.mo Prof. Enrico Drioli

Dr. Gianluca Di Profio

Candidato
Antonella Caridi

Coordinatore del Corso di Dottorato
Ch.mo Prof. Raffaele Molinari

AA 2013/2014

The PhD research project was in collaboration with:

- Institute on Membrane technology (CNR), Rende,IT

under the supervision of
Prof. Enrico Drioli and Dr. Gianluca Di Profio

- Technische Universiteit Delft, Delft, NL

TU Delft Delft University of Technology

under the supervision of Prof. **Joop H. ter Horst**

at Process & Energy
Intensified Reaction and Separation systems Department of (3mE),
in the semester November 2011-April 2012

- Université Paul Sabatier, Toulouse, FR

under the supervision of **Prof. Pierre Aimar**

at Laboratoire de Gènie Chimique (CNRS)
in the semester Septermber 2013- february 2014

Sommario

Questo elaborato finale del progetto di dottorato tratta lo studio del processo di cristallizzazione a membrana finalizzato alla produzione di composti farmaceutici in forma cristallina. Lo studio ha come obiettivo quello di dare una visione globale del processo di cristallizzazione a membrana andando oltre lo stato dell'arte, bensì proponendo l'implementazione della tecnica di cristallizzazione a membrana di base. A tal proposito il progetto è stato sviluppato seguendo in due diverse direzioni: da una parte la tecnica di cristallizzazione a membrana di base ha visto l'applicazione ad uno specifico settore dell'industria farmaceutica, dall'altra parte lo studio è proseguito investigando i meccanismi di cristallizzazione indotti dalla stessa membrana e successivamente ha visto una vera e propria progettazione di membrane opportunamente pensate per la cristallizzazione.

Dunque, il valore aggiunto di tale studio consiste nell'avere dimostrato la possibilità di ampliare il campo di applicazione del processo a membrana, di aver esteso la conoscenza di base dei meccanismi di nucleazione eterogenea sottesi dalla membrana e di aver progettato, prodotto e caratterizzato delle membrane con differenti materiali e strutture appositamente per essere testati nella tecnica di cristallizzazione. In dettaglio, il lavoro presenta uno studio iniziale sul processo di nucleazione eterogenea che parte da particelle libere in soluzione per poi continuare studiando il processo di nucleazione eterogenea sullle membrane stesse. Una seconda sezione tratta l'applicazione del processo a membrana alla cocristallizzazione farmaceutica. Successivamente inizia la parte di disegno e realizzazione di membrane eterogenee sia dal punto di vista chimico che strutturale: membrane fabbricate con tecniche e materiali differenti e membrane commerciali che sono state opportunamente funzionalizzate. Infine il lavoro si conclude con i tests di cristallizzazione condotti su tali membrane.

Abstract

This is the final work of the PhD project related to the study on the membrane crystallization process used for the production of pharmaceutical compounds in crystalline form. The study aims to give an overview of the membrane crystallization process beyond the state of the art, while proposing the implementation of the basic technique. On this regard, the project has been developed following two many directions: on one hand, the basic membrane crystallization technique has extended its scope to a specific field of the pharmaceutical world; on the other hand, the study followed by investigating the crystallization mechanisms when induced by the membrane and subsequently, a real design of membranes suitably for the crystallization followed. Therefore, the added value of this study is:

- having demonstrated the possibility of expanding the scope of the membrane process;
- having extended the basic understanding of the heterogeneous nucleation mechanisms induced by membranes;
- having investigated the process of design, manufacturing and characterization of the membranes with different materials and structures, specially to be tested in the art of crystallization .

In detail, the work presents an initial study on the process of heterogeneous nucleation by particles free in solution and then, it continued by investigating the process of heterogeneous nucleation on membranes. A second section deals with the application of the membrane-based process on pharmaceutical. Then, followed the section of design and realization of membranes heterogeneous by a chemical and structural point of view; these membranes were manufactured with different techniques and different materials or were appropriately functionalized. Finally, the paper was concluded by presenting the crystallization tests performed on the produced membranes.

Index

Introduction

This thesis is the final product of some years of study, experiences and elaborations. It would give an overview of membrane crystallization as a whole, without getting tied to the state of the art, rather investigating some new aspects of the process, such as the use of tailor-made membranes as nucleating agent, and the application of membrane technology to specific areas of pharmaceutical crystallization.

Initially, it is addressed the heterogeneous nucleation mechanism as the central core of the crystallization process and the ability to control this mechanism for the production of specific polymorphs through the use of free templates in solution. This study proved to be of great importance for expanding our fundamental knowledge about the heterogeneous nucleation mechanism and for introducing the following studies about the nucleation process onto polymeric surfaces of the membranes. Indeed, in the first chapter, the possibility of inducing nucleation of different pharmaceutical polymorphs, by using well-defined heterogeneous templates, was investigated. Synthetic zeolites with pores of well-defined size in the nanometer range, as well as titanium dioxide in two different forms, were used as templates. These researches were carried out at Mechanical, Maritime and Materials Engineering department of the Technical University of Delft, working with a research group leader in the field of industrial crystallization. During this experience, I had the opportunity to avail of cutting-edge equipment for researching on crystallization process, as well as having interesting and educational discussions with experts in the field. Later, the study on heterogeneous nucleation has been extended to the use of the membranes as heteronucleants.

The second chapter deals with the membrane crystallization process by using commercial membranes in a basic configuration. The newness of these investigations compared with past ones was the application of the basic

concept of membrane crystallization to the pharmaceutical cocrystallization process. The new membrane-based cocrystallization strategy has been used to induce the formation of carbamazepine-saccharin (CBZ-SAC) cocrystals or carbamazepine (CBZ) and saccharine (SAC) single crystals from water/ethanol solvent mixtures depending on the initial CBZ and SAC molar ratio. This study revealed the ability of the membrane-based technique of providing specific routes in the solubility phase diagram of CBZ-SAC system when opportunely choosing the initial solution conditions. The membrane had the specific role of limiting the maximum level of supersaturation reached in solution by controlling the solvent evaporation thorough its micropores. Furthermore, it was demonstrated the influence of trans-membrane flux on the polymorphic composition of the precipitates examining how as increasing the rate of supersaturation generation an increasing of the higher energetic polymorph occurred. After having successfully demonstrated the possibility of extending the basic membrane crystallization to other pharmaceutical applications. After this, the research continued by investigating the role of the membranes as nucleating agent. The strategy of study provided two steps: the manufacturing of various membranes typologies and the testing of the produced membrane as heteronucleants during crystallization. On this regard, chapter 3 deals with the manufacturing and the characterization of PVDF-based mixed matrix membranes with four different inorganic nanosized fillers and by using three different manufacturing procedures. The goal of the work was the fabrication of many different kind of membranes heterogeneous from a chemical and structural point of view, to eventually testing their performance in pharmaceutical crystallization. The membrane manufacturing and characterization was carried out at the Institute on Membrane Technology of the Italian National Council (ITM-CNR) and at Mechanical and Materials Engineering department of University of Calabria.

After the design and fabrication of various PVDF membranes, the research continued along the road of the membrane surface modification in order to create membranes opportunely functionalized. Thus, commercial polyproprylene (PP) membranes normally used in basic membrane crystallization have been subjected to UV-photografting treatment for the

grafting of acrylic acid monomer on the surfaces, in the chapter 4. While PP is basically inert, a successful stategy allowed the formation of a thin layer of polyacrylic acid on the membrane surface, resulting in the developing of double layered membranes: hydrophilic on one side and hydrophobic on the other side. Both flat sheet membrane and hollow fibers were treated with good outcomes. This work was performed at the Laboratoire de Geniè Chimique of Universitè Paul Sabatier in Toulouse, where it was possible to design and implement the full strategy of chemical modification of the polymeric surface and the following characterization.

After that, all produced or modified membranes discussed so far, were tested in crystallization of pharmaceutical model compounds in order to investigate their performance as heteronucleants. In chapter 5 this study is detailed by evaluating the crystals nucleation density on the membrane surface considered. The following table summarize whole research project.

PhD research project			
PhD year	**University/ Institute**	**Thesis Chapter**	**Study details**
I	ITM-CNR/ Unical, Italy	2	Basic membrane crystallization process and application on pharmaceutical crystallization.
II	TU Delft, The Netherlands	1	Study on crystal nucleation mechanism on nanosized templates
II	ITM-CNR/ Unical, Italy	3	Manufacturing of mixed matrix mebranes with nanosized fillers as heteronucleants
III	UPS Toulouse, France	4	Design and implementation of UV-photografted membranes for crystallization
III	ITM-CNR/ Unical, Italy	5	Crystallization of pharmaceuticals by means membranes as heteronucleant

Chapter 1

Crystallization of isonicotinamide polymorphs on heterogeneous nucleants

1.1Introduction

The first chapter deals with the potential of using well defined heterogeneous templates in controlling nucleation, as key step of crystallization process. This section aims of reasoning the fundamental aspects of the heterogeneous nucleation, which would anticipate some questions of the following sections about the crystallization process mediated by polymeric matrices such as membranes.

Nucleation is the formation of the first small crystalline embryos referred to as nuclei.[1] These nuclei become stable and grow up to mature crystals upon achieving a certain critical size.[1] Because nucleation is the primary step in the crystallization process, it determines the final characteristics of the rising crystalline phase, such us crystal size, size distribution, and polymorphism.[2,3] Therefore, control of the nucleation stage is crucial for the control of the macroscopic properties of the produced crystalline materials.

Nucleation mechanism is generally recognized as homogeneous (HON) or heterogeneous (HEN). The former occurs when a sufficient number of molecules cluster together in the same region and at the same time in the course of their random movement in the bulk and are able to form a critical nucleus.[1] HEN is the formation of critical nuclei at foreign body surfaces because of the creation of reduced interfacial energy regions that lower the thermodynamic barrier to nucleation.[4] HEN usually occurs in batch crystallization processes because the solution solid impurities, the dust particles or the container's walls act as heterogeneous surfaces promoting nucleation. Despite HEN is the dominant mechanism in solution crystallization, its control is still limited due to the ill-defined properties of the heterogeneous particles onto which HEN occurs. Also, concentration and surface of these particles are not known and/or impossible to be determined. On the other side, the opportunity to affect rationally the nucleation stage with the aid of intentionally added heterogeneous surfaces, would lead to improved control

over crystal properties. In the last years, several efforts have been devoted to the study and the development of tailored heterogeneous surfaces suitable to control nucleation for both biomacromolecules and small organic molecules. Several studies showed that the nucleation process can be modified by the presence of interfaces by various mechanisms: by means of favorable molecular interactions between the functional groups of target molecule and substrate surface; by epitaxial matching of the solute crystal lattice with the solid support; by confinement effects into porous or irregular structures. Several types of heteronucleants have been used for protein crystallization. Porous supports like porous silicon,[5] carbon nanotubes,[6] zeolites,[7] bio-active gel glass,[8] or porous polymeric membranes[9,10] were effective in enhancing nucleation rate; charged surfaces like polymeric films,[11] modified mica,[12] fluorinated layered silicate,[13] and poly-L-lysine surface[14] were used to support the electrostatic interaction with protein functional groups. Besides, many studies highlighted the possibility to affect polymorphism of organic crystals by using appropriate heterogeneous surfaces. Polymeric films with tailored chemical and structural surface properties were developed to modulate the nucleation rate of organic materials.[15,16,17] Phase-selective crystallization of acetaminophen has been performed by Lòpez-Mejìas *et al*.,[18] with polymer-induced heteronucleation, and by Chadwick *et al*.,[19] by epitaxial seeding on an opportunely chosen crystalline substrate. The induction of specific crystal forms and the control of crystal size of molecular crystals by means of heterogeneous templates have been successfully demonstrated by using patterned self-assembled monolayers,[20] porous glass,[21] and cross-linked polymer microgels with various mesh size.[15]

Despite the progress made in this field in the last years, the complete understanding of the fundamentals of the HEN mechanisms still remains demanding. The major challenge is to provide a description of the involved molecular mechanism and the interpretation of the structural relationships between heterogeneous surface and interacting molecules. Therefore, this work aimed to enhance the current knowledge of heterogeneous nucleation mechanisms at molecular level and to get improved control of polymorphic

selectivity in solution crystallization, by studying the potential of properly selected heterogeneous templates to stimulate HEN.

Templates exhibiting porous and regular surfaces structures in the nanometer range were selected and their influence on the nucleation kinetics and polymorphic selectivity of the model molecule Isonicotinamide (INA) was investigated by monitoring real-time the course of the crystallization process.

Association processes play a key role in the crystallization of INA.[14] Among the five different known polymorphs of INA[15,16] all metastable forms I, III, IV and V show various arrangements based on head-to-tail chains assembling of molecules, while form II, which is stable at room temperature, displays a head-to-head dimeric packing. Solvents like nitromethane and nitrobenzene enable the association of INA into chains leading to the formation of metastable forms. Solutions of INA in ethanol contain dimers and chains while crystallization using ethanol leads to the formation of the stable form II.

In this paper, we investigate whether templates can counterbalance this effect of self-association in the case of INA. If templates are sufficiently effective, then, a polymorph with a structure will be formed that does not reflect the association pattern in solution. Porous and regular inorganic templates, such as synthetic zeolite ZSM-5, mesoporous aluminosilicate MCM-41, and TiO_2 in both rutile and anatase phase, were selected. We first investigated whether the templates enhance nucleation, after that, we studied the polymorphic outcome of crystallization processes.

1.2Materials and Methods

Materials. Isonicotinamide (Cod. I17451), absolute ethanol, synthetic zeolite ZSM-5 (Cod. 419095) and MCM-41 (Cod. 643653), titanium dioxide in both rutile (Cod. 204757) and anatase (Cod. 637254) forms were provided by Sigma-Aldrich. All templates were used without further purification.

Solubility & Metastable Zone. The solubility of INA in ethanol was measured as a function of temperature using Crystal16 setup (Avantium, Amsterdam, the Netherlands). Slurries of INA, in different overall concentrations, were prepared by adding a known amount of crystalline material to 1 mL of solvent and stirring at 700 rpm. The saturation temperature was measured 3 times per sample through cycles of heating and cooling from 10 °C to 60 °C at 0.3 °C min^{-1}. Upon increasing the temperature the crystals completely dissolved and the suspension became a clear solution so that the light transmission reached the maximum value. The temperature at which light transmission reached the maximum value was the clear point, which we assumed to coincide with the saturation temperature. Then, by cooling down the solution with a rate of 0.3 °C min^{-1}, there was a temperature at which the first formed crystals were detected by a decrease in the light transmission (cloud point). The difference between cloud and clear point defined the metastable zone width (MSZW) of the system.

Induction time. The INA concentration used in induction time (t_i) experiments was 87.5 g L^{-1} in ethanol, corresponding to a supersaturation ratio S of 1.25 at a temperature of 25 °C, according to the experimentally determined solubility. Induction time measurements were performed on a 1 mL scale at 25 °C using the Crystal16 reactor. Each vial was magnetically stirred at 700 rpm; the heating rate was set at 0.3 °C min^{-1} and the cooling rate at 5 °C min^{-1}. Induction times were revealed by the initial decrease in the transmission of light through the sample since crystals started to form. The induction time is the period between the achievement of constant supersaturation at 25 °C and the moment the transmission started to decrease. To perform measurement of t_i

with templates, a stock solution with 0.3 mg*L^{-1} of templates in ethanol was prepared. Such a low contentration of template was reached by dilutions after suspending the templates. The suspension was obtained by treating the sample ultrasonically (Bransonic 2510E-MT 42 KHz +/-6%) for 15 min to break up the possible nano-powders aggregate particles. After that, a known amount of INA was dissolved into the 0.3 mg L^{-1} template suspention, to make the final supersaturation of INA to *S*=1.25. The sample was heated and again treated ultrasonically to dissolve INA powder and disperse the template particles. A hot bottle-top dispenser platform was used to avoid crystallization of INA during sample preparation and to dispense 1 mL of nano-suspension of template and dissolved INA into each vial. The amount of templates was chosen to be sufficiently low (0.3 mg L^{-1}) to avoid influence on the light transmittance. Suspensions were also stirred during the induction time measurements/crystallization tests, to uniformly suspend the template particles.

Crystallization experiments. For the crystallization experiments INA concentrations were 87.5 g L^{-1} and 98.0 g L^{-1} at 25 °C, corresponding to a supersaturation of 1.25 and 1.40, respectively, at 25 °C. Cooling crystallization experiments were carried out in the Crystalline multiple reactor setup (Avantium, Amsterdam, the Netherlands) by using 3 mL of INA solutions in ethanol with and without (blank experiments) templates. All tests were conducted under equal conditions except for the kind of template. 3 mg L^{-1} of templates were added to the vials. The solutions were treated ultrasonically for 15 min. The samples were heated to 60 °C and kept at constant temperature for 40 minutes to completely dissolve INA and then rapidly cooled down to 25 °C at 5 °C min^{-1} while stirring at 700 rpm. The samples were left stirring at 25 °C and in situ monitored by Raman spectroscopy while the light transmission was also measured. After induction and crystallization, the crystals were then filtered and dried overnight at 60 °C to characterize the solid state using powder X-ray diffraction.

Characterizations. Raman spectra of the dried samples were recorded by Hololab series 5000 instrument (Kaiser Optical System, Inc.). Powder X-ray diffraction (PXRD) patterns were recorded using a Bragg-Brentano geometry in

a Bruker D5005 diffractometer equipped with Huber incident-beam monochromator and Braun PSD detector. Data collection was carried out at room temperature using monochromatic Cu Kα1 radiation (λ = 0.154056 nm) in the 2θ region between 10° and 60°, step size 0.038° 2θ. All samples were measured under identical conditions. Samples of about 20 mg were deposited on a Si <510> wafer and were rotated during measurement. Data evaluation was done using the Bruker program EVA.

1.3Results and discussions

Metastable Zone (MSZ). The addition of effective heterogeneous templates to the crystallizing solution would induce nucleation at a lower supersaturation than normally required for HON, because of the reduction of the nucleation work. Thus, the effectiveness of the templates in inducing HEN can be verified by induction time measurements operating at relatively low supersaturation conditions, at which induction times in the absence of templates is relatively large. As the crystal growth being unaffected by the addition of template, we assume that the growth rate is constant for the sample with and without template in the given solution. In order to choose a suitable supersaturation region (the operational window) for these induction time measurements, the *metastable zone*, which is the zone between saturation temperature and cloud points, was determined experimentally. The saturation temperatures represent the solubility curve. Below, is located the *stable zone* where the solution is unsaturated and crystallization cannot occur. The cloud point is defined as the temperature at which crystals are detected using a constant cooling rate. Above the cloud point (MSZW upper limit) the *labile zone* is, where spontaneous and uncontrolled nucleation is observed.

The solubility line and MSZ limit are displayed in Figure 1. The measured temperature dependent solubility of INA in ethanol well agrees with previously reported data[21] and is therefore represented by a solid line. The measured cloud points for different concentrations in absence of any intentionally added heterogeneous templates can also be found in Figure 1.

Since cloud point measurements in small volumes are prone to fluctuations due to the stochastic nature of nucleation, we followed a recently published approach:[17,18] for measurements at the same concentration we chosed to use the lowest experimentally measured MSZW to construct the line for the MSZ limit at that concentration. The horizontal region between solubility line and cloud point is the metastable zone for a certain concentration. Within this zone the nucleation in absence of intentionally added heterogeneous templates is

sufficiently slow to measure relatively large induction times and the effect of intentionally added templates on these induction times. Thus, the concentrations used in the induction time measurements at 25 °C are chosen within the MSZW and indicated (blue dots) in Figure 1.

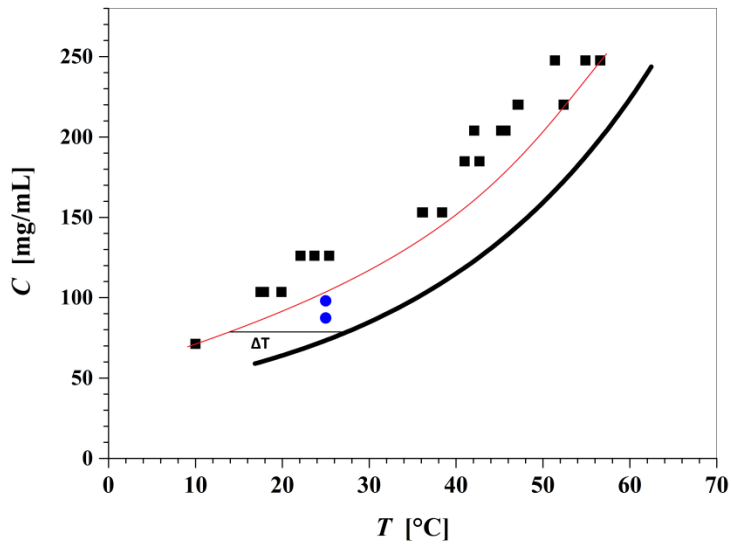

Figure 1. The solubility (solid line), the measured cloud points (squares), the MSZ limit (red solid line) of INA in ethanol when cooling at 5 °C min^{-1} in 1 mL solutions. The circles within the MSZ identify the concentrations and temperature used for the induction time experiments. ΔT is the minimum MSZW measured.

The horizontal region between solubility line and cloud point is the metastable zone for a certain concentration. Within this zone the nucleation in absence of intentionally added heterogeneous templates is sufficiently slow to measure relatively large induction times and the effect of intentionally added templates on these induction times. Thus, the concentrations used in the induction time measurements at 25 °C are chosen within the MSZW and indicated (blue dots) in Figure 1.

Template Induced Nucleation Rates. As the increasing of nucleation rate involves a reduction of induction time,[22] t_i measurements have been used for the indirect determination of crystal nucleation rate,[23,24] following a recently published procedure.[19,20] Accordingly, the potential of templates in promoting nucleation of INA was valuated measuring the induction times at equal supersaturation ratio used in blank experiments. The induction times for experiments in the absence of templates at a supersaturation ratio S=1.25 and a temperature of T=25 °C are reported in Figure 2a.

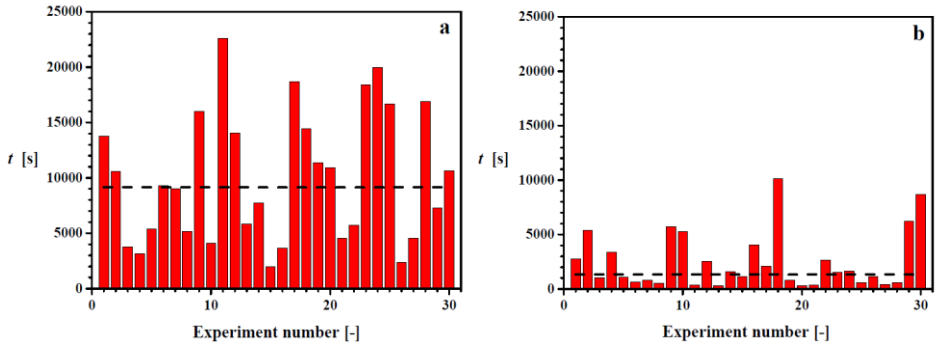

Figure 2. Induction time measurements for 87.5 mg mL^{-1} INA in ethanol, (a) in the absence of templates, (b) with 0.3 mg L^{-1} ZSM-5 template. Only 30 of the 80 measurements per supersaturation are shown in the graph. The measured induction times show a large variation due to the stochastic nature of the nucleation process. Horizontal lines indicate the median values of induction times.

Although the experiments were conducted under the same supersaturation conditions, the induction times show a broad variation: they range from around 2000 s to more than 22000 s. Since care was taken to eliminate any deviation in sample concentration and disturbance in experimental temperature to avoid variations due to experimental errors, this variation

reflects the stochastic nature of the nucleation process. Due to the large number of tests it was possible to converts the induction time measurements in to the probability distribution of induction time P(t).
According to theory, the probability P0 that no nuclei are formed within the time interval tJ is given by:

$$P_0 = \exp(-JVt_J) \quad (1)$$

Where J is the nucleation rate [n s^{-1} mL^{-1}] and V in the sample volume [mL]. The probability P*(t_J) that at least 1 nucleus has formed in the time interval t_J is:

$$P^*(t_J) = 1 - \exp(-JVt_J) \quad (2)$$

Taking into account the delay tg, the growth time, between the time t_J of appearance of a nucleus and the time t of detection: t_J =t - tg, the probability P(t) to detect crystals at time t which were nucleated at an earlier time can be determined by:

$$P(t) = 1 - \exp(-JV(t - t_g)) \quad (3)$$

For M isolated experiments, the probability P(t) to measure an induction time between zero and the time t is defined as:

$$P(t) = \frac{M^+(t)}{M} \quad (4)$$

where M+(t) is the number of experiments in which crystals are detected at time t. Therefore, after experimentally determining P(t) by eq. 4, it is possible to calculate the nucleation rate J and tg by fitting the ln(1-P(t)) vs. t curves with eq. 3.
Figure 3 shows the probability distribution *P*(*t*) for INA in ethanol at a concentration of 87.5 mg mL^{-1} in absence of templates. The probability *P*(*t*) refers to the probability to detect crystals until time *t*.[19]

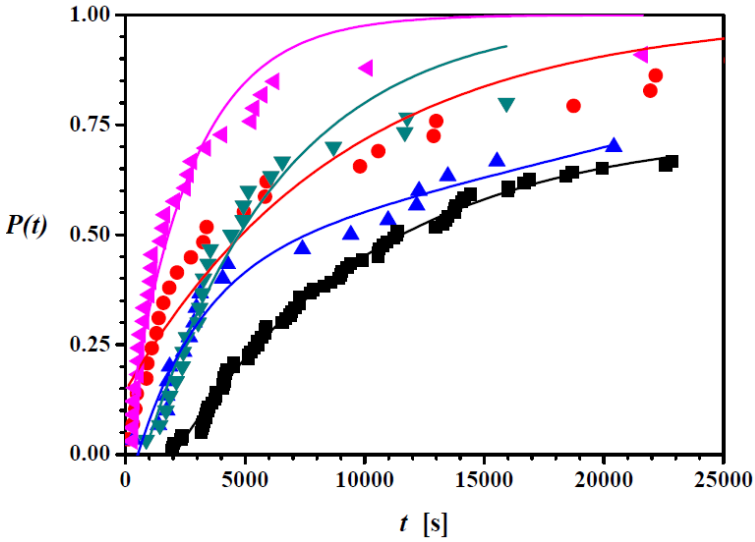

Figure 3. Probability distribution P(t) of induction times for INA in the absence (black squares) and in the presence of tempates at supersaturation ratio S=1.25: red circles – TiO2 Anatase; blue up triangles – TiO2 Rutile; green down triangles – MCM-41; pink left triangles – ZSM-5.

For the experiments without templates, for instance, in almost 40% of the samples crystals are detected when around 8000 s have passed. After around 6 hours the measurement was stopped since by then in at least 70% of the samples crystals were detected. The probability distribution $P(t)$ allows to determine the nucleation rate J and growth time t_g.[19] For the experiments in the absence of templates at a supersaturation ratio S=1.25 these are J=24 ± 0.3 $m^{-3}s^{-1}$ and t_g=1752 s (Table 1).

Table 1. Median induction time $\tilde{t}_i$ *and the determined nucleation rate J and growth time* t_g *from the fitting procedure using over 80 experiments.*

	$\tilde{t}_i$ [10^3 s]	J [$s^{-1}m^{-3}$]	ΔJ [$s^{-1}m^{-3}$]	t_g [s]	Δt_g [s]
Blank	7.2	24	0.3	$1.75 \cdot 10^3$	40
Rutile	3.1	59	0.7	585	80
MCM-41	3.4	74	5.8	$1.14 \cdot 10^3$	100
Anatase	3.0	85	2.8	1.3	20
ZSM-5	1.3	160	7.4	80	20

The potential of templates to promote nucleation of INA was evaluated by measuring the induction times at the same supersaturation ratio. As an example, Figure 2b displays the detected induction times for the first 30 experiments with the ZSM-5 template. Care was taken to use a sufficiently small amount of template particles so that the measurement was not influenced by the template particles but only by the presence of INA crystals. It can be seen that the induction times still show a large variation but that in average the induction time is substantially lower in presence of the template.

Figure 3 further shows the probability distribution *P*(*t*) of the induction time in the presence of templates. All heterogeneous particles resulted in higher probabilities compared to the experiments in the absence of templates (see Table 1). Figure 3 shows that after 10000 s induction time probabilities were 52% with rutile, 68% with MCM-41, 73% with anatase, and 89% with ZSM-5 respectively, while it was only 45% without templates.

After 1000 s all templated experiments had probabilities above 0 while for the experiments in absence of templates no induction times were measured smaller than 1000 s. It appears that all used templates decrease the induction time of INA.

Due to the large number of experiments it was possible to determine the nucleation rate J and growth time t_g from the probability distribution of the induction time P(t) using the method reported elsewhere.[19] The values for the nucleation rate J and the growth time t_g (Table 1) show that the observed

template effects at least partially can be attributed to an increase in the nucleation rate (Table 1).

Figure 3 also shows that the growth time tg is smaller in case of templated experiments as compared to templated experiment. The growth time (t_g) decreases due to fact that the crystal size reaches faster to the attrition size mainly because of template size added to crystal size. All determined nucleation rates in the presence of templates were larger than that in absence of templates, varying from twice to 6 times the nucleation rate in absence of templates (Figure 4). The order of the effectiveness of the 0.3 g/L templates to increase the nucleation rate is Rutile < MCM-41 < Anatase < ZSM-5 (Figure 4).

The growth times t_g in the presence of templates decreased from $1.8 \cdot 10^3$ s in the absence of templates to close to zero in the presence of Anatase. The growth time accounts for the delay in detection: a suspension of macroscopic crystals rather than the first nucleus is detected. The growth time thus is a function of the growth rate, the secondary nucleation rate and the outgrowth of the secondary nuclei.[17-19]

Probably, the secondary nucleation of the crystals on the template occurs more readily due to the larger size and larger solid density of the template particles causing more collisions of the crystal on the template with the stirrer. Growth times approaching zero indicate that nucleation might already occur during the cooling stage of the induction time measurement, before reaching constant temperature. This is the case for the template Anatase and the determined nucleation rate for the supersaturation used then is a lower limit and probably is higher.

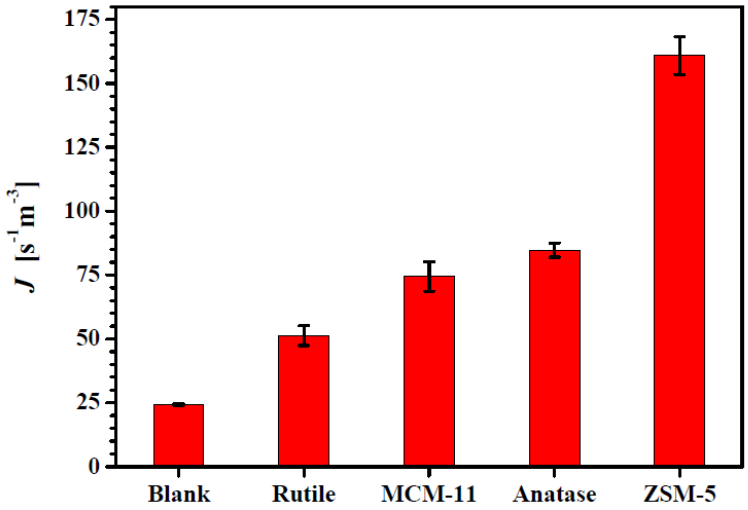

Figure 4. Nucleation rate determined from the induction time probability distributions by the fitting procedure published elsewhere.[19]

The increased nucleation rate obtained in the template experiments resulted in the production of a higher number of fine particles, drastically reducing the average crystal size. This is evident from the SEM images of dry product samples (Figure 5).

The heterogeneous nucleation rate is much higher than homogeneous nucleation rates for solution crystallization under non-extreme supersaturations because the decrease in the nucleation work (HEN<HON) dominates the decrease in the concentration of nucleation sites (HEN>HON). The concentration of nucleation sites can be assumed to be a function of the total template surface area. However, there is no direct relation between the measured nucleation rate and the specific surface area of the templates. In fact, between the two zeolite templates, ZSM-5 gave the highest enhancement of nucleation rate despite its lower specific surface area: 940-1000 m2g-1 for MCM-41 and around 900 $m^2 g^{-1}$ for ZSM-5

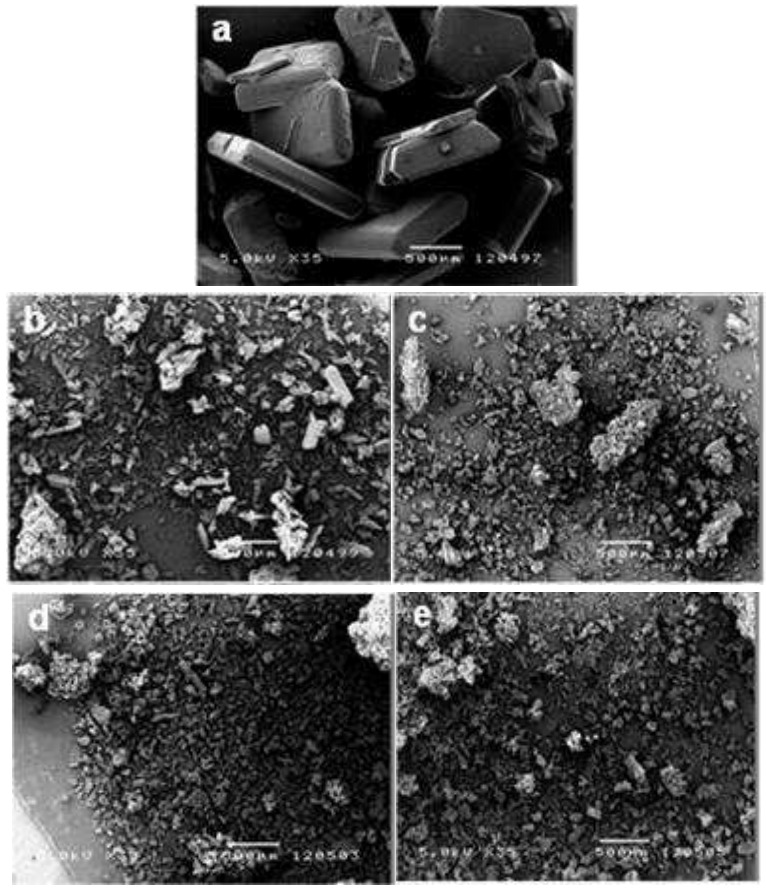

Figure 5. SEM images of dry INA crystals obtained (a) without templates, with (b) anatase, (c) rutile, (d) MCM-41, and (e) ZSM-5 templates. In all cases the size bar indicates 500 µm.

Template Controlled Polymorphism. For the crystallization of INA from ethanol in the absence of deliberately added templates it was shown previously[14] that it is indeed heterogeneous nucleation that is occurring.

Table 2. The detected INA polymorph directly after crystal detection during crystallization experiments in ethanol with various templates, at different INA supersaturation ratio S.

	Supersaturation *S*	
Type of Template	1.25	1.40
Blank	II	II
Rutile	II	II
MCM-41	II	II
Anatase	II	I + III
ZSM-5	II	II

For S=1.25 both blank and template experiments resulted in the formation of the stable form II. These results were consistent with the behavior of INA in strong proton donor solvents.[14] Increasing the initial supersaturation of INA to S=1.4 during crystallization, the blank experiment as well as those with titanium dioxide, rutile, and zeolites MCM-41 and ZSM-5 still resulted in the crystallization of form II. Interestingly, the experiments performed using titanium dioxide anatase resulted in the crystallization of mixtures of form I and form III, as detected by in situ Raman.

Since the dimeric form (form II) of INA and the chain forms show a different involvement of the pyridine group in hydrogen bonding,[14] the Raman spectra in the pyridine region (970-1010 cm^{-1}) enable to discriminate form II from the other polymorphs.[14] In Situ Raman spectroscopy was used to identify the polymorphic form obtained as soon as crystals were detected.

In solid Raman spectra form II, in which the pyridine does not interact with other groups, gives a peak at 991 cm^{-1} and the chain like forms, where pyridine is bounded to the amide group of another INA molecule, give peaks in the range 995-997 cm^{-1}. A similar behavior is in solution Raman spectra where free or bounded pyridine can be distinguished in different solvents.

The crystallization experiments of INA in ethanol were performed at two different supersaturations (1.25 and 1.4). For a supersaturation ratio S=1.25 both blank and template experiments resulted in the formation of the stable polymorph II. These results were consistent with the behavior of INA in strong proton donor solvents, indeed it is known that ethanol induce nucleation of form II. The use of templates in these conditions did not interfere with the role

played by the solvent. Increasing the concentration of INA for a S=1.4 the blank experiments resulted in the nucleation of form II as well as the experiments with titanium dioxide rutile, and zeolites MCM-11 and ZSM-5, while the experiments performed using titanium dioxide anatase resulted in nucleation of a chain like structure of INA.

In Figure 6a the Raman shifts along the time for blank experiment are shown; the figure present the behavior of INA in ethanol at 25 °C from t0 (the first moment at which 25°C was reached) until 250 minutes.

a)

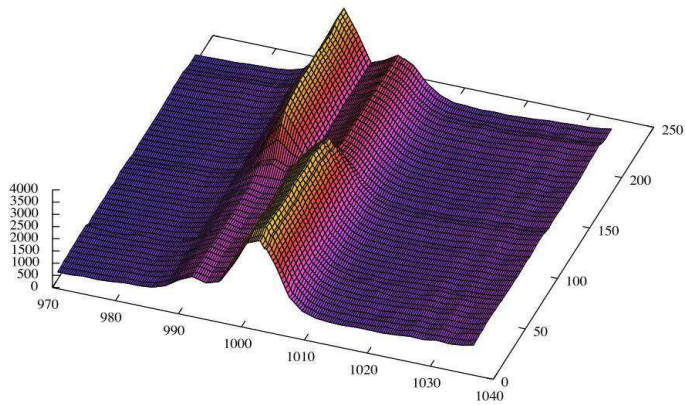

b)

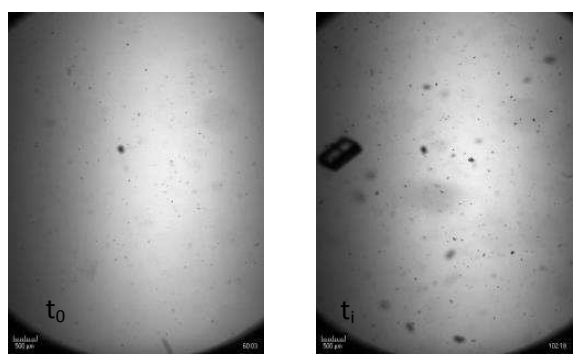

Figure 6. a) Raman shifts of INA blank experiments along the time; b) Pictures of the INA suspension at t_0 and a time t_i after the nucleation.

When cooling at 25°C the INA is still in solution a peak at 997 cm-1 is shown meaning that the pyridine is bounded by the hydroxyl group of ethanol. After a certain time a shift to 991 cm^{-1} indicated the nucleation of form II showing free pyridine groups. The time elapsed between t0 and the time at which the shift occurred was taken as induction time. This behavior was confirmed by some pictures of the sample at different times in figure 6b. At t0 a clear solution was seen while after the induction time some crystals are in solution. The same trend occurred for experiments with rutile titanium dioxide, zeolites MCM-11 and ZSM-5. When using anatase titanium dioxide only a peak at 997 cm^{-1} was detected when cooling at 25°C (t0) and for the whole duration of experiment; this means that the pyridine group of INA is bounded probably by the hydroxyl group of ethanol before nucleation and by amide group of another INA molecule forming a chain like structure after nucleation. The induction time was not detected (figure 7). Moreover, the presence of insoluble templates in the suspension made the real time visualization of crystals in suspension impossible.

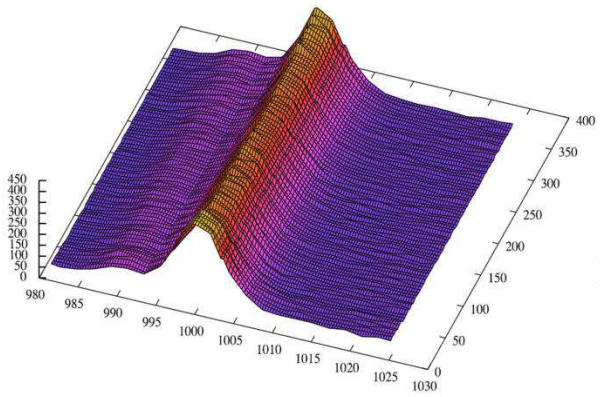

Figure 7. Raman shifts of anatase titanium dioxide experiment along the time.

The solid Raman spectra of the blank and template experiments at S=1.4 are reported in figure 8. For the experimets with anatase titanium dioxide the shift at 997 cm^{-1} confirmed the nucleation of a chain like form.

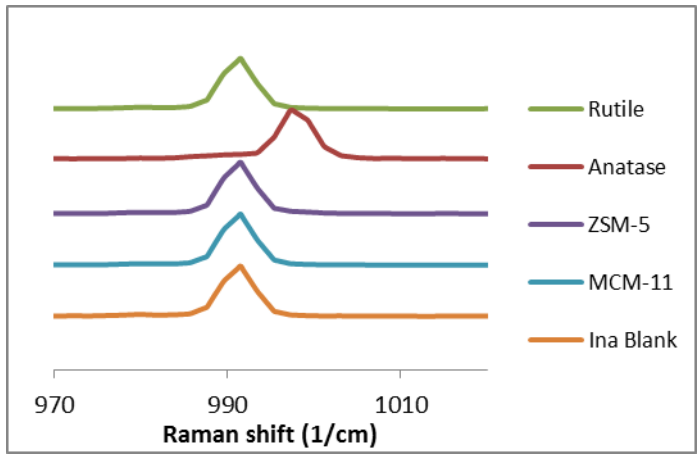

Figure 8 Solid Raman spectra of the blank and template experiments at S=1.4.

Thus, by deliberately adding templates that increase the nucleation rate we thus would change from one heterogeneous nucleation mechanism to another because nucleation would dominantly occur at another heterogeneous particle. A mixture of form I and III was also the outcome from an XRPD analysis of the powder obtained after suspension filtration (Figure 9). The crystals can grow on template surface due to the molecular interactions between the solute and template surface but can also occur because of physical confinement effects due to irregular topography of the surface. The lattice matching across the crystalline solid and substrate interface also play an important role in the process of heterogeneous nucleation. The size and shape of the pore of the template can also strongly affect the nucleation rate by confining the nucleus in one or more directions. The pore size might be a first factor involved in the effectiveness of the template to enhance the nucleation, indeed ZSM-5 with the narrowest pore size was the most effective in increasing nucleation rate (although with a lower specific surface area of MCM-41).

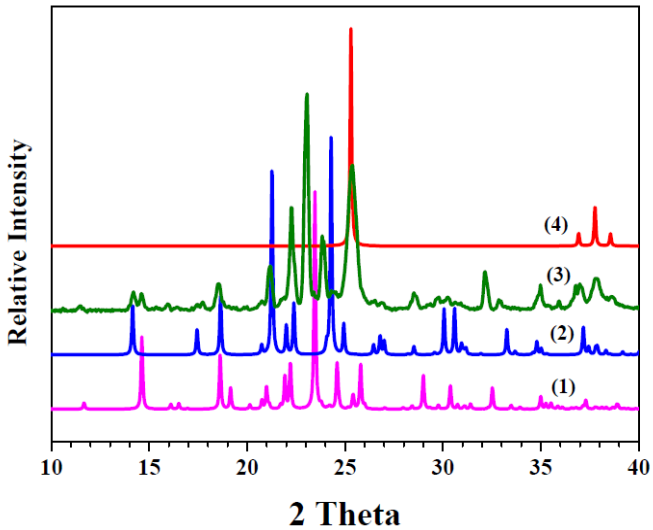

Figure 9. Powder X-Ray diffraction patterns of the known INA crystals compared with the experimentally obtained INA crystals using anatase as a template. (1) Reference form I, (2) Reference Form II, (3) experimentally obtained INA crystals and (4) Reference Anatase.

Rutile and anatase have the same chemical composition, although they show different reactivity of their surface, originated by the different spatial arrangement of atoms on exposed faces. The different surface structure accounts for the dissimilar surface energy for (110) rutile and (101) anatase facets, being 0.53 J/m^2 and 0.98 J/m^2, respectively. The existence in anatase of oxigen bicoordinate and titanium pentacoordinate, having the possibility to form extra coordination bonds makes this face more proud to interact with Lewis acid and basic groups, respectively, thus explaining the higher surface reactivity of anatase to interact with INA to form metastable form I and form III of INA. Thus, heterogeneous templates exhibiting porous and regular surfaces structures in the nanometer range, such as synthetic zeolite ZSM-5, mesoporous aluminosilicate MCM-41, and TiO_2 in both rutile and anatase phase, were effective in reducing induction time and enhancing the nucleation rate of INA. Among the used template, despite their similar chemical

composition, the two polymorphs of TiO_2 displayed a diverse effect on nucleation kinetics, as anatase was more effective than rutile to enhance nucleation rate and to reduce growth time. Furthermore, the ability of the TiO_2 template in anatase form to induce the formation of the metastable form I and form III of INA, thus diverting the expected course of nucleation induced by the solvent, was demonstrated by real time Raman analysis. Specific templates thus provide an additional tool in nucleation control as well as to achieve polymorphic selectivity in solution crystallization.

1.4Conclusions

This work demonstrated that heterogeneous templates exhibiting porous and regular surfaces structures in the nanometer range, such as synthetic zeolite ZSM-5, mesoporous aluminosilicate MCM-41, and TiO2 in both rutile and anatase phase, were effective in reducing induction time and enhancing nucleation rate of Isonicotinamide. Among the used template, despite their similar chemical composition, the two polymorphs of TiO2 displayed a diverse effect on nucleation kinetics, as anatase was more effective than rutile to enhance nucleation rate and to reduce growth time. Furthermore, in the crystallization experiments in ethanol with a supersaturation ratio S=1.4, for the anatase form of titanium dioxide instead of form II the metastable form I was obtained . Thus, the ability of the TiO2 template in anatase form to induce the formation of the metastable form I of INA, thus diverting the expected course of nucleation induced by the solvent, was demonstrated by real time Raman analysis, thus providing an additional tool to achieve polymorphic selectivity in solution crystallization.

1.5References

1. Kashchiev, D. Nucleation: Basic Theory with Applications; Butterworth-Heinemann, Oxford, 2000.

2. Mullin, J. W. Crystallization, 4th ed.; Butterworth-Heinemann, Boston, MA, 2001.

3. Lee, A. Y.; Erdemir, D.; Myerson, A. S. Ann. Rev. Chem. Biomol. Eng., 2011, 2, 259-80.

4. Davey, R. J.; Schroeder, S. L. M.; ter Horst, J. H. Angew. Chem. Int. Ed., 2013, 52, 2166-2179.

5. Chayen, N.; Saradakis, E.; El Bahar, R.; Nemirovsky, Y. J. Mol. Biol., 2011, 312, 591-595.

6. Asanithi, P.; Saridakis, E.; Govada, L.; Jurewicz, I. ACS Appl. Mater., 2009, 1, 1203-1210.

7. Sugahara, M.; Asada, Y.; Morikawa, Y.; Kageyama, Y.; Kunishima N. Acta Cryst. D, 2008, 64, 686-695.

8. Chayen, N. E.; Saridakis, E.; Sear, R. P. PNAS, 2006, 103, 597-601.

9. Kim, K.; Lee, I.; Centrone, A.; Hatton, T. A.; Myerson, A. S. J. Am. Chem Soc., 2009, 131, 18212-18213.

10. Di Profio, G.; Curcio, E.; Drioli, E. J. Struct. Biol., 2005, 150, 41-49 .

11. Curcio, E.; Fontananova, E.; Di Profio, G.; Drioli, E. J. Phys. Chem. B, 2006, 110, 12438-12445.

12. Lòpez-Mejìas, V.; Knight, J. L.; Brooks, C. L.; Matzger, A. J. Langmiur, 2011, 27, 7575-7579.

13. Chadwick, K.; Myerson, A.; Trout, B. CrystEngComm, 2011, 13, 6625-6627.

14. Kulkarni, S. A.; McGarrity, E. S.; Meekes, H.; ter Horst, J. H., Chem. Commun., 2012, 48, 4983-4985.

15. Eccles, K. S.; Deasy, R. E.; Fàbìan, L.; Braun, D. E.; Maguire, A. R.; Lawrence, S. E. CrystEngComm, 2011, 13, 6923-6925.

16. Li, J.; Bourne, S. A.; Caira, M. R. Chem. Commun., 2011, 1530-1532.

17. Kadam, S. S.; Kulkarni, S. A.; Coloma Ribera, R.; Stankiewicz, A. I.; ter Horst, J. H.; Kramer, H. J. M. Chem. Eng. Sci. 2012, 72, 10-19.
18. Kadam, S. S.; Kramer, H. J. M.; ter Horst, J. H. Crystal Growth Design 2011, 11, 1271-1277.
19. Jiang, S.; ter Horst, J. H., Cryst. Growth Design, 2011, 11, 256-261.
20. Krishnan, V. Probability and Random Processes; John Wiley & Sons: Hoboken, NJ, 2006.
21. Kashchiev, D.; van Rosmalen, G. M. Cryst. Res. Technol., 2003, 38, 555-574.
22. Mo, S. -D.; Ching, W. Y. Phys. Rev. B, 1995, 51, 13023-13032.
23. Diebold, U. Surf. Sci. Rep., 2003, 48, 53-229.

Section 2

Membranes as tool for pharmaceutical crystallization and co-crystallization

2.1 Introduction

The second chapter introduces the study on membrane crystallization process and its extension to cocrystallization.

Cocrystallization of active pharmaceutical ingredients (APIs) with cocrystal formers (or coformers) is gaining increasing interest in the drug-development area, since the resulting new solid forms are characterized by different physical-chemical properties compared to the original API.[1-5] Indeed cocrystallization increases the diversity of solid state forms of an API and enhances its pharmaceutical properties as chemical stability,[2] moisture uptake,[6] mechanical behavior,[7] solubility,[8] dissolution rate and bioavailability.[9] Therefore cocrystallization can directly impact scientific and legal aspects of drug development and life cycle management of the marketed products by providing alternative solid dosage forms and extended patent life.[4,5,10] Despite its great potentialities, cocrystallization is by now mainly considered as an empirical technique based on "trial and error" strategies. This is so because the basic mechanisms involved in cocrystals - and more general in crystal - formation are yet poorly understood; in addition, the cocrystallization process requires special control in the solution composition in order to avoid the overrunning of the thermodynamic stability region of a specific specie in the phase diagram, thus producing undesired or impure solid products.[2,3,5] Although ternary phase diagrams have been prepared for various systems such as API-coformer cocrystals,[11] API-coformer hydrate cocrystal,[12] and API-API cocrystals,[13] there is a great demand for the development of new and more efficient production technologies of solid dosage forms and, among them, particularly cocrystals.[2] In the last years, membrane crystallization technology has been recognized as a useful means for producing pharmaceutical crystals in controlled way.[14] Indeed, the interest in membrane technology arises from the possibility of improving the control over the course of the crystallization

process, particularly over the supersaturation stage, by using the proper combination of membrane characteristics and operating parameters.[15] The possibility of exploiting membrane crystallization technology, operating in antisolvent configuration,[16] to produce pharmaceutical cocrystals was recently proved for the Carbamazepine (CBZ) – Saccharin (SAC) system.[17] In this paper the application of membrane cocrystallization process is further investigated by performing a systematic study about the conditions promoting pure CBZ-SAC cocrystals or single components (CBZ/SAC) crystals from water/ethanol solvent mixtures. Particular attention has been devoted to improve control during the supersaturation stage, by operating in the proper zone of the solubility phase diagram of the chosen API/coformer/solvent system, in order to achieve full control in the crystallization of a specific solid form with the desired degree of purity.

2.2 Materials and methods

Crystallizing solutions. In this study a porous membrane is used to dose the amount of antisolvent in the solution, by finely controlling mass transfer in the vapor phase across the membrane. Membrane crystallization technology, operating in solvent/antisolvent demixing configuration has been successfully used for the direct production of cocrystals of the antiepileptic, poorly water soluble, API carbamazepine (CBZ) with the conformer saccharin (SAC) from water/ethanol solvent mixtures. When a gradient of vapor pressure was generated between the two sides of the membranes, by a temperature difference, ethanol (the main solvent for CBZ and SAC), which at the same temperature has a higher vapor pressure than water (the antisolvent), evaporated at higher rate, thus producing solvent/antisolvent demixing. As the amount of ethanol in the mixture (and the overall solution volume) decreased, the reduced solubility generated supersaturation and phase separation occurred once water exceeded a certain volume.

The API and the cocrystal former were dissolved in the solvent (ethanol) at different initial molar ratios and the solution was then added to a saturated aqueous solution of saccharin in different weight ratios in the following way: stock crystallizing solutions, with a final mass of 100 g, were prepared by dissolving different molar ratios of Carbamazepine (CBZ, C4024 from Sigma-Aldrich) and Saccharin (SAC, 240931 from Sigma-Aldrich) powders in bi-distilled water/ethanol (reagent grade, from Carlo Erba) solvent mixtures in the ratio 80%/20% wt. The overall procedure consisted in the following steps: (1) preparation of a saturated SAC solution (excess powder was dissolved in bi-distilled water at 50 °C, the suspension was equilibrated at 25 °C overnight and then the clear solution was separated from the solid residue by filtration); (2) mixing of the solution in (1) with an alcoholic solution containing weighted amounts of SAC and CBZ so that the desired overall CBZ/SAC molar ratio ranged from 0.01 to 1.1. The exact concentration of SAC in the aqueous

solution of step (1) was determined gravimetrically by drying a known amount of solution in an oven for 24 h and then weighing the dry residue (average among three measures). All solutions were filtered by 0.2 µm PES syringe filter to remove macroscopic impurities.

Experimental setup. Crystallizing solution was fed to an antisolvent membrane crystallization setup as sketched in Figure 1.

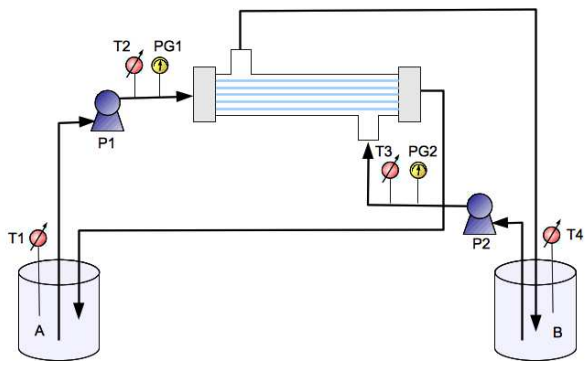

Figure 1. Membrane crystallization setup used in this work. It consists of a glass module containing polypropylene hollow fibers membrane, a crystallization tank (A), a distillate tank (B), recirculation pumps (P1-P2), pressure gauges (PG1-PG2) and temperature probes (T1-T4).

The setup contains a glass membrane module assembled with hydrophobic polypropylene hollow fibers membranes (nominal pore size 0.2 Gm), peristaltic pumps (P1-P2) for solutions recirculation, probes (T1-T4) to monitor temperature in the crystallization and the distillate vessels as well as at the inlet of the membrane module on both feed and distillate sides (T2-T3), and pressure gauges (PG1-PG2) to verify that liquid entry pressure for the used membranes was not reached during the process thus preventing membranes from wetting. Membrane module was made of 20 fibers of 1000 Gm outer diameter (Accurel PP, Q3/2, from Membrana GmbH), resulting in 9.1×10^{-3} m^2

surface area, or of 4 fibers of 1800 Gm outer diameter (Accurel PP, S6/2, from Membrana GmbH) for $3.3x10^{-3}$ m^2 surface area. The process operating mechanism provides that the higher vapor pressure of the solvent than the antisolvent determines the preferential evaporation of the former when the mixture is subjected to a thermal gradient so that T2 - T3 = LT > 0 (driving force).[16] In the present study, the temperature wasset to 25 °C on the feed (crystallizing) side and 10 °C on the distillate side. Since CBZ and SAC are more soluble in ethanol than in water, ethanol is the solvent and water is the antisolvent for the actual system. The preferential evaporation of ethanol from the crystallizing mixturereduces the ratio ethanol/water, resulting in the reduction of compounds solubility and thus increasing supersaturation. Experiments were carried out at the fixed solution circulating flow rate of 20 mL/min. During each test, water/ethanol composition in the crystallizing solution was quantified by means of exsitu refractive index measurements (Abbe 60/DR, Bellingham & Stanley Ltd) on samples of the distillate solution, after mass balance. The transmembrane flow rate, affected by both membrane module characteristics and crystallizing solution composition, was measured through the reduction rate of the volume of the crystallizing solutions.

Phase diagram. Solubility diagram were estimated by determining gravimetrically the solubility of pure components (CBZ, SAC, and cocrystal) in hydro-alcoholic solution at 85%/15% wt. ratio at 25°C. These conditions were chosen as those corresponding to the onset of the nucleation stage in the different tests. Namely, CBZ (SAC) solubility was determined equilibrating an excess of CBZ (SAC) in the presence of unsaturated SAC (CBZ) solutions at increasing concentration; the sample was equilibrated overnight and the solution was filtered by 0.2 µm filter. The filtered solution was dried at 70 °C for 24 h and the solid residue was weighted. The effective amount of CBZ (SAC) was estimated by mass balance.

Cocrystal solubility dependence on the CBZ/coformer concentration was determined by equilibrating an excess of cocrystal in solutions containing API and coformer at different concentrations using the same procedure. This method, although generally considered not as much accurate, is extensively

preferred to estimate solubility data because of its robustness, simplicity, without the need to perform any calibration.[18]

Characterizations. All dry samples from solubility tests and from crystallization trials were analyzed by infrared (IR) analysis and powder X-ray diffraction (PXRD) to verify their composition. IR analyses were performed by using a Fourier transformed infrared (FT-IR) spectrophotometer (Spectrum One, Perkin Elmer), in transmission mode by KBr pellets. Averages of 50 scans at 4 cm-1 resolution were taken for each sample.

FT-IR patterns were visualized and analyzed using principal component analysis (PCA).[19] Data were pretreated by standard normal variate. Such scaling takes care of the fact that the amount of KBr pellet in the sample was not the same in all the measurements. A hierarchical clustering procedure based on the group average method was applied in the space of the principal components to classify the spectra. The calculations were performed with the MultiSpectra software.[20]

PXRD spectra were processed by the program Quanto,[21] using the Rietved method22 for phase quantification with accuracy within 1%. Full-pattern fits were then performed for each sample to derive the weight fraction of each crystalline phase present in the polycrystalline mixture. Previous to the quantification process, identification of all possible phases in all their polymorphic forms was controlled in each mixture. Therefore, the possible occurrence of the five known anhydrous polymorphic forms of CBZ (CBZ I-V), of its dihydrate form (CBZ DH), of SAC and of the two known polymorphic forms of CBZ-SAC cocrystal (Cocrystal I-II) was checked.

2.3 Results and discussions

Crystals obtained from the different tests have been characterized by both infrared (FTIR) and powder X-ray diffraction (PXRD) analyses. Infrared spectra of the pure forms of CBZ (commercial formulation), CBZ crystals from experiments, SAC, and CBZ–SAC cocrystals are displayed in Figure 2.

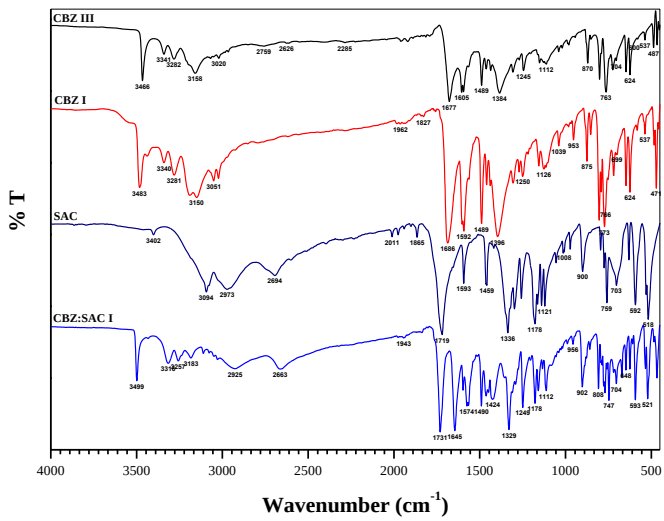

Figure 2. FTIR spectra of carbamazepine form III (commercial), CBZ form I, saccharin, and CBZ-SAC cocrystal form I.

The PXRD spectra provided accurate estimation of the weight fraction of the diverse crystalline phases composing the solid mixtures. Precipitate characterizations revealed that when decreasing the CBZ/SAC molar ratio from 1.1 to 0.01 (while keeping all the other parameters constant) the composition of the precipitate drastically changed, as depicted in Figure 3.

The figure clearly indicates the different regions where a pure crystal form or a mixture of the several phases were obtained. CBZ 100% pure crystals were

obtained for CBZ/SAC molar ration higher than 0.3, while further decreasing the molar ratio in the range 0.3-0.22 CBZ-SAC I cocrystals were produced as mixture with CBZ.

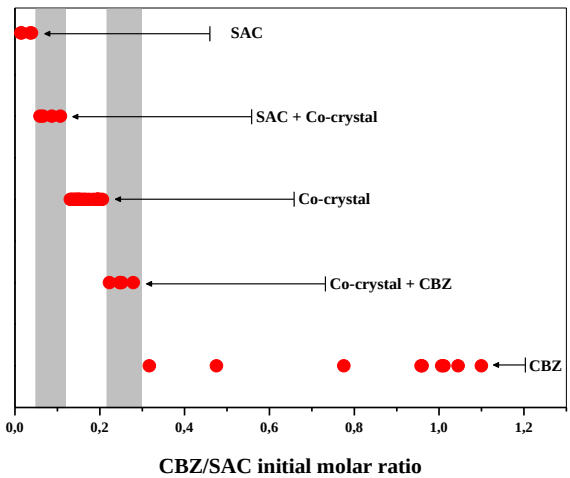

Figure 3. Zones of occurrence of the different products (indicated by the arrows) of the crystallization tests versus the CBZ/SAC molar ratio in the initial solution.

100% pure cocrystals were obtained for solution composition consisting in 0.12-0.22 molar ratio. It was also found that a further decreasing of molar from 0.12 to 0.01 allowed to produce first cocrystals/SAC (up to 0.05) and then pure SAC crystals. This observation confirms the great importance of the initial solution composition in addressing the final outcome of the cocrystallization process and it can be explained exploring the phase solubility diagram of the cocrystal system.[24-26] Since the cocrystal nucleation and growth depends on solution composition, temperature, and solvent evaporation rate in a rather complex way, the solubility phase diagram is the most effective design terminology in cocrystallization. Examination of solution composition in the context of a phase diagram can demonstrate how the preferential supersaturation of the cocrystal can be generated. The ternary phase diagram

(TPD), which shows the solubility of cocrystal and pure components, could be useful to give a detailed visualization of the system.[24,27] The diagram is shown in Figure 4; here the CBZ solubility curve in presence of increasing SAC, the SAC solubility curve in presence of increasing amount of CBZ, and the CBZ-SAC cocrystal solubility data, together with results from the crystallization tests, concurred to build the different regions and to individuate intersections of the single components curves in the eutectic points. The determination of these zones allowed to direct the cocrystallization process toward the preferential formation of the CBZ-SAC cocrystals or the CBZ and SAC single component crystals by simply choosing the starting conditions as the proper CBZ/SAC initial molar ratio in the crystallizing solution.

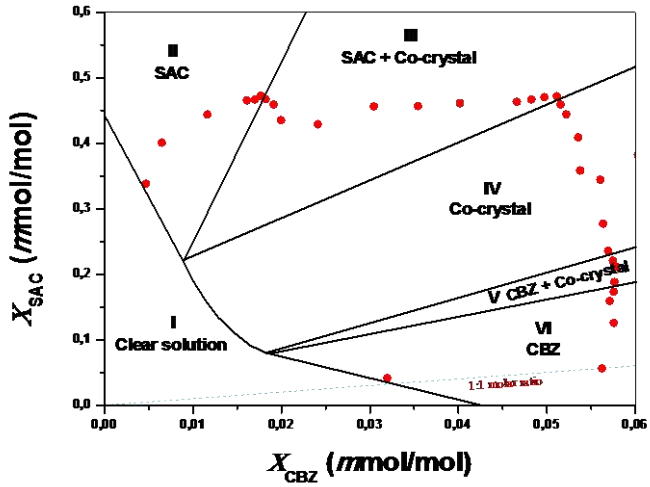

Figure 4. Solubility phases diagram of CBZ-SAC system in 15%/85% wt. ethanol/water mixture at 25 °C. The determination of these curves combined with experimental evidences allowed to approximately divide the graph in six regions: I. region of undersaturated solution; II. region where SAC is thermodynamically stable; III. region where mixtures of SAC and CBZ-SAC cocrystal are stable; IV. region where only CBZ-SAC cocrystal is thermodynamically stable; V. region where a mixture of CBZ and CBZ-SAC cocrystal is stable; VI. region where only CBZ is stable.

The choice of suited solution composition enable to create specific pathway in the phase diagram; indeed, changing the initial molar ratios was possible to reach preferentially the area of stability of cocrystal or the other regions where the single components are more stable. To achieve this purpose, the role of the membrane was crucial to control the concentration mechanism of solution, limiting the maximum level of supersaturation and thus, inducing the reaching of a specific point of the phase diagram. It is evident the necessity to operate in the proper zone of the diagram, avoiding to overrun the thermodynamic stability region of a specific specie by excessive/uncontrolled supersaturation, in order to obtain the desired product. In order to rationalize the experimental results about the conditions favoring the cocrystal and the other different crystalline forms, the specific phase diagram for the CBZ/SAC system in 85%/15% water/ethanol solvent mixture at 25 °C was estimated. The percentage of ethanol was chosen accordingto the value of ethanol measured on the onset of nucleation during the experiments. It was useless to construct a TPD for the CBZ/SAC system in water/ethanol mixtures because of the reduced solubility of the two components in this solvent mixture. Figure 4 shows a trend consistent with the behavior of the noncongruently saturating systems[5,24,25] where an equimolar solution of the two components (CBZ and SAC) will not help in producing the pure cocrystal. To achieve such a finding, an initial solution with a nonequimolar composition, where the molar ratio is shifted towards the more soluble component, was necessary.[28] Indeed, by changing the CBZ/SAC molar ratio in favor of SAC (the more soluble component) made it possible to drive the overall composition in a region of the phase diagram where the cocrystal was the only thermodynamically stable solid phase. The choice of suited solution compositions (circles in Figure 4) enables to create specific pathways in the phase diagram, leading to crystallization points (diamonds in Figure 4) giving rise to the desired product with the required level of purity; indeed, by changing the initial molar ratios it was possible to reach preferentially the area of stability of cocrystal or the other regions where the single components are more stable.

Controlled crystallization of the CBZ polymorphs. Interesting additional results concern with the polymorphic nature of the CBZ precipitate. It is known that CBZ exists in a dihydrate form (CBZ DH) and at least five anhydrous forms:[29,30] primitive monoclinic (CBZ III), triclinic (CBZ I), C-centered monoclinic (CBZ IV) and trigonal (CBZ II), sorted by thermodynamic stability in decreasing order,[29] and the recently discovered orthorhombic form V.[30] Regarding the experiments yielding CBZ, increasing the transmembrane flow rate the amount of CBZ I decreases and the higher energetic form CBZ IV increases as it is shown in Figure 5.

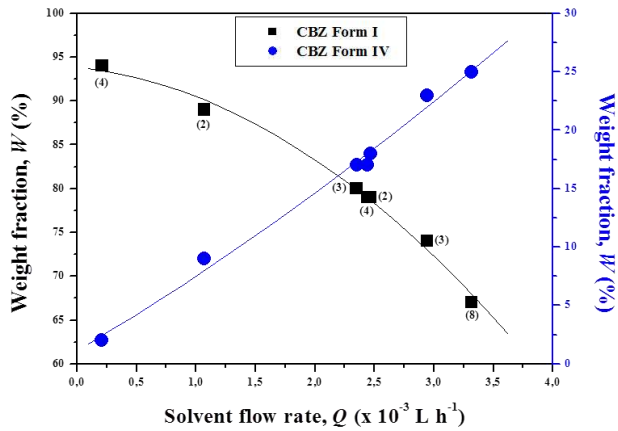

Figure 5. Weight fraction of CBZ crystalline polymorphs in the precipitate as function of the solvent flow rate (in parentheses the weight fraction of the dihydrate form).

In a membrane crystallizer, the transmembrane flow rate can be controlled by choosing the appropriate membrane properties or by acting on process variables.[16] This means that the crystallization trend can be properly addressed towards a specific pathway by operating on the process conditions, giving rise to the selective crystallization of different polymorphs.[15,31] Accordingly, the preferential formation of metastable higher energetic forms are promoted at

high rates of supersaturation. These findings are in good agreement with recent studies[32] where the rate of generation of supersaturation was found to be a controlling factor in the polymorphic composition of the resulting crystals. These results have also been rationalized by valuating the thermodynamic and kinetic interplay in crystallization process and it is concluded that the CBZ crystallization has been kinetically rather than thermodynamically controlled at high transmembrane flux.

Generally speaking, when the thermodynamic and kinetic paths of crystallization are similar, the system has every chance to sample all the possible multi-molecular clusters in solution before selecting the one with lowest energy. In this situation, the system is able to select that path which will minimize the energy at each stage; in other words, the crystal will chose the most stable form (thermodynamic product). When instead the crystallization process is under kinetic control, the system, when leaving an unstable state, does not seek out the most stable state, rather the nearest metastable state which can be reached with loss of free energy, according to the Ostwald's law of stages.[33] In this case, the system is localized into a relative energy minimum, leading to the formation of a metastable structure (kinetic product).

Results confirm the great importance of the initial solution composition in addressing the final outcome of the cocrystallization process. However, in order to achieve the desired product with the right level of purity, it is necessary to operate in the proper conditions without overcoming its region of thermodynamic existence. To achieve this purpose, the role of the membrane was crucial to control the concentration mechanism of solution limiting the maximum level of supersaturation. The operating mechanism of the membrane-based strategy involves using a porous membrane as mean to control the solvent/antisolvent demixing in the crystallizing solution, by finely modulating solvent removal in vapor phase.[14-16] Accordingly, the specific role of the membrane is to limit the maximum level of supersaturation reached in solution by controlling the solvent evaporation, so as providing specific routes in the phase diagram, thus avoiding the overrunning of the thermodynamic stability region of a specific specie, giving rise to the desired solid form.

The phase composition of the CBZ precipitates highlighted the kinetic nature of CBZ crystallization pathway. Indeed, solid samples were composed mainly by CBZ I and CBZ IV phases while CBZ DH was only obtained as byproduct. It is interesting to note that CBZ III, the most thermodynamically stable phase and the only one present in the initial solution, never appeared during the crystallization test. CBZ IV is a polymorph of low thermodynamic stability, which requires higher energy than CBZ III and CBZ I to be formed. On the other hand, CBZ I is the polymorph with lower symmetry and more populated asymmetric unit (Z=4), that can be obtained from the other phases upon heating up to 160-190 °C.[29] Crystal forms with more than one independent molecule in the asymmetric unit (Z'>1) have often been referred as kinetic products.[34] In fact, the Z'>1 crystals represent a form which has been trapped before the molecules have adjusted themselves in a form with higher symmetry and Z'=1. In other words, the Z'>1 occurrence is related to the molecules organization in stable clusters prior to reaching the highest symmetry arrangement in strong hydrogen-bonded structures.[35] It is joint opinion that high Z' packing is due to kinetic trapping in metastable state during the crystallization process. In this regards, high Z' structures have been referred to as "fossil relic,[36] "snapshot picture of crystallization[37] or "crystals on the way,[35] particularly when a lower Z' form also exists. Therefore, the preferential formation of CBZ polymorphs eitherthermodynamically unfavoured (CBZ IV) or with Z'>1, hence resulting from an interrupted crystallization (CBZ I) confirms that the CBZ crystallization mechanism occurred in the explored transmembrane conditions under kinetic control.

2.5 Conclusions

A successful crystallization strategy based on the use of membranes crystallization technology was designed and developed for the CBZ/SAC/water-ethanol system. The implementation of this methodology allowed controlling the production of pure CBZ, SAC crystals or CBZ-SAC cocrystals from water/ethanol solvent mixtures by using the appropriate initial solution composition. The choose of opportune CBZ/SAC molar ratios, combined with the use of the membrane to control supersaturation, made it possible driving the process towards the achievement of a specific region of the solubility phase diagram thus producing the desired product with the required degree of purity. The membrane, used as device to modulate solvent removal in vapor phase, had a key role in controlling the solution composition and confining the level of supersaturation reached in solution. As it concerns the CBZ crystals production, the crystallographic analysis has shown the preferential formation of the high Z' polymorph, so as confirming that the crystallization process was kinetically controlled. The transmembrane flow rate was seen to be a controlling factor in the polymorphic composition of the produced crystals, as proportionally affecting the rate of supersaturation generation.

The direct correlation between transmembrane flow rate and polymorphic form produced may cause the adoption of membrane-based crystallization technique in the production of specific metastable phases of interest in pharmaceutical industry.

2.5 References

1. (a) Almarsson, O.; Zaworotko, M. J. Chem. Comm., 2004, 17, 1889. (b) Blagden, N.; Berry, D. J.; Parkin, A.; Javed, H.; Ibrahim, A.; Gavan, P. T.; De Matos, L. L.; Seaton, C. C. New J. Chem., 2008, 32, 1659. (c) Sheikh, A. Y.; Rahim, S. A.; Hammond, R. B.; Roberts, K. J. CrystEngComm, 2009, 11, 501. (d) Weyna, D. R.; Shattock, T.; Wishweshwar, P.; Zaworotko, M. J. Cryst. Growth Des., 2009, 9, 1106, (e) Schultheiss, N.; Bethune, S.; Henck, J.-O. CrystEngComm, 2010, 12, 2436. (f) Upadhyay, N.; Shukla, T. P.; Mathur, A.; Jha, S. K. Int. J. Pharm. Sc., 2011, 8, 26. (g) Brittain, H. Cryst. Growth Des., 2012, 12, 1046.

2. Childs, S. L.; Chyall, L. J.; Dunlap, J. T.; Smolenskaya, V. N.; Stahly, B. C.; Stahly, G. P. J. Am. Chem. Soc., 2004, 126, 13335.

3. Trask, A. V. Mol. Pharmaceutics, 2007, 4, 301.

4. Chen, J.; Sarma, B.; Evans, J. M. B.; Myerson, A. Cryst. Growth Des., 2011, 11, 887.

5. Gagniere, E.; Mangin, D.; Puel, F.; Valour, J.; Klein, J. J. Cryst. Growth, 2011, 316, 118.

6. Trask, A. V.; Motherwell, W. D. S.; Jones, W. Cryst. Growth Des., 2005, 5, 1013.

7. Sun, C. C.; Hou, H. Cryst. Growth Des., 2008, 8, 1575.

8. Jones, W.; Motherwell, W. D. S.; Trask, A. V. Phar. Mater. Sci., 2006, 31, 875.

9. (a) Hickey, M. B.; Peterson, M. L.; Scoppettuolo, L. A.; Morrisette, S. L.; Vetter, A.; Guzman, H.; Remenar, J. F.; Zhang, Z.; Tawa, M. D.; Haley, S.; Zaworotko, M. J.; Almarsson, O. Eur. J. Biopharm., 2007, 67, 112. (b) Stanton, M. K.; Bak, A. Cryst. Growth Des., 2008, 8, 3856. (c) Good, D. J.; Rodriguez-Hornedo, N. Cryst. Growth Des., 2009, 9, 2252. (d) Bethune, S. J.; Schultheiss, N.; Henk, J.- O. Cryst. Growth Des., 2011, 11, 2817.

10. Gardner, C. R.; Walsh, C. T.; Almarsson, O. Nat. Rev.: Drug Discovery, 2004, 3, 926.

11. (a) Padrela, L., Rodriguez, M. A., Velaga, S. P., Matos, H. A., de Azevedo E. G., Eur. J. Pharm. Sci., 2009, 38, 9. (b) Gagniere, E., Mangin, D., Puel, F., Rivoire, A., Monnier, O, Garcia, E., Klein, J.P., J. Cryst. Growth, 2009, 311, 2689. (c) Takata, N., Takano, R., Uekusa, H., Hayashi, Y., Terada, K., Cryst. Growth Des., 2010, 10, 2116.
12. Karki, S., Friščić, T., Jones, W., Motherwell, W. D. S. Mol. Pharm, 2007, 4, 347.
13. Bhatt, P. M., Azim, Y., Thakur, T. S., Desiraju, G. R, Cryst. Growth Des., 2008, 9, 951.
14. Di Profio, G.; Curcio, E.; Drioli, E. Ind. Eng. Chem. Res., 2010, 49, 11878.
15. Di Profio, G.; Tucci, S.; Curcio, E.; Drioli, E. Cryst. Growth Des., 2007, 7, 526.
16. Di Profio, G.; Stabile, C.; Caridi, A.; Curcio, E.; Drioli, E. J. Pharm. Sci., 2009, 98, 4902.
17. Di Profio, G.; Grosso, V.; Caridi, A.; Caliandro, R.; Guagliardi, A.; Chita, G.; Curcio, E.; Drioli,E. CrystEngComm, 2011, 13, 5670.
18. (a) Ono, T.; Kramer, H. J. M.; ter Horst, J. H.; Jansens, P. J. Cryst. Growth Des., 2004, 4, 1161. (b) Scholl, J.; Lindenberg, C.; Vicum, L.; Mazzotti, M. Cryst. Growth Des., 2007, 7, 1653. (c) Guo, K.; Sadiq, G.; Seaton, C.; Davey, R.; Yin, Q. Cryst. Growth Des., 2010, 10, 268. (d) Rager, T.; Hilfiker, R. Cryst. Growth Des., 2010, 10, 3237.
19. Beebe, K., Pell, R., Seasholtz, M. Chemiometrics: A practical Guide; John Wiley & Sons, Inc: New York, 1998.
20. Caliandro, R., Guagliardi, A., Di Profio, G., Nicolotti, O., Masciocchi, N. in preparation.
21. Altomare, A.; Burla, M. C.; Giacovazzo, C.; Guagliardi, A.; Moliterni, A. G. G.; Polidori, G.; Rizzi, G. J. Appl. Cryst., 2001, 34, 392.
22. Rietved, H. M. Acta Cryst. 1967, 22, 151.
23. Porter, W. W.; Elie, S. C.; Matzger, A. J. Cryst. Growth Des., 2008, 8, 14.
24. Childs, S. L.; Rodriguez-Hornedo, N.; Reddy, L. S.; Jayasankar, A.; Maheshwari, C.; McCausland, L.; Shipplett, R.; Stahly, B. C. CrystEngComm, 2008, 10, 856.
25. ter Horst, J. H.; Cains, P. W. Cryst. Growth Des., 2008, 8, 2537.

26. Urbanus, J.; Roelands, C. P.; Verdoes, D.; Jansen, P.; ter Horst, J. H. Cryst. Growth Des., 2010, 10, 1171.
27. (a) Chirella, R. A.; Davey, R.; Peterson, M. L., 2007, 7, 1223. (b) Ainouz, A.; Authelin, J.-R.; Billot, P.; Lieberman, H. Int. J. Pharmac., 2009, 374, 82. (c) Jayasankar, A.; Reddy, L. S.; Bethune, S. J.; Rodriguez-Hornedo, N. Cryst. Growth Des., 2009, 9, 889.
28. Childs, S. L.; Wood, P. A.; Rodriguez-Hornedo, N.; Reddy, L. S.; Hardcastle, K. I. Cryst. Growth Des, 2009, 9, 1869.
29. Grzesiak, A. L.; Lang, M.; Kim, K.; Matzger, A. J. J. Pharm. Sci., 2003, 92, 2260.
30. Arlin, J.-P.; Price, L. S.; Price, S. L.; Florence, A. J. Chem. Commun. 2011, 47, 7074.
31. Di Profio, G.; Caridi, A.; Caliandro, R.; Guagliardi, A.; Curcio, E.; Drioli, E. Cryst. Growth Des., 2010, 10, 449.
32. (a) He, G.; Wong, A. B. H.; Chow, P. S.; Tan, R. B. H. J. Cryst. Growth, 2011, 314, 220. (b) Barrett, M.; Hao, H.; Maher, A.; Hodnett, K.; Glennon, B.; Croker, D. Org. Res. Develop., 2011, 15, 681.
33. Ostwald, W. Zeitschrift für Physikalische Chemie, 1897, 22, 289.
34. (a) Desiraju, G. R. Angew Chem. Int. Ed., 2007, 46, 8342. (b) Desiraju, G. R. CrystEngComm., 2007, 9, 91. (c) Bernstein, J.; Dunitz, J. D.; Gavezzotti, A. Cryst. Growth Des., 2008, 8, 2011. (d) Bishop, R.; Scudder, M. L. Cryst. Growth Des., 2009, 9, 2890.
35. Das, D.; Banerjee, R.; Mondal, R.; Howard, J. A. K.; Boese, R.; Desiraju, G. R. Chem. Com., 2006, 5, 555.
36. Anderson, K. M.; Steed, J. W. CrystEngComm, 2007, 9, 328.
37. Steed, J. W. CrystEngComm., 2003, 5, 169.

Chapter 3

Manufacturing of PVDF-based Mixed Matrix Membranes as heterogeneous support for crystallization

3.1 Introduction

The increasing technological and economic prominence of membrane processes in various fields, such as water treatment, desalination, fuel cells, food industry, has driven for the development of a large array of membrane typologies. Researches on membrane manufacturing have been going towards two main directions, both aiming the preparation of new membranes tailored to specific applications: the development of new composite materials, on one hand, and the modification of the structural properties, on the other hand.

Among the polymer materials for membrane production, PVDF is one the most widely used due to its thermal stability, chemical resistance, semi-crystalline structure and versatility in manufacturing.

Various routes of PVDF membrane modification have been used, such as coating, chemical grafting, blending or combinations of these methods. Blending resulted a simple, versatile and tunable method as of the recently proposed approaches. Specifically, the blending of inorganic fillers into PVDF polymer matrix, resulting in the production of mixed matrix membranes (MMMs), has been seen to improve PVDF mechanical strength and stiffness and sometimes strongly influence the final membranes properties. The production of PVDF based MMMs, provided benefits in a variety of applications, such as mitigation of membrane fouling in water treatments, increasing transmembrane flux in gas separation, and enhancement of catalytic effect in membrane reactors.

Apart the chemical nature, the utility of the membranes in specific application is largely dependent on the structural nature, such as morphology, porosity and pore size. Therefore, the study of manufacturing procedures and the technical parameters affecting the structural features arouse great interest in the last years and it is constantly evolving.

Despite the structural characteristics are not easy of controlling, because of the influence of several concurrent factors, there is, today, a general

consensus among researchers about the possibility of diversify the membrane structure by using different manufacturing methods. Various procedures give rise to the formation of membranes different in porosity degree (from dense to highly porous), pore size, symmetry along the cross section, membranes with skin layer of variable thickness, and different connectivity of the polymer matrix.

Therefore, the objective of this study was the preparation of PVDF membranes, opportunely modified from both chemical and structural point of view, by varying the blend composition and changing the manufacturing procedure. The implementation of sets of membranes, made with the same polymer constituent and appropriately modified in chemical and structural features, aims a better definition of the relations between membrane manufacturing parameters (chemical composition, preparation techniques) and membrane properties (hydrophobicity, wettability, porosity, roughness, pore size, thickness). The idea of producing PVDF membranes, different in both chemical composition and morphological features arose from the awareness that sets of modified membranes are needed in the systematic screening of the membranes performances for the selection of the membrane type which best suits for specific applications.

Here, the chemical modification was achieved by embedding different inorganic nano-sized fillers into the polymeric matrix, while the morphological modification was achieved by changing preparation method. Four kinds of inorganic fillers – titanium dioxide nanoparticles in anatase and rutile form, molecular sieves ZSM-5 and mesoporous MCM-41 - were embedded into the PVDF matrix to prepare mixed matrix membranes (MMMs). Blank PVDF membranes (without fillers) were also prepared as standard. Each polymeric blend (PVDF, PVDF/TiO_2 Rut., PVDF/TiO_2 Anat., PVDF/MCM-41, PVDF/ZSM-5) was manufactured via three phase inversion/separation methods, giving rise to a total of 15 PVDF-based membrane type, different for chemical and physical nature jointly. The membrane manufacturing methods, used in this work, are three different phase separation techniques, reported as: non-solvent induced phase separation (NIPS), vapour induced phase separation (VIPS), and dry/wet non-solvent induced phase separation (Dry/Wet-NIPS).

The mechanism of the phase separation, associated to these techniques, takes place because of the simultaneous occurrence of the non-solvent penetration and the solvent elimination in the homogeneous polymer solution. The mass exchanges between the non-solvent and the polymer ffsolution, make the polymer solution thermodynamically unstable because the gradual reduction of the polymer solubility, leading to a complete phase separation.

Depending on the thermodynamic and kinetic parameters, the demixing process of the homogeneous polymer solution strongly influences the morphology of the final material.

The first phase separation procedures (NIPS) involved using the non-solvent in liquid phase. The polymer solution was cast as a thin film on a support and was immediately immersed in the non-solvent (water) bath. This process is generally associated with rapid mass exchanges between the polymer solution and coagulation bath, resulting in formation of asymmetric membranes with a less porous skin layer and a more porous support layer.

In the second phase separation methods (VIPS), the non-solvent was used in vapour phase. The cast film was left evaporate at athmosphere with controlled moisture degree. During this process, phase separation of the polymer solution is led by the evaporation of the solvent and the penetration of non-solvent vapour (water molecules in the air). The polymer solution demixing is here much slower, generally giving rise to more porous and symmetric membranes or structures in which the pore size decrease gradually.

The third procedures (Dry-Wet-NIPS) involves exposing the casted film on the atmosphere humidity for a fixed time and then immerging it into the liquid coagulation bath. This manufacturing method reproduces both the previous mentioned techniques, inducing the solvent/non-solvent demixing in liquid/vapour phase at first, and in liquid/liquid phase, at a second time. The procedures would lead to asymmetric membranes with tunable features, depending on the evaporation time.

3.2 Materials and methods

Materials. Poly-vinylidene fluoride (PVDF) Solef 6010, purchased by Solvay, was the membranes polymer constituent. N,N-Dimethyl formamide (DMF), from Sigma-Aldrich, was the solvent for polymeric blends. Titanium dioxide in both anatase and rutile form, microporous molecular sieves ZSM-5, mesoporous silica nanoparticles MCM-41, from Sigma-Aldrich, were used as fillers, without further purification, for membranes preparation. Lithium chloride (LiCl) from Sigma-Aldrich was added to the polymeric blends to enhance the membrane porosity.[1]

Casting mixtures preparation. All polymeric mixtures were prepared with the same formula (detailed in *Table 1*): 15% polymer (PVDF), 2% $LiCl_2$, 1.5% additive (TiO_2 anatase, TiO_2 rutile, ZSM-5, MCM-41), 81.5% solvent (DMF). For the blank-type membranes (without additive) 83% solvent was used. The casting mixture was prepared by firstly dissolving LiCl in DMF at room temperature and then, adding the appropriate amounts of PVDF and filler. The polymeric mixture was left stirring at 50°C for about 24 hours, until the polymer complete dissolution. Solvent loss by evaporation was negligible due to the high boiling point of DMF (153 °C). Since the poor solubility of the inorganic fillers in the polymeric blend, all samples were treated ultrasonically (VWR ultrasonic USC600TH, 120 W) for 30 minutes yielding an evenly spread suspension. Then, the casting blend was gradually quenched at room temperature for 2 hours, for reducing any possible air bubble formed during the treatments.

Membranes manufacturing. Three different manufacturing techniques were used for membranes preparation (NIPS, Dry-Wet-NIPS, VIPS, schematically shown in Figure 1), giving rise to the formation of three membranes different in terms of scaffolding and surface texture for each chemical composition respectively (five different polymeric blends). All manufactured membranes are listed in Table 1.

Table 1. List of the manufactured membranes: polymeric mixture compositions (fillers, solvent) and casting details (technique used, temperature, moisture degree, casting thickness)

N.	Fillers	Solvent	T (°C)	RH	Technique	Casting thickness
29	-	DMF 83%	24.6	66-68%	NIPS	250
30	-	DMF 83%	24-26	66-68%	VIPS	250
70	-	DMF 83%	26,9	61%	Dw-NIPS	250
38	TiO2 An.1.5%	DMF 81.5%	26.6	72%	NIPS	250
33	TiO2 An.1.5%	DMF 81.5%	23.4-26	66-56%	VIPS	250
72	TiO_2 An. 1.5%	DMF 81.5%	27,3	61%	Dw-NIPS	250
35	TiO_2 Rut.1.5%	DMF 81.5%	25	59%	NIPS	250
36	TiO_2 Rut.1.5%	DMF 81.5%	25-26.8	59-62%	VIPS	250
73	TiO_2 Rut.1.5%	DMF 81.5%			Dw-NIPS	250
39	MCM-41 1.5%	DMF 81.5%	25,4	59%	NIPS	250
40	MCM-41 1.5%	DMF 81.5%	25,4	59%	VIPS	250
74	MCM-41 1.5%	DMF 81.5%			Dw-NIPS	250
42	ZSM-5 1.5%	DMF 81.5%	25,4	59%	NIPS	250
43	ZSM-5 1.5%	DMF 81.5%	25,4	59%	VIPS	250
75	ZSM-5 1.5%	DMF 81.5%			Dw-NIPS	250

Each polymeric mixture was manually cast onto a glass slide thorough a micrometric film applicator (Elcometer 3570) at a nominal thickness of 250 µm. In the case of the NIPS made membranes, the cast films were immediately plunged into a distilled water bath (with a temperature ranging from 16°C to 26°C and humidity between 59% and 72%) for 12 hours to ensure the PVDF complete phase separation. Then, the coagulation bath was renovated with fresh distilled water, for a further 12 hours.

For the Dry-Wet-NIPS produced membranes, the cast films were evaporated for 60 s before being immersed into the coagulation bath (distilled water with a temperature between 16°C and 27°C, and humidity between 58% and 66%) for 24 hours, (water bath refreshed after 12 hours).

Lastly, as the VIPS made membranes concerned, the cast films were exposed to the atmosphere at room temperature (in the range of 16-27°C) with

controlled moisture content (57-68%) until complete solidification (about 72 hours).

All coagulated films were repeatedly rinsed with distilled water to flush away the solvent residuals, before being dried up.

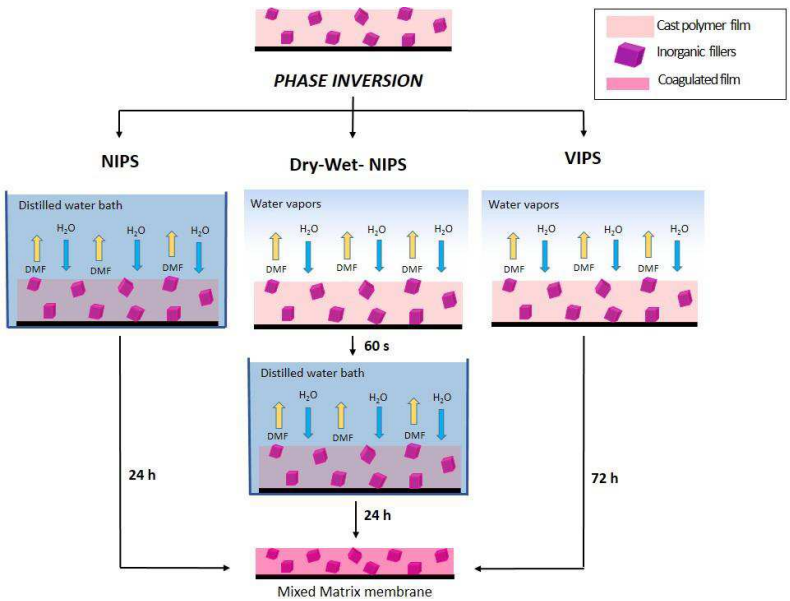

Figure 1 Three different methods to induce the polymer phase inversion, used for membranes preparation: Non-solvent induced phase separation (NIPS), Dry-wet-non-solvent induced phase separation (Dry-Wet-NIPS) and Vapor induced phase separation (VIPS).

Membranes characterization. The membrane wettability was evaluated thorough contact angle measurements with sessile drop technique in static and motion mode (growing/shrinking), according to the classical procedures, by using a CAM 200 contact angle meter (KSV Instruments 109 Ltd.) equipped with a micro- syringe, automatic dispenser and images processing software. The membrane sample was stuck onto a glass slide with a double-sided tape to ensure its top surface was flat and motionless. Static contact angles (θ_{eq}) were

measured with tangent method, by depositing a deionized water droplet (5 µL) on the membrane surface and catching one frame per second until the equilibration (10 s). Advancing contact angles (θ_a) were measured by catching image frames every 0.5 seconds, while increasing the volume of a deposited droplet of 5 µL up to 10 µ, with a constant dosing rate of 0.2 µL/s. Receding contact angles (θ_r) were measured by catching image frames every 0.5 seconds, while reducing the volume of 10 µL droplet till 5 µL, at the same dosing rate. Contact angle hysteresis was determined as difference between advancing and receding contact angles ($H= \theta_a - \theta_a$). The reported contact angles were average values of three measurements to minimize random errors.

Surface morphology was assessed by means of and Nanoscope III atomic force microscope (AFM Digital Instruments, VEECO Metrology group).

Moreover, the scanning electron microscope (SEM Quanta 200 F FEI Philips) allowed a further analysis of the membrane morphology along the top/down surfaces and the sections. To observe their cross sections, the membranes were frozen in liquid nitrogen and then cut by a rip. Energy Dispersive X-ray spectroscopy (SEM-EDX) analysis confirmed the presence of the fillers into the polymer structures.

The crystalline phases of PVDF polymer matrix were detected by Fourier Transform Infrared Spectroscopy (FTIR) analysis.

The thickness of each membrane was measured with a digital micrometer (40E Carl Mahr D 7300 Esslingen).

Pore size distribution of membranes (2cm diameter samples) was determined by Capillary Flow Porometer (CFP 1500 AEXL, Porous materials Inc., USA) with dry up-wet up method, which measures gas flow as a function of transmembrane pressure through the wetted (with a low surface tension liquid) and dried membrane. The relationship between capillary pressure and pore size was given by the Laplace equation. The membrane wetting liquid used for the experiments was Porewick (surface tension 16 dynes/cm).

Membrane total porosity was determined by imbibition method. The membrane sample was immersed in Kerosene overnight to ensure it was fully saturated. It was assumed that all the pores of the membranes were completely filled with Kerosene. The sample was weighed in a digital balance

before and after the impregnation in kerosene. A further weighing was after drying the membrane sample in the oven at 70°C overnight, as evidence of the membrane endurance in kerosene. The porosity $\varepsilon\%$ was calculated according to the following equation:[2]

$$\varepsilon\% = \frac{(w_w - w_d)/\rho_w}{(w_w - w_d)/\rho_w + w_d/\rho_d} * 100$$

where w_w is the mass of wet in kerosene membrane, w_d is the mass of dry membrane, $\rho_w$and ρ_d are the density of kerosene (0,82 g/cm^3) and PVDF (1,77 g/cm^3), respectively.

3.3 Results and discussion

Chemical modification of PVDF membranes. The inorganic fillers are observable by the SEM images of the MMMs (Figure 2), revealing the attempt to make chemically heterogeneous PVDF membranes has been successful. The images show the filler particles have tended to congregate, appearing as withe spots scattered around in the polymer matrix, in line with many SEM pictures from other author[3,4]. Indeed, a good dispersion of filler particles in a polymer matrix is inherently challenging because of the strong interparticles interactions and weak polymer-nanoparticles and solvent-nanoparticles interfacial interactions.

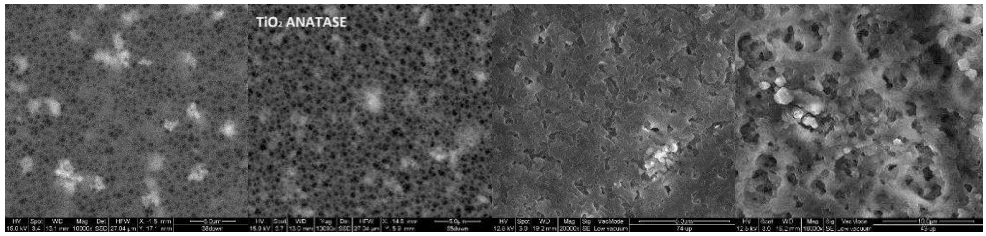

Figure 2. Down surface SEM images of produced MMMs membranes by NIPS technique, (5µm magnification).From the left to the right: TiO2 rut, TiO2 anat, MCM.41, ZSM-5.

As concerning the TiO_2, the nanoparticles dispersion into a polymer cast solution is the result of their thermodynamic stability when in contact with both solvent and polymer. Mackay et al.[5], studying strategies for controlling the nanoparticle dispersion in polymer melts, found that the nanoparticles are thermodynamically stable in the cast polymer solution when the radius of gyration (R_g) of the linear polymer is greater than the radius of the nanoparticles (Rp). According to the molecular dynamic simulation reported by Sukitpaneet et.al.[3] the radius of gyration of PVDF chain in NMP is 24.98 Å, which is much smaller than the radius of anatase and rutile, whose dimensions

are about 25 nm and 100 nm respectively, as specified by the supplier. This would explain the difficulty in obtaining a good TiO_2 distribution in the polymer matrix. Moreover, Teow et al.[6] studying the preparation of PVDF/TiO2 MMMs via in situ colloidal precipitation, reported the tendency of DMF to favour the formation of larger TiO_2 aggregates with respect other less water-miscible, because of the higher surface tension between DMF and TiO_2 which promote particles aggregation. Nevertheless, the good solvent properties of DMF for a highly hydrophobic polymer such as PVDF, have justified our choice of the solvent, in this work.

Elementary analysis by Energy-Dispersive X-ray spectroscopy (SEM-EDX) further revealed the filler particles embedded in MMMs.

In Figure 3, the EDX spectra of the NIPS produced membranes are shown; the same results were for the membranes manufactured by Dry-Wet-Nips and VIPS methods (not shown).

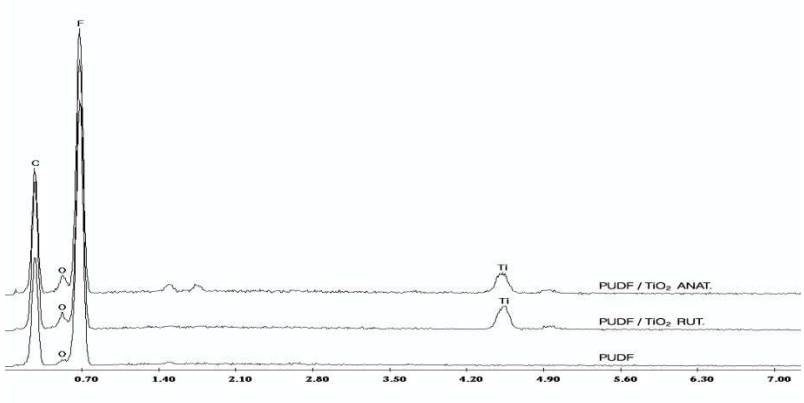

Fig. 3 Qualitative analysis of membranes materials by Energy Dispersive X-ray spectroscopy (SEM-EDX): spectra for PVDF, PVDF/TiO2 Rut., PVDF/TiO2 Anat., PVDF/MCM-11, and PVDF/ZSM-5, produced by NIPS technique. Mancano EDX delle membrane 39 e 42 (PVDF/MCM-11, and PVDF/ZSM-5)

The presence of the TiO_2 rutile and TiO_2 anatase in the PVDF matrix was also confirmed by UV-vis Diffuse Reflectance Spectroscopy analysis. The spectra of PVDF/TiO_2 Rut., PVDF/TiO_2 Anat. and PVDF membranes, at wavelengths

between 200 and 800 nm, are shown in Figure 4. Pure PVDF does not show any absorption band in UV range (black flat line), while characteristic absorption peak of Ti–O bond are clearly visible at 310 nm for PVDF/TiO2 Anat. and 330 nm for PVDF/TiO2 Rut. The absorption band for rutile embedded membrane resulted shifted and attenuated with respect the anatase, probably due to a worst dispersion of the rutile nanoparticles.

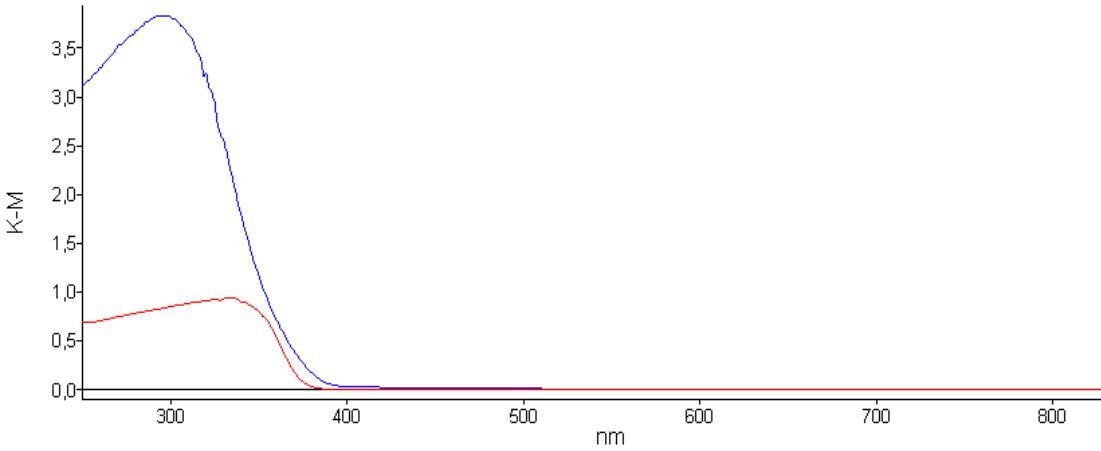

Fig. 4 UV-vis DR spectra of PVDF/TiO_2 Rut. (red), PVDF/TiO_2 Anat. (blue), and PVDF blank membranes (black flat line) , at wavelengths between 200 and 800 nm.

Membranes morphology. Many studies about the non-solvent induced phase separation techniques demonstrated that the factors affecting the rate of liquid-liquid and solid-liquid demixing ultimately determine the physical morphology of membranes. The SEM characterization confirmed how different manufacturing parameters strongly affect the membrane morphology.

Figure 5 shows the cross-section morphologies of the PVDF blank-type membranes produced membranes. The membranes produced by NIPS and Dry-Wet-Nips seems to have correlated morphologies, while membranes produced by VIPS appears significantly different. These differences can be explained by looking at the process of phase inversion. In the NIPS method, a

film of the homogeneous polymeric solution is generally cast on a glass support and immersed in a non-solvent bath. When the non-solvent in liquid phase comes in contact with polymer solution, mass exchanges between the polymer solution and coagulation bath is very rapid and the polymer solution starts to demixing in two liquid phases. The solvent/non-solvent exchange induces an increase of the polymer concentration in the concentrated phase surrounding the pores. The phase with the higher polymer concentration forms the membrane matrix, and the phase with the lower polymer concentration generates the pores. The phase inversion process explains why the final film morphology is strictly dependent on the rate of the solvent/non-solvent diffusion. Differently, the VIPS method proceeded by exposing the cast liquid film to water vapors. The phase inversion in VIPS process is induced by the diffusion of the non-solvent in the polymer solution (influx) and the evaporation of the solvent (outflux). Therefore, in the NIPS process, the mass transfer rates is usually higher than in VIPS.

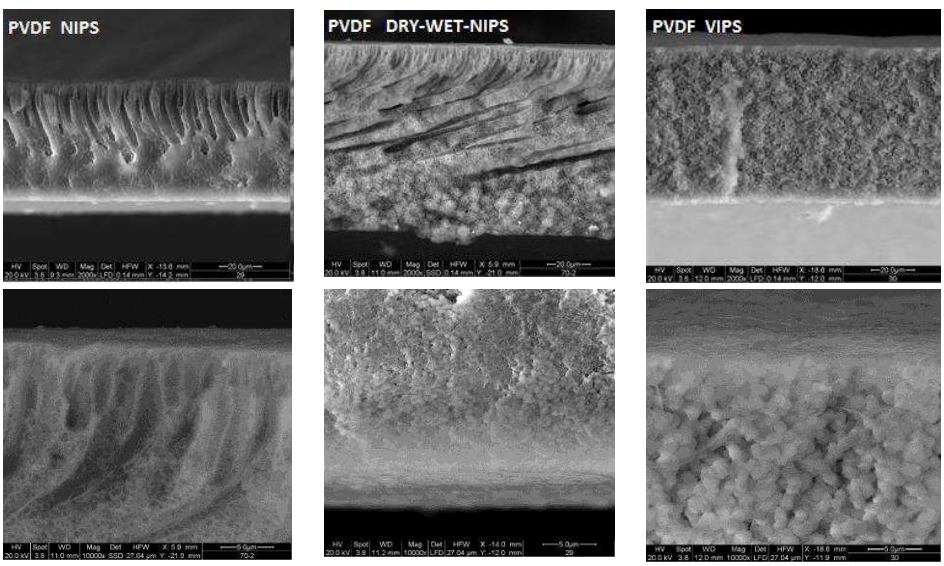

Figure 5 . Cross section SEM images of PVDF membranes prepared by NIPS, Dry-Wet-Nips and VIPS techniques respectively, at 20 µm (in the top row) and 5 µm (in the bottom row) magnification.

The SEM images in figure 5 showed that in NIPS made membranes, finger-like macrovoids are present in the bulk of the membranes under a dense skin surface. Macrovoids are very large elongated pores which can extend over the entire membrane thickness. Macrovoids are, in general, undesirable, because they cause mechanical weaknesses in the membrane. The formation of these finger-like cavities under a skin layer in membranes can be associated with a high rate of precipitation of the polymer from the casting solution upon immersion in the non-solvent, due to the high tendency of the solvent to mix with the non-solvent. The rapid solvent/non-solvent exchange induces the polymer precipitation at the liquid/polymer interface and reduces the exchanges rate in the sublayers.[7]

On the contrary, a spong-like and symmetric structure was observable in the VIPS made membranes. The distinguish morphology was given by the slow diffusion of the vapor phase to the film surface. During the evaporation of the solvent and the concomitant penetration of non-solvent vapour in the solution, the solubility of the polymer decreases gradually, leading to an uniform polymer concentration profile along the film cross section during the phase separation process.

Figure 6 shows the PVDF based MMMs made with Titanium dioxide embedded, in both rutile and anatase form, prepared with the same three technical procedures. For PVDF/MCM-11 and PVDF/ZSM-5 membranes the same trend is shown in Figure 7.

In the Table 2 the physical membrane features, such as membrane thickness, the average pore diameter, and the overall porosity ($\varepsilon\%$) calculated according with equation 1, are reported.

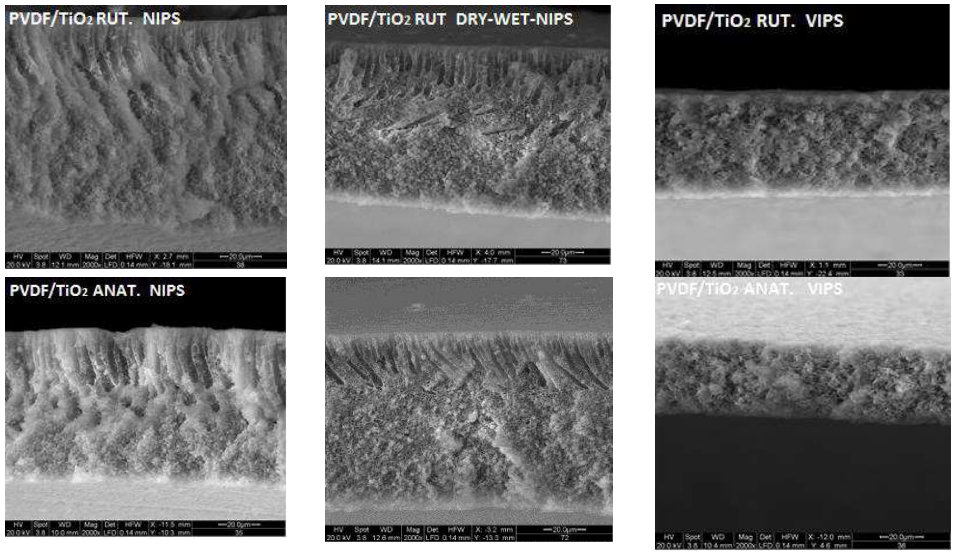

Fig. 6 PVDF based MMMs made with Titanium dioxide in both rutile and anatase form prepared by NIPS, Dry-Wet-Nips and VIPS techniques respectively, at 20 magnification.

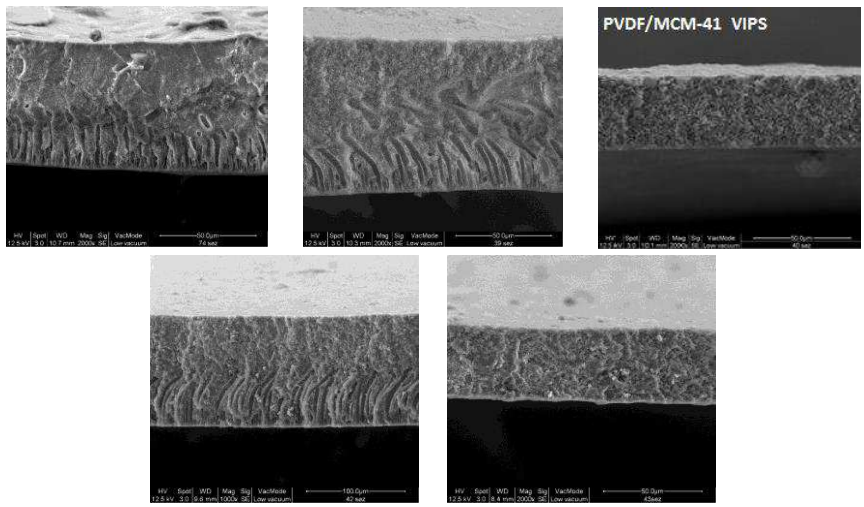

Figure 7. PVDF based MMMs made with MCM-41 prepared by NIPS, Dry-Wet-Nips and VIPS techniques in the first row, and with ZSM-5 made by NIPS and VIPS in the second row at 50 µm magnification.

Table 2. Membrane physical properties (thickness, total porosity, average pore diameter)

		Thickness (*μm*)	**Total porosity (ε%)**	**Average pore diameter (*μm*)**
NIPS	PVDF	0,047	69,53%	0,0275
	PVDF/TiO2 RUT.	0,083	68,97%	0,0326
	PVDF/TiO2 ANAT.	0,076	63,17%	0,0354
	PVDF/MCM-41	0,082	68,34%	0,0768
	PVDF/ZSM-5	0,110	68,97%	0,0459
DRY-WET-NIPS	PVDF	0,071	72,45%	0,0219
	PVDF/TiO2 RUT.	0,075	71,31%	0,0224
	PVDF/TiO2 ANAT.	0,069	70,15%	0,022
	PVDF/MCM-41	0,092	31,55%	0,0748
	PVDF/ZSM-5	0,068	59,43%	0,0413
VIPS	PVDF	0,056	53,50%	0,4624
	PVDF/TiO2 RUT.	0,054	58,94%	0,2916
	PVDF/TiO2 ANAT.	0,028	61,96%	0,6758
	PVDF/MCM-41	0,055	55,70%	0,3572
	PVDF/ZSM-5	0,032	54,46%	0,5912

Results demonstrated that the VIPS procedure leads to the formation of thinner membranes, ranging from 0,028 to 0,056 μm, regardless of the presence of the fillers. Instead, the NIPS and VIPS made MMMs appeared thicker, with an average thickness of about 0,08 μm. Only the blank type membrane produced by NIPS show a lower thickness value. Although the casting thickness was 250 μm for all membranes, the difference in the final thickness can be recognized looking at the precipitation mechanism. Again, a lower precipitation rate of VIPS method, making possible an uniform polymer concentration profile along the section, induced the formation of homogeneous and compact structure occupying a lower volume. Differently, the NIPS and Dry-Wet-NIPS method induced the formation of inhomogeneous and less compact structured showing many macrovoids which contributed to increase the volume and thus the thickness.

All membranes show an acceptable porosity. Results revealed that the preparation method influences the membrane porosity, as well. The VIPS produced membranes, although looking more porous by the SEM images, having a spong-like structure and bigger average pore diameters, shows the lower porosity in the range of 53-61%, while NIPS made membranes show membrane porosity in the range of 63-69%. The membranes produced by Dry-Wet-NIPS show the higher porosity in the range of 59-73%. This could be probabily due to the fact that NIPS and Dry-Wet-NIPS techniques resulted in asymmetric membranes rich in finger-like macrovoids, which increased the free volume of the membranes contributing to the calculation of higher total porosity percentage values. Thus, the study of the membrane morphology from the SEM images was conclusive in the reading of these results.

As concerning the pore size, VIPS made membranes showed bigger pore size than NIPS and Dry-Wet-NIPS MMMs (Table 2). Figure 8 shows of the pore size distributions of the pore dimensions for the TiO2/PVDF MMMs made by NIPS, Dry-Wet-NIPS and VIPS respectively as example. As shown, VIPS MMM presents bigger pore size (according with the average pore diameter measurements in Table 2) and a narrow distribution of pore dimensions confirming a structure with homogeneous features. While, NIPS and Dry-Wet-NIPs made MMMs show smaller pore size dimensions but a wider distribution including pore size of about 1.5 μm which indicate the macrovoids. Keeping in mind that the same trend is reflected by the MMMs made with other additive, we can conclude that the pore size and pore size distributions was strongly affected by the preparation method and not affected by the chemical composition.

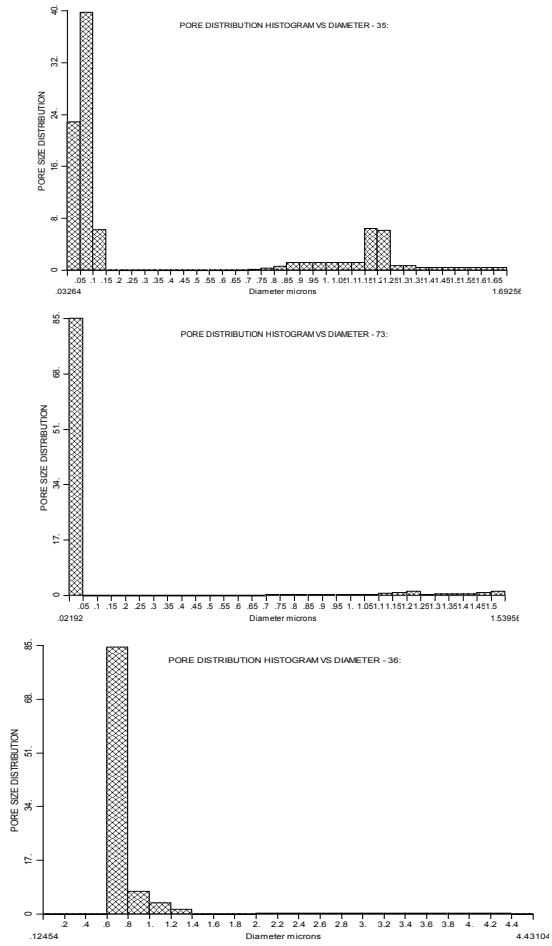

Figure 8. Pore size distribution of TiO2Rutilio/PVDF MMMs made by NIPS, Dry-Wet-NIPS and VIPS respectively.

PVDF crystallinity. PVDF is known to exhibit different crystalline forms; in this study, the crystallinity phases of PVDF in MMMs were determined using Fourier-transform infrared spectroscopy (FT-IR). Three are the main and most studied crystalline forms, known as α, β, γ.[8] PVDF α form shows a unit cell containing trans-Gauche sequences and it is the kinetically favourite crystalline form. The β form shows polymer chains containing only trans structure and it

is the thermodynamically favoured. Finally, the γ form shows sequences of three trans bonds separated by one Gauche bond.

Depending on the membrane preparation conditions PVDF can precipitate in one or more of the different crystalline phases. *Bormashenko et al*.[8] studied the effect of the precipitation temperature on the crystalline phase, demonstrating that α phase predominates at melt-crystallization below 160 °C, while the polar γ phase may be obtained from both solution and melt-crystallization at temperatures above 160 °C or by annealing α phase samples between 175 and 185 °C. A β phase is normally obtained at temperatures below 70 °C. The effects of some important membrane preparation conditions on the PVDF crystallization such as the composition of the casting solution, the precipitation temperature and the harshness of the precipitation bath were studied by *Buonomenna* et al.[9]

Also *Gregorio et al*.[10] studing PVDF crystallinity, reported the characteristic spectra of the PVDF crystalline forms indicating well-defined absorption bands for the α phase at 408, 532, 614, 764, 796, 855, and 976 cm^{-1}. The bands at 445, 510, and 840, 1275 cm-^{1} were considered characteristic of the β phase.[11] To distinguish unequivocally between β and γ phase in a sample, we should look for the existence or not of the 431, 776, 812, and 833 cm-1 bands, exclusively of the γ phase. Indeed, they noted that the peak, which is located close to 833 cm^{-1}, strengthened when the fraction of the γ phase in the sample increased, so this peak is obviously assigned to the γ phase. A peak at 1233 cm^{-1} was also attributed to the γ form by Boccaccio et al.[12] and Fontananova et al.[13] Our characterization provided partial FT-IR spectra ranging from 700 to 4000 cm^{-1} so that, apart the absorption bands common to all PVDF crystalline forms, only few peaks reported in literature were used as references. In the figure 9 the partial spectrum of NIPS made membrane without any additive is shown. Here, we can clearly observe peaks at about 839 and 1274 cm^{-1} uniquely attributable to the β form and a less pronounced peak at 1233 cm^{-1} indicating the γ form.

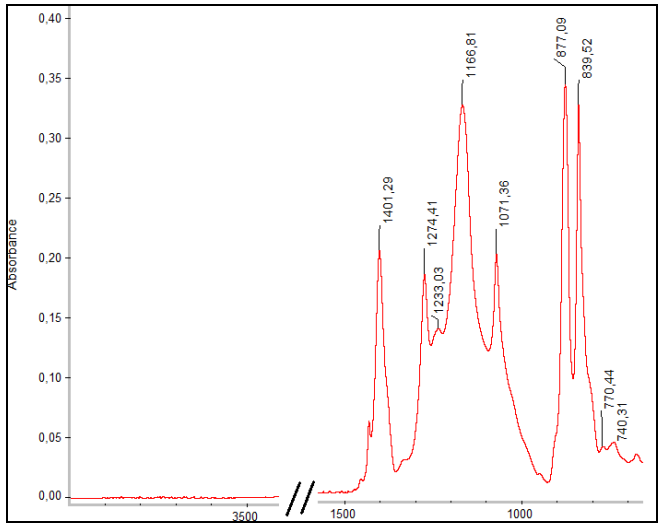

Figure 9. Partial spectra of blank PVDF membrane produced through NIPS procedure.

Although the other distinguish peak of γ form at 833 cm^{-1} is not clearly visible, this could be simply hidden by the small hill at approximately 820 cm^{-1} band. Thus, it was possible to conclude that in the membrane considered, both β and γ phases coexists.

The same peaks were detectable in the spectra of all membranes produced by NIPS and Dry-Wet-NIPS techniques, independently from the chemical compositions (in blank PVDF membranes and PVDF MMMs). No substantial differences were recognized between the upper and bottom membranes surfaces. Some spectra of upper and bottom MMMs surfaces were reported in figure 10 as example. The typical signals of the kinetically favoured α phase were not present in our manufactured membranes.

In all NIPS and Dry-Wet NIPS produced membranes the peak at 1274 cm^{-1} is higher than the peak at 1233 cm^{-1} meaning that the the β phase would be the dominant phase of the polymer.

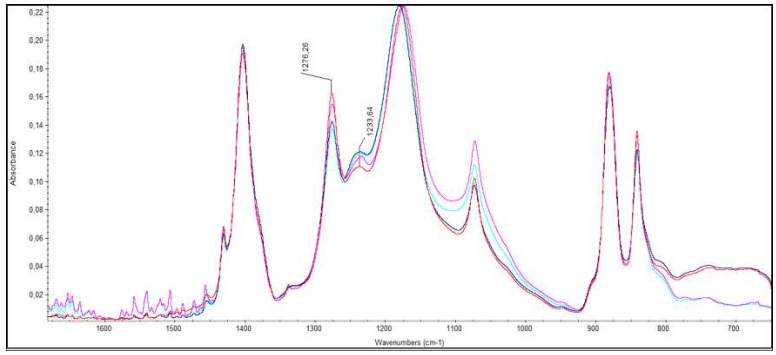

Figure 10. Recorded spactra of TiO_2Anatasio/PVDF MMM up (red spectrum)and down surface (blue spectrum) and MCM-41/PVDF MMM up (pink spectrum) and down surface (light blue).

Interestingly, different results were from MMMs produced by VIPS method. All VIPS made MMMs showed an inverted ratio of the peaks and 1233 cm^{-1} indicating β and γ form respectively: the peak at 1233 cm^{-1} became higher than peack 1274 cm^{-1}. Picture 11 shows the spectra of different VIPS made PVDF membranes (a blank type and with additives).

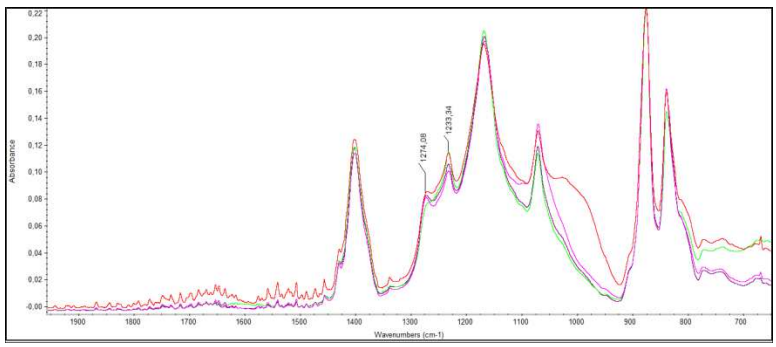

Figure 11. Recorded FTIR spectra on the upper surface of MMMs made by VIPS technique: blank PVDF membrane is the blue spectrum, TiO_2Anatasio/PVDF MMM is green, MCM-11/PVDF MMM is pink and ZSM-5/PVDF is showed in red.

This inversion in the relative heights of the peaks has been interpreted as an increasing of the portion of γ crystalline form in the polymer. This trend is constant for all VIPS made MMMs and no meaningful differences were detected between upper and bottom surfaces spectra. This demonstrated that the manufacturing conditions strongly affected the crystalline form of the PVDF and VIPS technique tended to increment the γ phase, independently from the initial blending composition. The reason of this behaviour was attributable to the kinetics factors during the phase inversion process including solvent-non solvent demixing (liquid-liquid demixing for NIPS, vapour-liquid demixing for VIPS) and PVDF crystallization (liquid-solid demixing). The two mechanisms are in balance so that the formed membranes often exhibit characteristics from both types of phase separations.

As reported in literature, the fast demixing process induces the formation of cellular pores whereas the crystallization tend to form interlinked crystalline particles. During the liquid-liquid demixing (in the NIPS) a high mass transfer occurs between the polymer and the precipitation bath increasing the polymer concentration to the interface region. This results in the dense skin layer, as showed in the picture 5, which creates a resistance to mass transfer in the sublayers. Thus, the liquid-solid demixing consisting in the crystallization of the polymer takes place later than the liquid-liquid demixing, leading to the formation of crystalline particles (as well as macrovoids). The crystalline particles in our membranes were β and γ phase with a greater portion of the thermodynamically stable β phase.

While, the exposure to air in the VIPS technique instead of immersion in the coagulation bath, caused the slow absorption of humidity by the non-solvent meaning that the vapour- liquid demixing process went hand in hand with the liquid-solid demixing (PVDF crystallization). In this case, although the total process was slowed down, the PVDF crystallization was probably instantaneous with respect the vapour-liquid demixing at microscopic level, encouraging the formation of the γ phase which is less thermodynamically stable crystalline phase than β. Our results were in good agreement with the studies of Buonamenna et al.[8] where the increasing of the casting solution

temperature and the air exposure time induced the formation of less stable crystalline phases.

Membrane wettability. The surface wettability is one of the significant properties of the membranes, which can affect the trans-membrane flux and the antifouling ability of the membranes. Wettability, here intended as the wetting degree of the membrane surface when interact with water, involved the contact angles measurements. Small contact angles correspond to high wettability, while large contact angles correspond to low wettability.
Here, the adding of inorganic fillers and the manufacturing techniques as well, were seen to influence the membrane surface wettability. In Figure 12, the static contact angle values, measured on the upper membrane surface, are shown.
For NIPS and Dry-Wet-NIPS produced membranes similarly, the embedding of fillers into the PVDF polymer matrix increases the upper surface wettability. The adding of TiO_2 in rutile form seems to slightly decreased the upper surface contact angles; indeed, for the NIPS produced membranes, the θ_{eq} varied from 110° for the PVDF to 91,1° for the PVDF/TiO_2 Rut., and for Dry-Wet-NIPS produced membranes, the θ_{eq} reached a value of 99,3°. While, a noticeable reduction of the static contact angle can be appreciated looking at the anatase embedded membranes. The adding of anatase nanoparticles reduced the upper suface θ_{eq} from 110° to 81,9° for the NIPS membranes and up to 83,8° for the Dry-Wet- produced membranes. Athough anatase and rutile are chemically identical, the hydrophilization effect of the PVDF membrane surface is more evident when the anatase is used, probably due to the better distribution of the nanoparticles.
For the membranes produced by VIPS, a different trend was seen. Primarily, all VIPS made membranes showed higher θ_{eq} values than the NIPS and Dry-Wet-NIPS made membranes. These values were related to structural surface features associated with the VIPS technique.

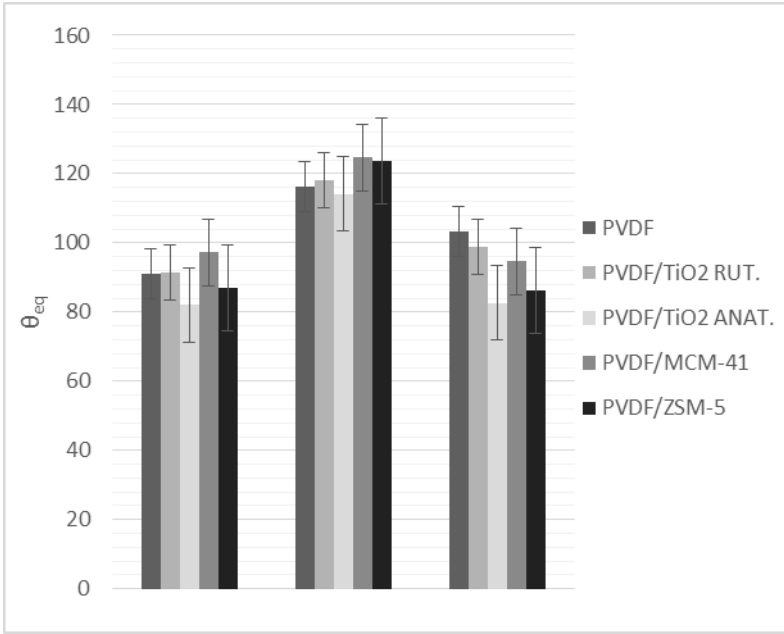

Figure 12. Top surface static contact angles of the produced membranes by NIPS, VIPS and DRY-Wet-NIPS techniques.

The increased contact angles can be specifically attributed to the increasing in surface roughness. The roughness parameters measured (Ra and Rq) are reported in Table 2. Unlike ideal surfaces, real surfaces do not have perfect smoothness, rigidity, or chemical homogeneity. A well-known departure from ideality is when the surface of interest has a rough texture. In the hydrophilic rough texture of a surface the liquid can fills in the roughness grooves following the Wenzel model, while, on hydrophobic rough texture surface a nonwetting liquid may not penetrate into surface cavities resulting in the formation of air pockets, according to the Cassie–Baxter model. Here, the rough hydrophobic PVDF surface, followed the second model, showing an increasing of the water contact angles with increasing of surface roughness.
Accordingly, the VIPS made MMMs having higher contact angles values than NIPS and Dry-wet membranes, showed more rough surfaces. Thus, it was

possible concluding that the manufacturing procedures played a role in influencing the surface wettability.

Secondly, only the PVDF/TiO2 Anat. MMM showed lower θ_{eq} than PVDF blank membrane, while the other MMMs showed higher $\theta_{eq.}$ It follows that the final θ_{eq} value is probably the result of two opposing factors, the tendency of the hydrophilic fillers to enhance the wettability, on one side, and the the tendency of surface roughness to reduce the wettability, on the other side.

While, the adding of MCM-41 and ZSM-5 significantly increases the upper surfaces contact angles, up to a value of 129,7° for PVDF/MCM-41 membrane and to 133,2° for PVDF/ZSM-5 membrane. This behavior can be related to the different roughness of the membranes as shown in Table 2.

Table 2. Roughness of the prepared membranes for UP and down surfaces

		UP surface		**DOWN surface**	
		Ra	**Rq**	**Ra**	**Rq**
NIPS	PVDF	92,67	75,95	58,57	48,39
	PVDF/TiO2 RUT.	152,91	117,03	23,11	18,50
	PVDF/TiO2 ANAT.	108,23	85,42	60,38	48,48
	PVDF/MCM-41	111,20	91,15	203,83	166,19
	PVDF/ZSM-5	183,49	140,44	159,48	129,47
DRY-WET-NIPS	PVDF	169,85	138,49	46,52	37,85
	PVDF/TiO2 RUT.	132,90	107,89	28,12	21,84
	PVDF/TiO2 ANAT.	103,29	86,04	37,96	31,35
	PVDF/MCM-41	168,63	134,96	27,73	22,20
	PVDF/ZSM-5	74,45	58,43	72,46	58,18
VIPS	PVDF	266,55	204,50	173,54	143,32
	PVDF/TiO2 RUT.	140,52	112,47	63,74	51,58
	PVDF/TiO2 ANAT.	62,04	48,69	26,03	21,33
	PVDF/MCM-41	129,88	102,50	123,94	103,25
	PVDF/ZSM-5	319,86	245,40	70,28	58,07

3.4 Conclusions

Different kind of PVDF membranes were successfully produced by varying the blend compositions and the manufacturing technique. Inorganic materials used in the first chapter for the basic study on heterogeneous nucleation were embedded into the PVDF polymer in order to create membranes heterogeneous from a chemical point of view and eventually testing the membranes in crystallization test to investigate the effect of the materials on nucleation when they were free in solution and when they were included in a macroscopic structure as a membrane. The subsequent test will be presented in the last chapter and will give an overview on membrane composition and membrane performance in crystallization. Considering the effect of the inorganic fillers to the mixed matrix membranes, we concluded that the presence of the titanium dioxide slightly affected the membrane wettability even a deep influence on this characteristic derived from the roughness. The roughness was strongly affected by the manufacturing method.

The most interesting findings of this study have been about the structural features of the membranes when changing a different manufacturing method. Although three different phase inversion methods were used, two of these, NIPS and Dry-Wet-NIPS did not produced substantial different structures. This was related to the fact that in the Dry-Wet-NIPS techniques the polymer casting solution was exposed to the air only a minute before immersion in the coagulation bath and this time was not sufficient to induce visible effects on the morphology of the membranes. While when leaving the membranes to evaporate at controlled moisture degree, the membrane morphology resulted strongly influenced. Membranes with homogeneous and compact profile along the section, with a spong-like morphology, thinner and with bigger pore size were produced through VIPS technique. These membrane strongly differ from the MMMs produced by NIPS and Dry-Wet-NIPS technique which present a dense skin layer followed by a more porous sublayer showing finger-like

macrovoids. These structured were featured by a wide distribution of pore size and a different morphology when considering the upper and bottom surface. Moreover, it was worth to notice the effect of the technique on the crystallinity of PVDF polymer, depending on the precipitation kinetics during the phase inversion. Finally, the subsequent testing of these MMMs in membrane crystallization experiments will help in the determination of the membranes performance in enhancing the heterogeneous nucleation mechanism.

3.5 Reference

1. K. L. W. T. Dongliang Wang, Porous PVDF asymmetric hollow fiber membranes prepared with the use of small molecular additives, Volume 178, Issues 1–2, 15, Pages 13–23, 2000.

2. A. V. M. Margulies, Porous structure of membranes of an acrylonitrile copolymer. Porosity, H-NMR permeability, Eur. Phys. J. E, 2, 117-123, 2000.

3. C. Panu Sukitpaneenit, Molecular elucidation of morphology and mechanical properties of PVDF hollow fiber membranes from aspects of phase inversion, crystallization and rheology, Journal of Membrane Science 340, 192–205, 2009.

4. X. Zhang, «Preparation, performance and adsorpion activity of TiO2 nanoparticles entrapped PVDF Hybryd membranes,» Applied Surface Science, vol. 263, pp. 660- 665, 2012.

5. M. E. Mackay, A. Tuteja, P. M. Duxbury, C. J. Hawker, B. V. Horn, Z. Guan, G. Chen, and R. S. Krishnan, "General strategies for nanoparticle dispersion," Science vol. 311, no. 56-78, pp. 1740-1743, March 2006.

6. Y. Teow, Preparation and characterization of PVDF/TiO2 mixed matrix membrane via in situ colloidal precipitation method, Desalination 295, 61-69, 2012.

7. K. Michael E. Mackay, «General Strategies for Nanoparticle Dispersion,» Science, vol. 311, n. 5768, pp. 1740-1743 , 2006.

8. Bormashenko Ye., Pogreb R., Stanevsky O, Bormashenko Ed., Vibrational spectrum of PVDF and its interpretation, Polymer Testing, 23 (2004) 791-796.

9. Gregorio R. , Ueno E. M.m, Effect of crystalline phase, orientation and temperature on the dielectric properties of poly (vinylidene fluoride) (PVDF),. 34, Issue 18, pp 4489-4500

10. Gregorio R Jr, Cestari M, Chaves N, Nociti PS, Mendonca JA and Lucas AA, The Polymer Materials Encyclopedia, CRC, Boca Raton (1996)

11. Venault A., Chang Y., Wu Y., Wang D.M., Influence of solvent composition and non-solvent activity on the crystalline morphology of PVDF membranes prepared by VIPS process and on their arising mechanical properties, Journal of Materials Science, 2004.

12. Fontananova E., Jansen J.C., Cristiano A., Curcio E., Drioli E., Effect of additives in the casting solution on the formation of PVDF membranes, Desalination 2006; 192:190-197.

Chapter 4

Development of UV-photografted membranes designed for membrane crystallization process

4.1 Introdution

This work aimed the manufacturing of new membranes tailored to MCr having hydrophobic matrices, which guarantee the integrity of the distillation mechanism, and surfaces opportunely functionalized, capable to affect the crystal formation.

We proceeded thorough the chemical modification of hydrophobic polypropylene membranes surface by means of UV-photografting; the hydrophilic monomer acrylic acid (AA) was grafted at different monomer concentration by using benzophenone as photoinitiator. This strategy would allow the surface properties to be tailored in order to meet a specific requirement, while retaining beneficial properties deriving by the hydrophobic microporous matrix.

Thus, the whole study was performed in two stages (as described in figure 1) : the first focused on the accomplishment of chemically modified membranes; the second focused on the testing of the modified membranes in crystallization (discussed in the following chapter 5). The modification of commercial polypropylene membrane surfaces was obtained by means of grafting of specific functional groups; this allowed the surface properties to be tailored, while retaining beneficial properties deriving by the hydrophobic microporous matrix.

Among the used polymer modification processes, grafting polymerization is one of the most promising.[5] Grafting, refers to the addition of special chemical functionalities onto a surface by covalent bond formation, differently from coating whereby oligomer mixtures adheres to the substrate by physical forces. The covalent attachment of monomer chains onto the polymer surface is crucial for membranes designed for MCr process to assures long-term chemical stability of introduced chains; indeed, an unintended release of the material during the process would be to irreversibly alter the crystallizing solution, turning off the crystallization process.

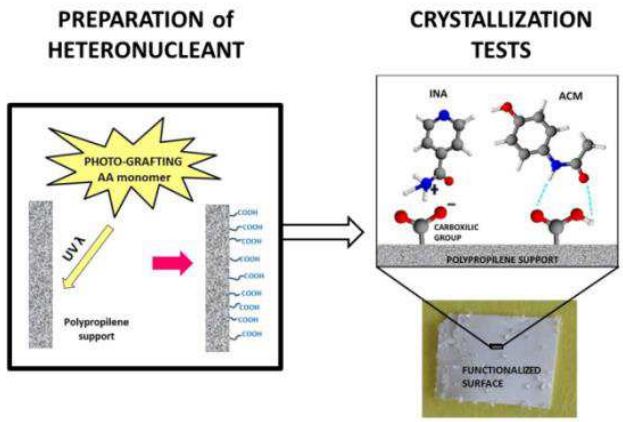

Figure 1. Research strategy: the first step regards the functionalization of polypropylene membrane surfaces with acrylic acid through UV-photografting; the second step regards the tests of the modified membrane surfaces in crystallization. As shown, the carboxylic groups on PP surface could induce the orientation of the crystallizing molecules thorough ionic interactions or H-bonding.

Surface grafting techniques including photo-initiated grafting, living radical grafting, ceric ion induced grafting, layer-by-layer ionic grafting and plasma polymerization have proven to be effective to graft poly-functional monomers or polymers onto different kind of surfaces. Among the methods to modify polymer surfaces, radical photo-grafting polymerisation appears as an attractive method to impart a variety of functional groups to a polymer. The advantages of photografting over other available methods are: low cost of operations, mild reaction conditions, permanent alteration of the membrane surface with control of the chemistry .

Low energy radiation, such as UV light, is frequently used to initiate surface modification.[6] UV photografting technology has been used for producing membranes for different applications such as the reduction of membrane fouling[7] and the removal of dye from wastewater.[8]

The surface modification of polypropylene was done by UV photografting of the hydrophilic monomer Acrylic acid (AA). AA was selected as the monomer to be grafted because, being a hydrophilic monomer, gave the possibility to change the surface features of the membranes; moreover, the chemical and physico-chemical properties of this monomer were readily available in literature.[9]

The grafting process by a photochemical technique can proceed with or without a sensitizer.[5] When a macromolecule bearing a chromophore absorbs light, it goes to an excited state, which can dissociate into reactive free-radicals, whence the grafting process is initiated This mechanism without sensitizer involves the generation of free radicals on the backbone, which react with the monomer free radical to form the grafted co-polymer. If the polymer does not contains a chromophore or is stable (such as in the case of polyolefines), the absorption of light does not lead to the formation of free-radical sites through bond rupture. This process can be promoted by the addition of photosensitizers. In the mechanism 'with sensitizer', the sensitizer forms free radicals, which can undergo diffusion so that they abstract hydrogen atoms from the base polymer, producing the radical sites required for grafting. Aromatic ketones are known to be good photosentitizer.

Despite the difficulty of grafting mostly inert polyolefin polymers such as PP, few but relevant examples have been reported in the literature by Ulbrich et al.[10,11] and Ma et al.[12]

Many studies suggested the use of benzophenone (BP) as good photoinitiator for AA.[13]

When absorbing UV light at 340±360 nm, benzophenone is excited to singlet state (S°) and it transforms to triplet state (T°) by intersystem crossing and abstracting an hydrogen from the substrate.

Therefore, AA photografting was performed on PP flat sheet membranes, at first, in order to test different conditions and then, on PP hollow fibers to be employed in continuous membrane crystallization process.

This strategy allowed the modification of the membrane surface without affecting the core of the membrane which, remaining hydrophobic, ensures the correct course of membrane crystallization process.

An important aspect to be consider is that the carboxylic functional groups introduced on the membrane surface could induce specific chemical interaction with the solute molecules during the crystallization process, leading to molecular orientation and hence facilitate the nucleation of specific polymorphs or crystal morphologies.

4.2 Materials and methods

Hydrophobic, polypropylene hollow fibers membranes (Accurel PP, nominal pore diameter 0.22 µm; thickness 530 µm (from Membrana GmbH, Germany) were used. AA anhydrous, contains 180-200 ppm MEHQ as inhibitor, 99% and Benzophenone ReagentPlus®, 99% were from Fisher and used as received. Methanol was from Sigma-Aldrich. Pure water was used for all experiments. UV graft polymerization was performed with two different procedures shown in figure 2 for both flat sheet and hollow fiber membranes:

- one step method (I), consisting of one cycle of UV exposure of PP membrane surface, after immersion in monomer/initiator mixture;
- two steps method (II), consisting of a first UV irradiation cycle after immersion on photoinitiator solution, followed by a second irradiation after immersion in a monomer solution.

For the flat sheet membranes grafting, a UV lamp system (a polychromatic lamp, UV Hanau Heraeus TQ 150 (Hg medium pressure) equipped with a glass filter ($\lambda > 300$) providing an intensity energy UVA and UVB of 50 mW/cm^2 was used. In the procedure I, the pre-weighed membranes samples of 5x10 cm^2 were soaked in 10 mL of BP/AA in methanol solution at different AA percentage, for 5 minutes and immediately incubated under UV lamp for 20 minutes.

In method II the pre-weighed membrane samples were soaked in a methanol solution saturated in benzophenone for 5 minutes and subject to UV irradiation for 20 minutes; after, the samples were immersed into 20 mL of AA solution in methanol at different monomer concentration and subject to a second cycle of UV- irradiation for further 20 minutes.

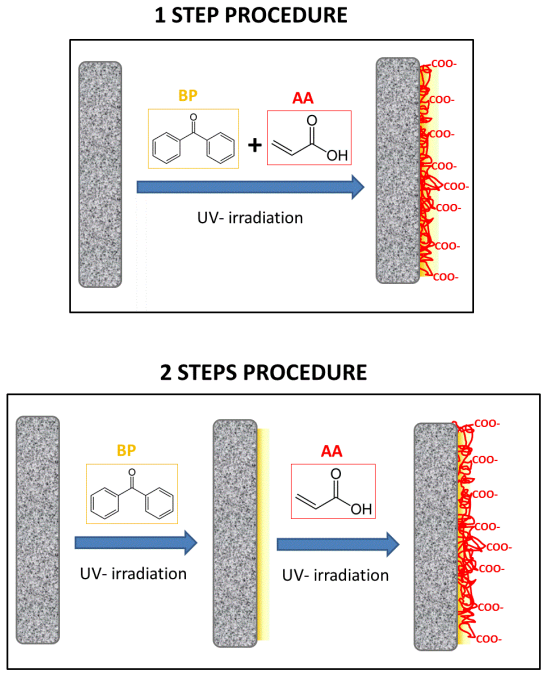

Figure 2. Schematic representation of the UV photografted procedure used: method I provided one cycle of UV exposure of PP membrane surface, after immersion in monomer/initiator mixture; method II provided a first UV irradiation cycle after immersion in the photoinitiator solution, followed by a second irradiation after immersion in a monomer solution.

While, for the hollow fiber photografting a continuous process was used. A schematic representation of process is shown in figure 3. It consists of two successive steps: after dipping the fibers in a bath containing the monomer/photoinitiator solutions (dip-coating step) the hollow fiber was irradiated by the UV lamps (irradiation step). For the method I, the fibers were dipped in AA/BP in methanol solution and then, were passed through the cylindrical UV-lamp of 50 cm, equipped with a filter quartz, with a speed of 2 mm/sec. With the method II, the fibers were first dipped in a saturated in BP methanol solution for 5 minutes and subjected to a first cycle of UV-irradiation at 2 mm/sec; then, the same fibers were dipped in the monomer bath (AA in

methanol solutions at different AA percentage) and again passed through the cylindrical UV-lamp at the same velocity. The energy irradiation of the UV-lamp for the fibers grating was 1400 mW/cm^2.

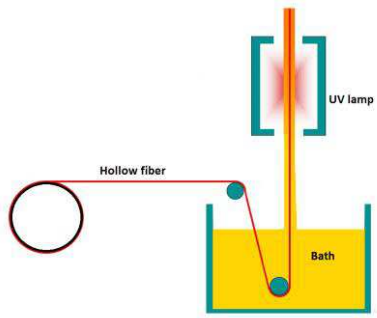

Figure 3. Schematic rapresentation of the UV-photografting continuous process.

All conditions tested (monomer and photoinitiator concentrations, photografting procedure) for both flat sheet and hollow fiber membranes, are listed in Table 1.

All the sample prepared with both procedures were washed with 100 mL of pure water under stirring for 30 minutes and then left standing in refreshed water overnight. Then, the membranes were quickly wiped with filter paper and dried at room temperature for 24 hours.

Membrane were characterized by infrared analysis, scanning electron microscope and contact angle measurements. Tests to visibly verify the presence of the PAA grafted on the membrane surface were done with toluidine blue water solution 5*10^{-4} M; membrane samples were dipped in toluidine blue solution for 1 hour and then dried.

Table 1. Experimental conditions of AA grafting on PP flat shet membranes (PP) and hollow fibers(HF)

Membrane	AA%	BP%	Typology	Method
PP0	-	-	Flat sheet	-
PP1	10	1,5	Flat sheet	I
PP2	20	1,5	Flat sheet	I
PP3	30	1,5	Flat sheet	I
PP4	40	1,5	Flat sheet	I
PP5	50	1,5	Flat sheet	I
PP6	60	1,5	Flat sheet	I
PP7	20	1,5	Flat sheet	II
PP8	40	1,5	Flat sheet	II
PP9	60	1,5	Flat sheet	II
PP10	20	1,5	Flat sheet	II
PP11	40	1,5	Flat sheet	II
PP12	80	Satured	Flat sheet	II
PP13	20	Satured	Flat sheet	II
PP14	40	Satured	Flat sheet	II
PP15	60	Satured	Flat sheet	II
HF0	-	-	Hollow fiber	-
HF1	60	1,5	Hollow fiber	I
HF2	20	Satured	Hollow fiber	II
HF3	40	Satured	Hollow fiber	II
HF4	60	Satured	Hollow fiber	II
HF5	80	Satured	Hollow fiber	II

The degree of grafting (DG%) was determined gravimetrically from the weight of each sample before and after functionalization. The degree of grafting (DG) was calculated according to:

$$DG\% = \frac{(m_{gr} - m_0)}{m_0} * 100$$

Where m_0 is initial sample weight and m_{gr} is the weight after modification.

4.3 Results and discussions

After UV-graft polymerization a thin grafting layer of polyacrylic acid (PAA) was generated on the PP membrane surface. The mechanism provides that the radiation from the UV lamps create radicals on the surface of the polymer and thus starts a radical polymerization reaction. The radiation heats the fiber and causes a progressive evaporation of the liquid film leaving a dried layer of PPA. The PPA layer can be confirmed by FT-IR-ATR spectroscopy analysis. As can be seen from Figure 4, there is no absorption peak around 1720 cm^{-1} of the native PP membrane, while a strong vibration peak can be seen at 1720 cm^{-1} for the spectrum of the grafted membrane, which can be attributed to the C=O group stretching (red curve).

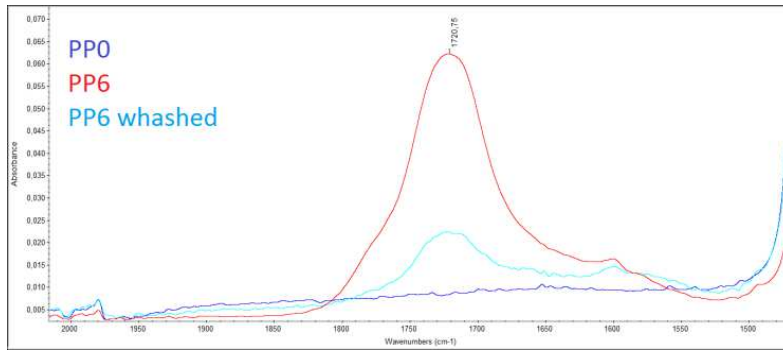

Figure 4. FT-IR-ATR of native PP (blue curve) and PP grafted with 60% AA flat sheet membranes immediately irradiation(red) and after washed (light blue).

The same characterization were done after having washed the grafted membrane in pure water all night to remove the excess of unreacted AA and dissolve the film of homopolymer PPA and dried the membrane. After the treatment, the adsorption peak at around 1720 cm^{-1}, is strongly decreased in

intensity but it is still present, proving that the AA is covalently bonded on the membrane surface (blue curve).

For the hollow fiber the same can be seen (figure 5), but differently from the flat sheet membranes, after washing the fiber the peak at 1720 cm^{-1} is significantly present. This means that the PPA layer on the fiber is securely bonded whit the polypropylene surface.

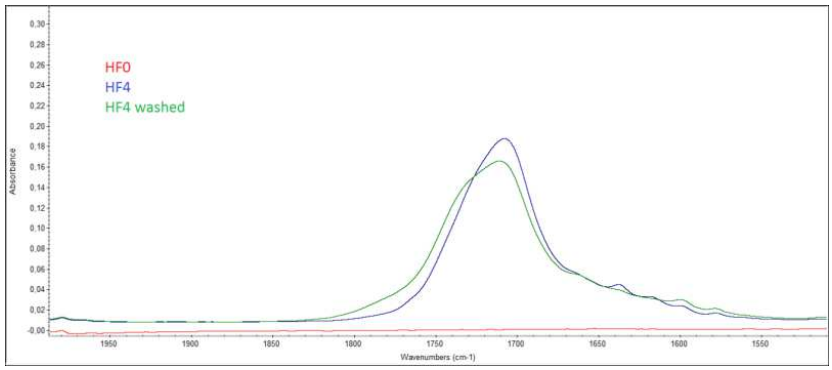

Figure 5. FT-IR-ATR of PP grafted with AA membranes and after washed

The fact that the FTIR spectra of the fibers indicate a higher amount of PAA linked on the surface than the flat sheet membranes is probably due to the difference in energy power of the UV source. Indeed, for the hollow fiber the UV-source the energy power was about 1000 times higher.

Simple tests to optically appreciate the grafting on the membrane surface were done with toluidine blue O (TBO) . TBO being a cationic blue dye derivative of phenothiazine, complex the negative charge of the membrane surface, if the negative charges are present. The flat sheet membranes showed a stronger blue coloration immediately at the time of immersion and then a slow discoloration; this would indicate the dissolution of the PAA homopolymer layer in water. In the case of the hollow fibers the strong coloration is still present after 1 hours of immersion in toluidine solution, indicating the covalent bonding of the PAA layer to the polypropylene surface.

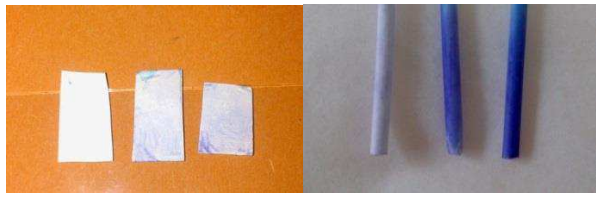

Figure 6. Membranes treated with toluidine blue: PP0, PP8 and PP15 to the left, and HF0, HF1, HF4 to the right.

The SEM characterization allowed the study the membrane morphology of the grafted and native membranes. For the flat sheet membranes, no relevant visible effects are for the grafted membranes. Figure 7 shows the surfaces and the sections of the native and grafted flat sheet membranes with method I and II respectively. No sign are present on the surface of the membranes treated with method I and the section thickness is not affected. The surface of the membrane treated with method II seems slightly eroded with respect the native polypropylene; also the thickness of this membrane is smaller. Nevertheless, no layers of heteropolymer are shown on the surfaces.

Differently from the flat sheet membranes, on the the hollow fiber surface a visible layer of polyacrylic acid is present, even after having left the fiber in pure water for one night. Figure 8 shows the sections and the surfaces of the native and grafted fibers with method I and II. From the sections was possible to observe the difference between the native PP hollow fiber and the grafted one. In the second section (corresponding to HF1, namely 60% AA grafted fiber with method I) the PPA layer is clearly shown and it appears darker than the polypropylene matrix. Also in the third section (HF4, 60% AA grafted fiber with method II) the PAA layer is shown. The thickness of the grafted layer was about 50 µm average in both sections. From the section a reduction of porosity it is noted; although porosity measurements were not yet done, these would point out the decreasing of porosity due to the penetration of the AA monomer within the matrix pores during the dipping in the monomer bath. Moreover, the surface of the native polypropylene fiber appears to be smoother than the

PPA layer. Also in this case topographic and roughness measurements would be a further interesting investigations.

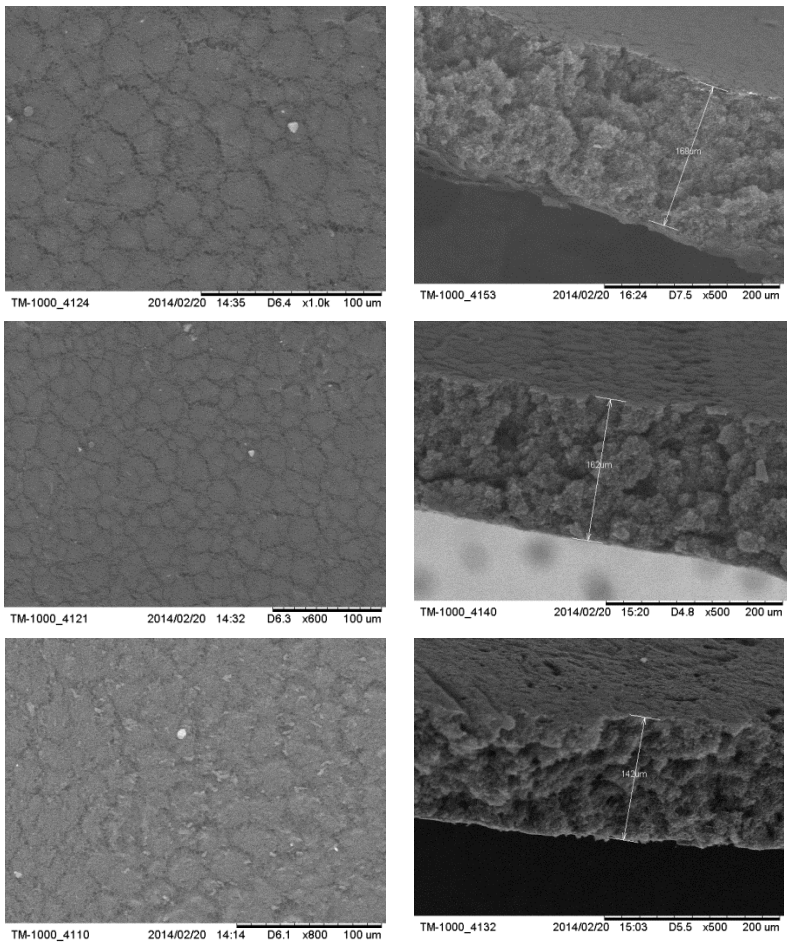

Figure 7. Surfaces (left) and sections of PPO, PP8 and PP15 flat sheet membranes.

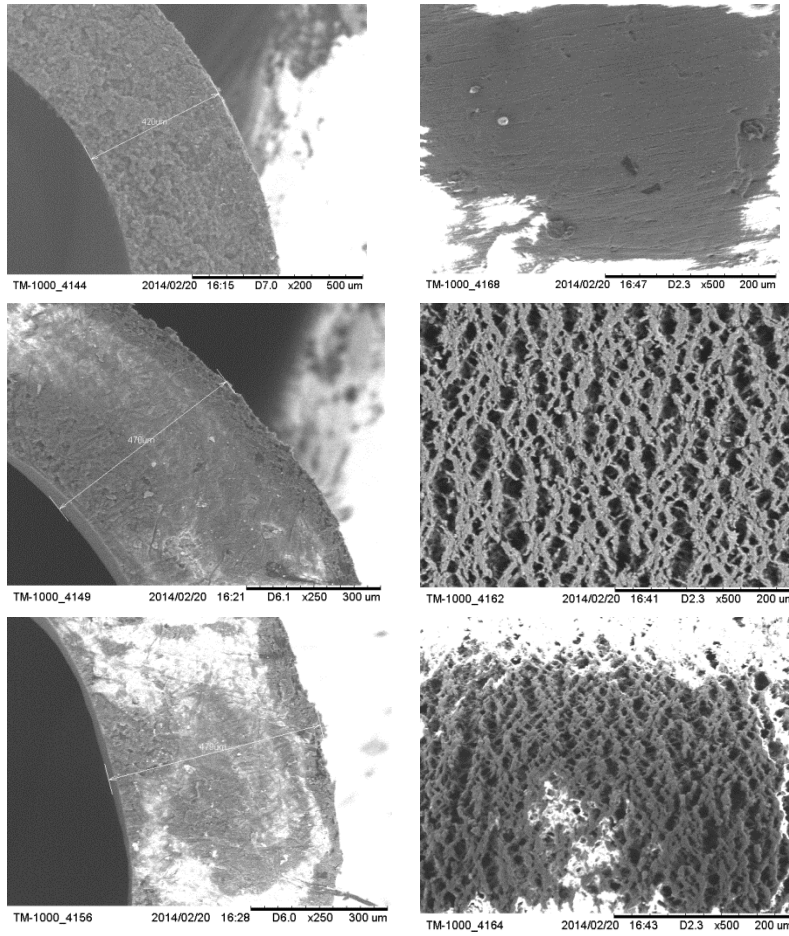

Figure 8. Sections (left) and surfaces (right) of HF0, HF1 and HF4

Figure 9 shows the effect of monomer concentration on the DG% for the flat sheet membranes when using the two different grafting procedures. An increasing of DG as a function of AA concentration was observed. The method II of grafting made it possible to increase the degree of grafting on flat membranes, although this still does not exceed the 2,5%.

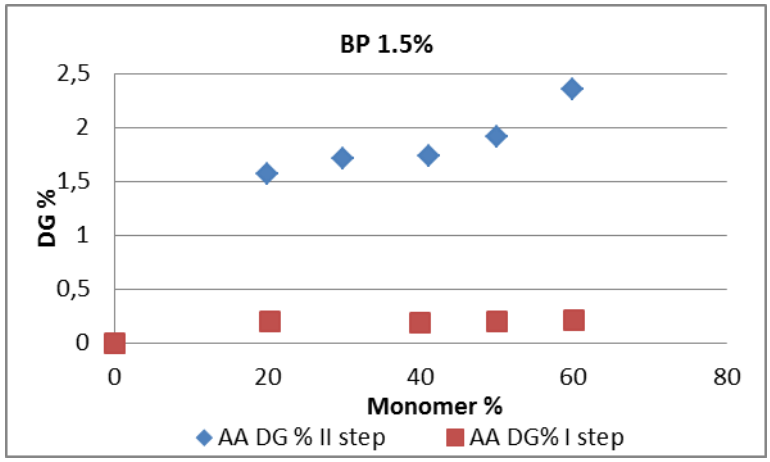

Figure 9. DG as a function of monomer concentration when using 1,5% photoinitiator, for the membranes prepared with method I and II respectively.

The grafting technique II, was developed by Ma et al. [16] in order to significantly reduce the homopolymer and crosslinked polymer and induce the preferential formation of linear polymer chains. The radical mechanism is different than that in mechanism I.

Here, in the first step, benzophenone abstracts an hydrogen from the substrate to generate surface radicals which combine to form surface photoinitiators in the absence of monomer solutions. In the subsequent step, monomer solutions without any additional benzophenone are contacted with the active substrate, and the surface initiators initiate the graft polymerization when exposed to UV irradiation. Both homopolymer and crosslinked polymer are reduced in the novel grafting method, since benzophenone is not present at the same time with monomer or grafted polymer.

The reason of the low GD% could reasonably due to two reasons: the low power of the UV-equipment for the flat sheet modification or the low % of photoinitiator. Thus, figure 10 shows the GD% as a function of monomer concentration when using a saturated solution of benzophenone.

It is noted that the GD% increased up to 43% but it does not show an increasing trend with increasing monomer concentration. This means that the

high amount of benzophenone used introduced an high error in weighing. Thus, the gravimetric method does not seem a reliable procedure for the DG measurement. Titration procedure could be an appropriate way for evaluating the amount of AA molecules on the membrane surfaces.

The membrane surface wettability was evaluated by measuring the contact angles. The presence of PAA on the membrane increase the surface hydrophilicity, indeed, for all grafted membranes the contact angle value was lower than for the native polypropylene.

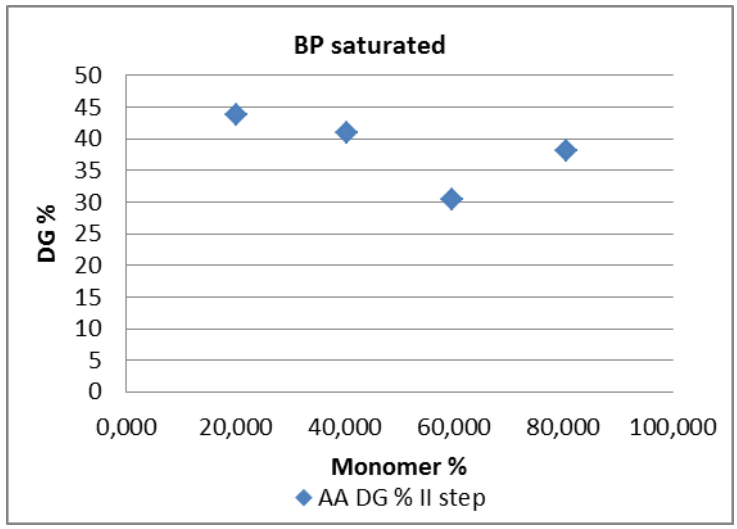

Figure 10. DG as a function of monomer concentration when using saturated BP methanol solution, for the membranes prepared with method II.

In figure 11 the contact angles values are shown for the native and grafted flat sheet membranes with method I, at different monomer concentration, measured on the up and down surface. For the up surface, the water contact angle decreased from ~140° for the native polypropylene to 106° for the grafted membranes with 40% of AA. For the bottom membrane surface, the contact angle varied from 143° to about 123°. Although the bottom surface was not irradiated, and the membranes were washed after irradiation, the decreasing of contact angles indicated the presence of AA, probably absorbed

through the polymer matrix and deposited; indeed the contact angle decreases from 143° to about 124. Thus, it is possible to deduce that the variation of contact angle, although is an indication of the presence of PAA, it does not prove the covalent bonding of PPA with PP matrix.

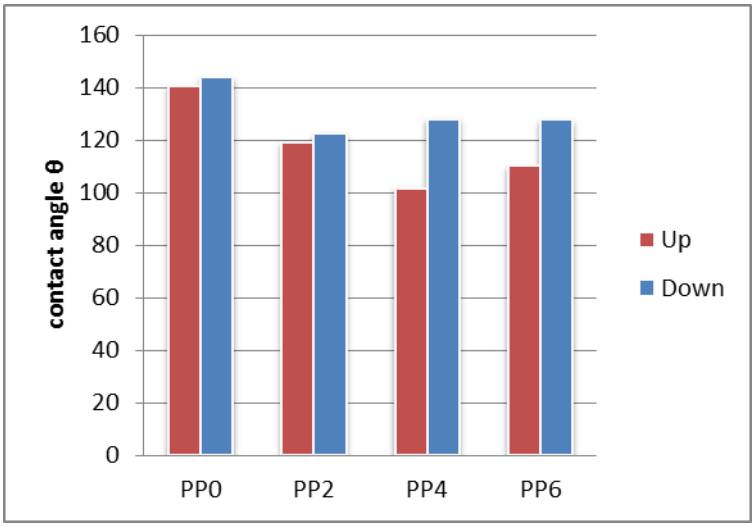

Figure 11. Contact angles of native and grafted (method I) polypropylene flat sheet membranes at different monomer concentration when using 1,5% BP.

When considering the membranes grafted with method II, the contact angles decreases from 140° for the native polypropyleneup to 107° for the membrane. The contact angle seems to decrease when increasing the DG% calculated by mass difference.

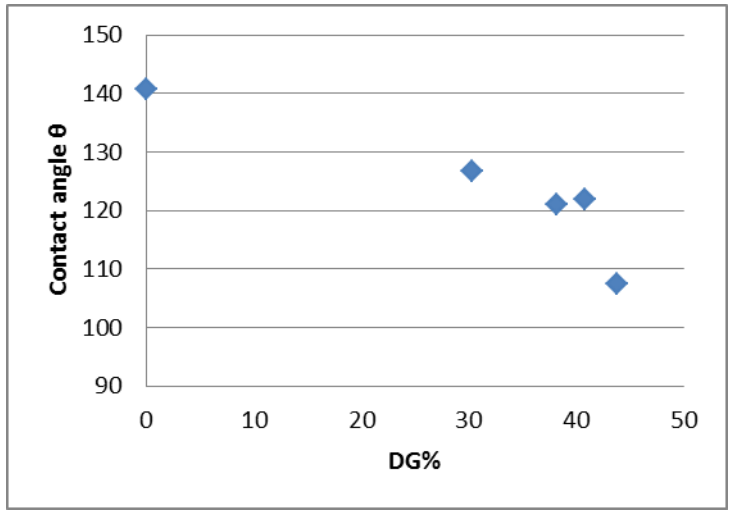

Figure 12. Contact angles of native and grafted (method II) polypropylene flat sheet membranes as function of DG% (calculated by mass difference).

Since only the grafted area of the membranes is necessary for conducting the crystallization experiments, an evaluation about the distribution of the PPA along the flat membrane surface was done. The distribution of PAA along the flat membrane surface was evaluated by measuring the variation in the absorbance intensity of the FT-IR peak at 1720 cm^{-1} (corresponding to the carboxilic group of AA), at different distances by the UV light source. Also the variation of contact angles along the membrane surfaces was measured (figure 13). The measurements were done on the membrane PP15 corresponding to the flat sheet membrane grafted with 60% AA monomer and saturated BP solution thorough method II. As shown in the figure, the absorbance intensity decrease linearly with the distance from the light source while the contact angle value increases meaning that the distribution of the PPA is not uniform. Thus, only the membrane area in the radius of 2,5 cm from the UV-light source was used for crystallization experiments.

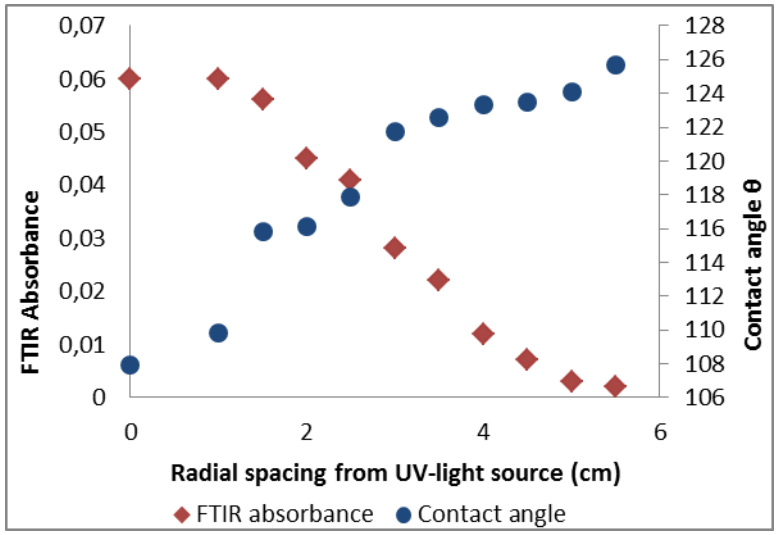

Figure 13. Variation of the absorbance intensity in the FT-IR peak at 1720 cm^{-1} and contact angle values along the membrane surfaces at different radial spacing from UV-light source for the flat sheet membrane PP15.

4.4 Conclusions

The FT-IR analysis revealed the UV-photografting procedures investigated in this study was effective in modifying the polypropylene membranes surface. Indeed, in all spectra of the grafted membranes, a vibration peak attributed to the C=O group stretching, can be seen, while no absorption peaks of the acidic gropup is detectable for the native PP membrane. Also after washing the grafted membranes in pure water for a night, the adsorption peak indicating the acidic groups on the membrane surfaces, is still present, proving that the AA is covalently bonded on the membrane surface. Moreover, a linear increasing of grafting degree (DG%) as a function of AA concentration was observed for the flat sheet when using 1,5% of benzophenone. Between the two grafting procedures tested (one step method and two step method), the two step method resulted more effective, indicating higher grafting degree level when increasing the monomer concentration. A significant improvement of the grafting degree was gained when dipping the PP membrane into an alcoholic solution saturated in benzophenone, revealing that the low concentration of photoinitiator can act as limiting factor of the grafting degree, even if can introduce a calculation error of the DG% when using the gravimetric method.

As concern the hollow fiber grafting, the SEM pictures revealed the formation of a real poly-acrylic acid coating on the PP membrane surface. The pictures clearly showed the difference between the native PP hollow fiber and the grafted one. The PPA layer obtained was about 50 µm. From the section also a reduction of porosity was noted.

Finally we can conclude that the UV-photographing procedures here investigated, proved to be a useful method for producing double layer flat sheet membranes with a hydrophobic surface in polypropylene and a hydrophilic one with acrylic acid substituents. The same procedures made it possible to create hollow fibers with a hydrophobic core in PP and grafted outer surface, these fibers showing a double hydropobic/hydrophilic nature,

have an high potential of application and seems to be particularly suited for membrane crystallization process. Indeed, both flat sheet and hollow fibers grafted membranes will be used for conducting crystallization test, in the following study.

4.5 References

1. Grafting: a versatile means to modify polymers. Techniques, factors, and applications. A. Bhattacharya, B.N.Misra. 2004, Prog. Polym. Sci, Elsevier, pp. 767-814.

2. Modification of hollow fibers by UV sirface grafting. Goma-Bilongo T., Remigy J.C., Clifton M.J. 304-308, s.l. : J. Mem. Sci., 2010, Vol. 364.

3. Photochemical modification of poly(ether sulfone) and sulfonated poly(sulfone) nanofiltration membranes for control of fouling by natural organic matter. J.E. Kilduff, S. Mattaraj, J.P. Pieracci, G. Belfort. 308-317, s.l. : J. Mem. Sci. Elsevier, 2000, Vol. 278.

4. Treatment of textile dye effluent using a new photografted nanofiltration membranes. A. Akbari, S. Desclaux, J. C. Remigy, P. Aptel,. 101-107, s.l. : Desalination, 2002, Vol. 149.

5. Braudrup J., Immergent E. H, Grulke E. A.,. Polymer handbook 4th ed.,. New York : Wiley-Interscience, 1998

6. Porous polypropylene membranes with different carboxyl polymer brush layers for reversible protein via surface-initiated graft copolymerization. Ulbricht M., Yang H.,. 17, 2005, Vol. Chem. Mater. 2622-2631.

7. Photograft-polymer modified microporous membranes with environment-sensitive permeabilities. M., Ulbricht. 31, 1996, Vol. React. Func. Polym. 165-177.

8. Membrane flouling reduction by backpulsing and surface modification. H. Ma, C. N. Bowman, R. H. Davis. 191- 200, s.l. : J. Mem. Sci., 2000, Vol. 173.

9. Surface functionalization of thermoplastic polymers for the fabrication of microfluidic devices by photoinitiated grafting. Rohr T., Ogletree D. F., Svec F., Frécht J.M.J. 4, s.l. : Adv. Func. Mater., 2003, Vol.

10. FT-IR and raman spectroscopic methods for identification and quantitation of orthorhombic and monoclinic paracetamol in powder mixes. Al-Zoubi N. Koundourellis J.E., Malamataris S. 459-467, 2002, Vol. 29.

11. The use of polymer heteronuclei for crystalline polymorph selection. Lang M., Grzesiak A.L., Matzer A.J. 14834-14835, s.l. : J. Am. Chem. Soc, 2002, Vol. 124.

12. On the mechanism of crystalline polymorph selection by polymer heteronuclei. Lopez-Mejias V., Knight J.L., Brooks C. L., Matzger A. J. 7575-7579, s.l. : Langmuir, 2011, Vol. 27.

13. Isonicotinamide self-association: the link between solvent and polymorph nucleation, S. A. Kulkarni, E. S. McGarrity, H. Meekes, J. H. ter Horst, (2012)

14. Template-Induced Nucleation of Isonicotinamide Polymorphs, A. Caridi, S. A. Kulkarni, G. Di Profio, E. Curcio, J. H. ter Horst (2014).

Chapter 5

Crystallization of pharmaceuticals by means of tailor-made membranes

5.1 Introduction

In Membrane Crystallization process (Mcr), the membrane is a microporous and hydrophobic medium playing as support for controlling solvent evaporation and as heterogeneous surface promoting crystals nucleation.[1-3]
Although advances have been done in DCMD/MCr, nowadays this technology suffers the lack of membranes specifically designed for distillation applications. Indeed, the membranes commonly used in DCMD/MCr are commercial hydrophobic membranes in polypropylene (PP) or Polyvilidenfluoride (PVDF) primarily designed for microfiltration process.[4]
Hence, improvements in MCr point to the need of developing new types of membranes which meet the requirements of both distillation and crystallization processes, namely, the necessity of enhancing the membrane potentiality in controlling nucleation mechanism while maintaining high distillation performances. On these basis, we proposed the design and the development of membranes tailored for membrane crystallization. Indeed, 15 typologies of PVDF-masked MMMs were produced and discussed in the chapter 3 for the following testing in crystallization. Moreover, commercial PP membranes were opportunely functionalized on the upper surface through photografting of acrylic acid in the chapter 4. In this chapter, the discussion on these membrane continued by discussing about the testing of these membranes on nucleation of pharmaceutical compounds. All the produced and characterized membranes were tested in order to discriminate the chemicals and structural characteristics of the membranes that best suit for enhancing nucleation mechanism. Thus, the goal of this work is to present the crystallization tests performed by using the hand-made membranes. Crystallization tests aimed a better definition of the relationship between membrane properties and membrane performances in MCr.
The MMMs membranes were tested on two different model compounds: isonicotinamide (INA) and Acetaminophen (ACM) at different initial concentration. As concerning the photografted membranes, both native and functionalized membranes were used for the crystallization of INA and ACM.

Crystallization experiments were performed with ACM and INA as model compounds because being polymorphic compounds, enables us to eventually investigate a possible role played by the membrane material on the polymorphs selection. Studies about the control of polymorphism of the PAR with different polymer heteronuclei, are present in the literature. [5,6]

About Isonicotinamide the few paper present in letterature demonstrated the possibility to control the polymorphism in batch crystallization by using different solvents[7] or using specific heterogeneous nanotemplates.[8]

Membranes in MCr were seen to play a relevant role in affecting the nucleation mechanism. Therefore, membranes showing a different surface chemistry, can differently affect the crystals nucleation thorough preferential solute-membrane interactions. For instance, INA molecules could form acid-base interactions between its basic group and the acid groups of the AA grafted membranes, and ACM could form preferential H-bonding with the superficial functional groups. Moreover, the nonspecific chemical interaction between the membrane and the solute molecules might lead to molecular orientation and hence facilitate the nucleation of specific polymorphs or crystal morphologies.

The native and modified flat sheet membranes were tested thorough MCr experiments in static conditions. While, the native and modified hollow fibers will be used for assembling membrane modules for the continuous MCr process and tested successively.

5.2 Materials and methods

Membrane crystallization experiments were performed with all membranes produced and using different initial concentrations of model compound. For MCr tests stock crystallizing solutions were prepared by dissolving different amount of acetaminophen and Isonicotinamide (from Across Organics) in ultrapure water at final supersaturation values of 1.2, 1.5 and 1.8 at 10 °C, respectively. All solutions were filtered by PES filter of 0,2 µm.

The MMMs were tested by dipping a 100x70 mm^2 piece of every polymeric film into 1mL of crystallizing solution, using crystallization plates and repeating the same condition experiments for 10 times (10 wells of the plate with the same crystallizing solution and the same membrane). Standard experiments with blank type PVDF were also carried out as reference. Control experiments were performed by filling some wells with crystallizing solutions and without membranes. For the grafted membranes 10 vials were filled with each crystallizing solution, and 130x70 mm^2 pieces of polymeric film were dipped in the solution. For the tests made using hollow fiber, 1 cm long piece of any fiber type was dipped in 1 mL of crystallizing solutions of INA in water at 1.42 and 1.79 supersaturation degree, respectively. The same experiments were performed with both original (Flat sheet PP membrane, nominal pore diameter 0.22 µm, thickness 600 µm , from Membrana GmbH, Wuppertal, Germany) and modified membranes. 10 vials of each crystallizing solution without any polymeric film (blank tests) were also prepared as standard. Both plates and vials were quenceed at 10°C until the crystals formation.

After incubation in all experiments, crystals attached on the membrane surfaces and present on the bottom of the vial, (supposedly detached from the surface during the incubation time), were included in the counting. Then, polymer films were extracted from the vials and were photographed. It was verified that crystals did not appear in control tests over the incubation time. Nucleation density of crystals on membrane surfaces has been quantified by the ratio between the number of crystals nucleated in each of the 10 vials of

the same membrane type, over the sum of all the crystals nucleated in all vials of the same concentration. Crystals were characterized by FTIR after drying at room temperature for 24 hours. Pictures of the crystals were done by optical microscope.

5.3 Results

Crystallization tests with the produced PVDF based MMMs. In the Figure 1 the nucleation density percentage for superficial unit of INA at different supersaturation values is shown when using MMMs discussed in chapter 3. The membrane corresponding number is detailed in Table 2 chapter 3.

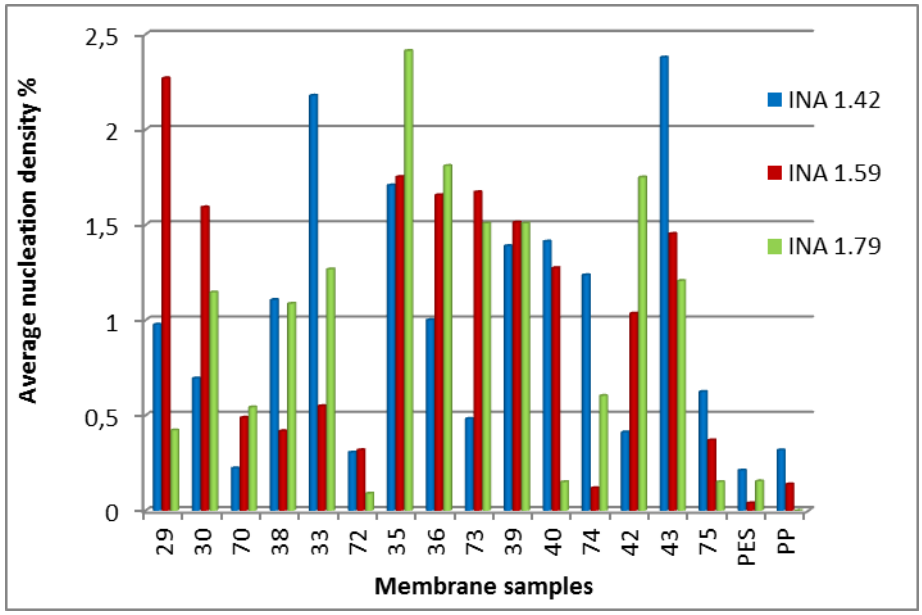

Figure 1. Nucleation density % of INA at different supersaturation values on the PVDF based MMMs.

As shown in the pictures above, all PVDF based membranes enhanced nucleation if compared with the commercial PP and PES membranes. This could be related to the fact that the PP is smoother than the hand-made PVDF membranes. As we know the roughness can induce nucleation by creating high local supersaturation in the porour portion of the surfaces. If not considering some discarding data all VIPS made MMMs seems to enhance the nucleation of INA more than NIPS and Dry-Wet-NIPS membranes, probably because of the higher surface roughness. The presence of the inorganic fillers do not seems to influence the nucleation density of INA, probably because the fillers, although at high concentration (15% on the total polymer solution mass) were distribuited in the whole polymer matrix and not only on the membrane surface. Thus, the effect of the fillers was not visible in this kind of experiments.

Crystallization tests with flat sheet grafted membranes. For INA crystallization experiments in water, when using a super saturation of 1.2 at 10°C no crystals were detected during the time range these experiments were followed. When increasing the INA supersaturation at 1.5 at 10°C only two samples gave rise to the formation of INA crystals with the membrane PP13, corresponding to a grafted membranes with 60% of AA thorough of method II (figure 2).

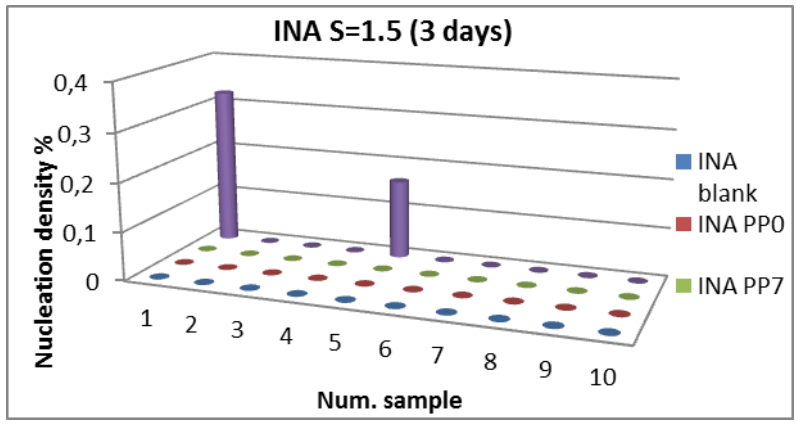

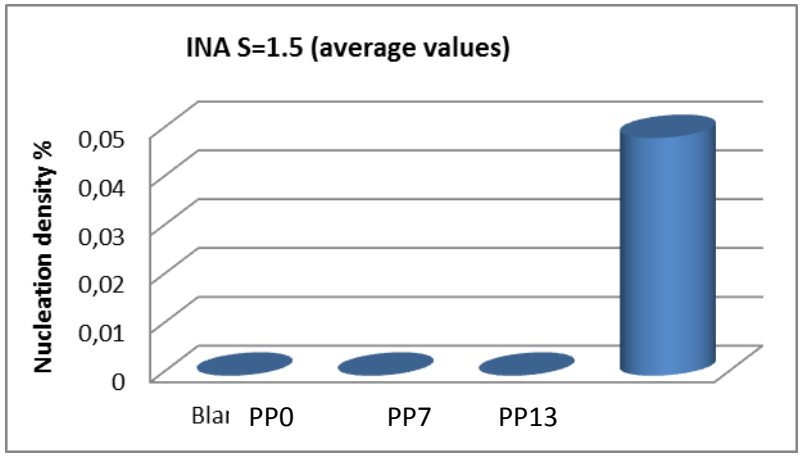

Figure 2. Nucleation density % of INA samples at a supersaturation value of 1.5 without membranes (blank experiments) and with native polypropylene and grafted membranes (methods I and II, respectively).

While, with a supersaturation at 1.8, although the blank samples did not nucleate, the vials containing the membranes showed higher nucleation density. Polypropylene induced the nucleation of INA with a percentage of about 2%, while when using the grafted membrane PP13 the nucleation density increased up to 40% (figure 3).

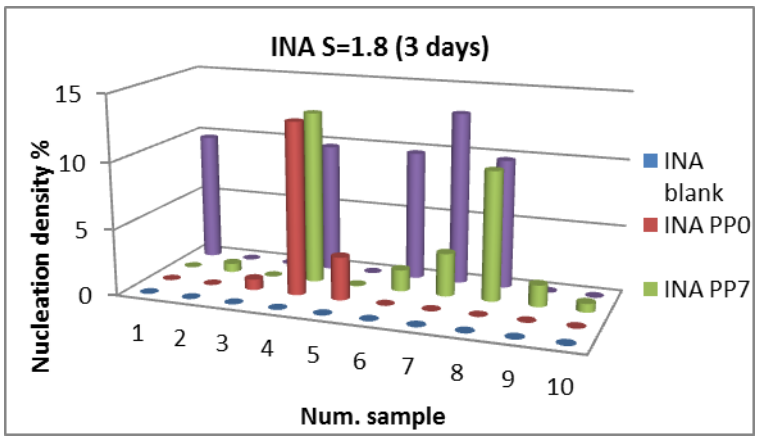

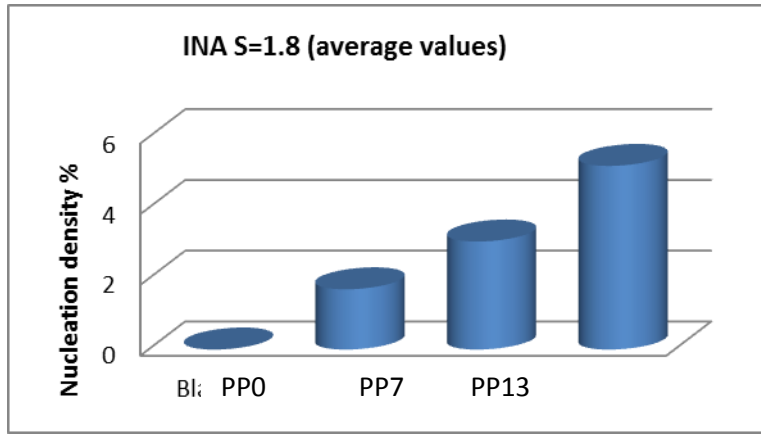

Figure 3. Nucleation density % of INA samples at a supersaturation value of 1.8 without membranes (blank experiments) and with native polypropylene ang grafted membranes (methods I and II respectively).

The morphology of INA crystals was needle-like with dimensions overcoming 1 centimeter for all vials.

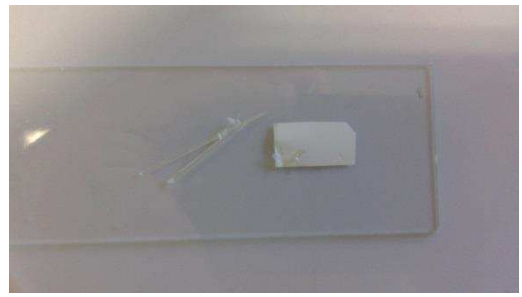

Figure 4. Pictures of INA crystals growed at 1.8 supersaturation in presence di PP7

Isonicotinamide is known to crystallize as five different polymophs named as form I, II, III, IV and V, respectively. The crystal nucleation of INA is a most

interesting process because of the strongly differing packing of form II and the other forms.

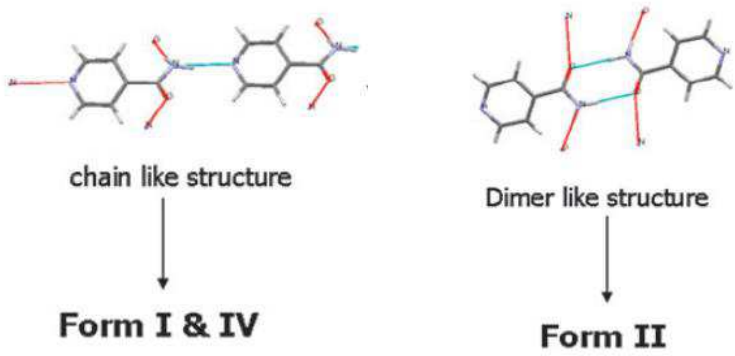

Figure 4. Hydrogen bonding in INA stable and metastable polymorphs.

Isonicotinamide form II has been reported to be the most stable form at room temperature.[7] In the structure of form II the amide groups form amide–amide homosynthons (head-to-head dimers), which in turn are hydrogen bonded through the oxygen atom and the remaining hydrogen of the amide group. Interestingly, the pyridine group does not participate in hydrogen bonding in the crystal structure of form II, contrary to all other currently known forms of INA. These metastable forms consist of differently packed head-to-tail chains connected through heterosynthons of the amide and the pyridine group.
With ATR-FTIR spectroscopy the type of hydrogen bonding of the amide group of INA crystals could be identified. Indeed, since in the dimeric form II the amidic $–NH_2$ group forms hydrogen bonding with carbonyl group, while in the chain-like structure the $–NH_2$ group forms hydrogen bonding with the pyridine nitrogen, a shift of N-H vibration band around 3200 cm^{-1} and 1670-1650 cm^{-1} confirm the crystallization of INA in different packing.

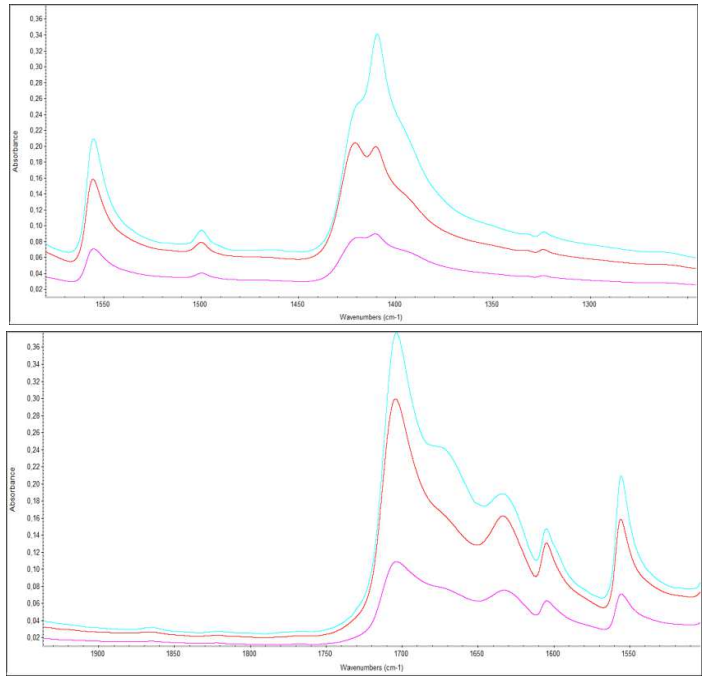

Figure 5. Partial prectra of INA crystals grew at 1.8 on PP0(pink), PP7 (red) and PP13 (light bue)

From picture 5 it is possible to see a difference between the spectra of INA when nucleated on native polypropylene (PP0), and grafted fibers with a monomer concentration of 80% (PP13). This induce to think that the the functionalized membranes showed the capability to affect the polymorphism of INA. The mechanism of polymorphic selection is probably the molecular orientation of INA given by the ionic bonding between the INA amide group and the acidic groups of the fiber surfaces. This ionic bond induce the exposure of the pyridine portion of the INA molecule leading the formation of head to tail INA metastable form. This result was reliable only with the fiber grafted with 80% of AA monomer, meaning that an high amount of acidic groups need for inducing the INA molecular interaction.

As regarding ACM crystallization experiments, when using a supersaturation of 1.2 no crystals were formed in the vials in the time range we followed these

experiments (7 days). When increasing the supersaturation value of ACM to 1.5 and 1.8 at 10°C, crystals nucleated after 5 days and 1 day, respectively. The nucleation density of ACM at different supersaturation values are shown in figure 6 and 7. Results revealed that the nucleation of ACM is encouraged by the native polypropylene, differently from INA which demonstrated to crystallize on the grafted membranes preferentially

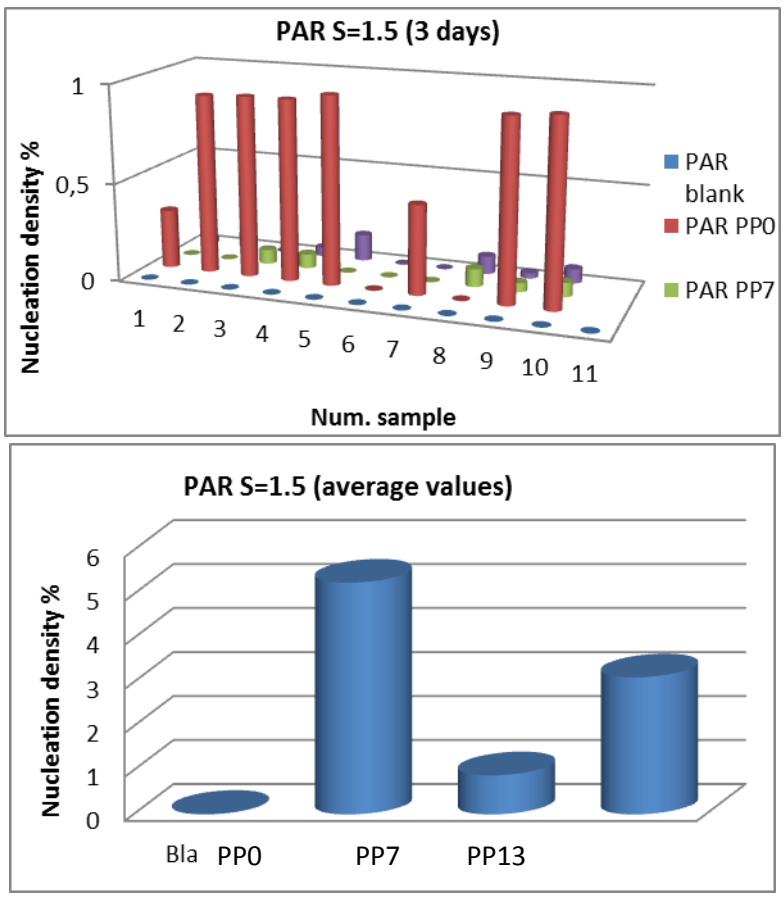

Figure 6. Nucleation density % of PAR samples at a supersaturation value of 1.5 without membranes (blank experiments) and with native polypropylene ang grafted membranes (methods I and II respectively).

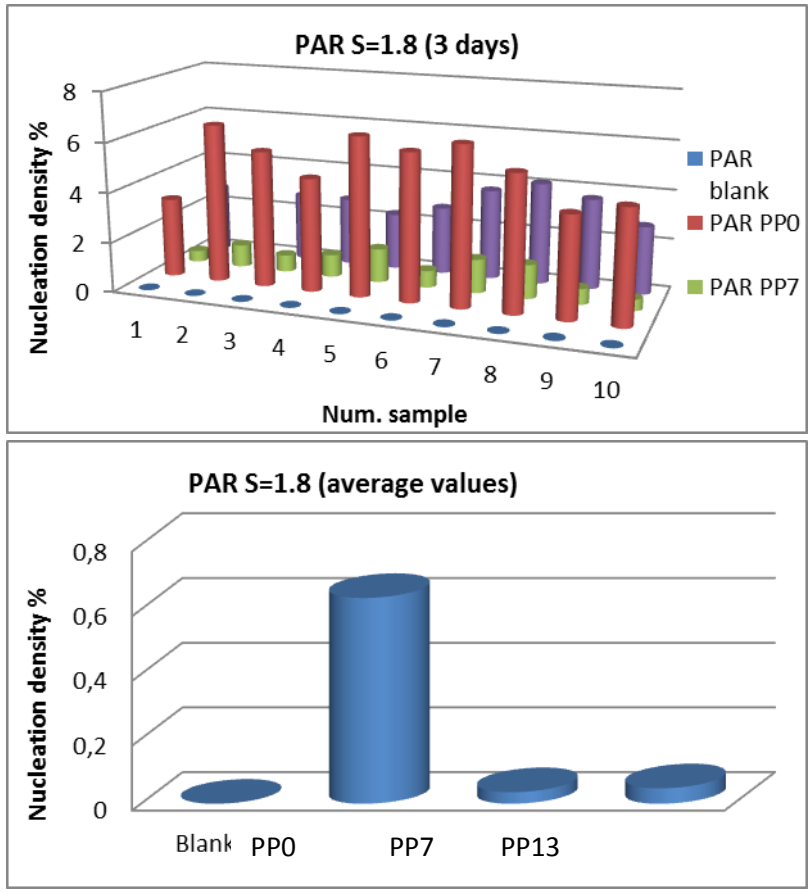

Figure 7. Nucleation density % of PAR samples at a supersaturation value of 1.5 without membranes (blank experiments) and with native polypropylene ang grafted membranes (methods I and II respectively).

The increasing of ACM nucleation density obtained when the membrane substrate is present in batch solution resulted in the production of a higher number of crystals with drastically reduced average size. This is evident from the crystals pictures showed in figure 8.

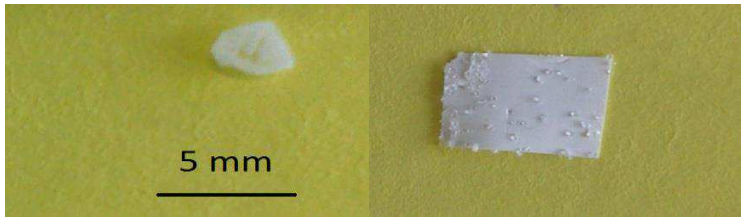

Figure 8. ACM crystallized in batch solution of 16,99 g/L at 10 °C without membrane (a) and ACM crystallized upon PP membranes at the same conditions.

Picture 9 shows the microscope pictures of ACM crystals taken from a solution, probably grew on the membrane surface and successively detached.

Figure 9. Optical microscope pictures of ACM crystals in batch solution at 16,99 g/L crystallized on PP membrane. These crystals supposedly detached by the membrane surface during the growth.

Crystals characterization revealed ACM crystallized as monoclinic form I under all the conditions investigated. Distinctive peaks at 1649 and 3314 cm^{-1} of the ACM form I are visible in the ACM FT-IR spectra shown in figure 10.

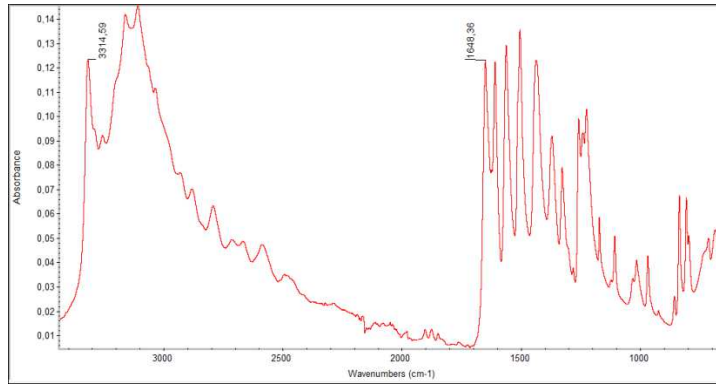

Figure 10. FT-IR spectra of ACM form I crystallized by using PP membranes.

Crystallization tests with hollow fibers. For INA batch crystallization experiments in water using hollow fibers, two different solution concentration were tested: supersaturation value of 1,42 and 1,79 at 10°C. Batch crystallization tests were carried out by dipping 1 cm long piece of fiber in to 1 ml bacth solution. Native and grafted polypropylene (grafted with an initial monomer percentage of 20%, 40%, 60% and 80%, respectively) were tested. Blank experiments were carried out also as reference. Figure 11a shows the ND% of 5 samples for all fiber tested and 5 blank samples when using INA S=1.42 . In figure 11b the ND% average of 5 samples is shown. It was observed how the Nucleation density reached a maximum value when using 60% AA-grafted fibers, while is lower for the other tests. The ND% seems to follow the trend: AA 60% > AA 20% > AA40% > AA 80% > Bianco > PP0. This would demonstrate that the acrylic acid molecules grafted on the PP membranes tends to enhance the nucleation of INA with respect the blank experiments (batch crystallization tests without fibers). Also, PP0 (not grafted fiber) did not significantly influenced the ND% with respect the blank experiments. Nevertheless, the ND% trend did not follow the same trend of the AA grafted percentage as expected. The low ND% value given by the 80% AA grafted fiber could be related to a not corrected grafting procedure, resulting in a low

grafting degree. A similar behavior was revealed from the crystallization tests at supersaturation 1.79.

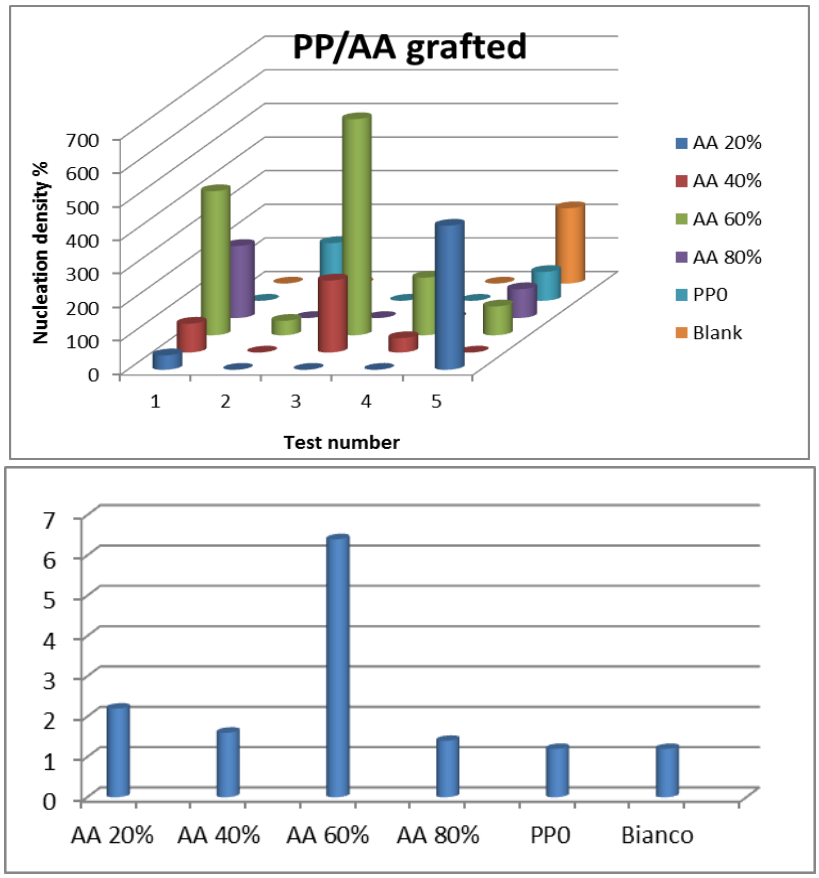

Figure 11. Nucleation density % for INA S=1.42 when tested PP fibers (PP0) and grafted PP at different initial monomer percentage (AA 20%, 40%, 60%, 80%): a) ND% for all experiments series ; b) ND% calcultated as average of 5 samples.

Figure 12a shows the ND% of 5 samples for all fiber tested and 5 blank samples when using INA S=1.79, while in figure 24b the ND% average of 5 samples is shown.

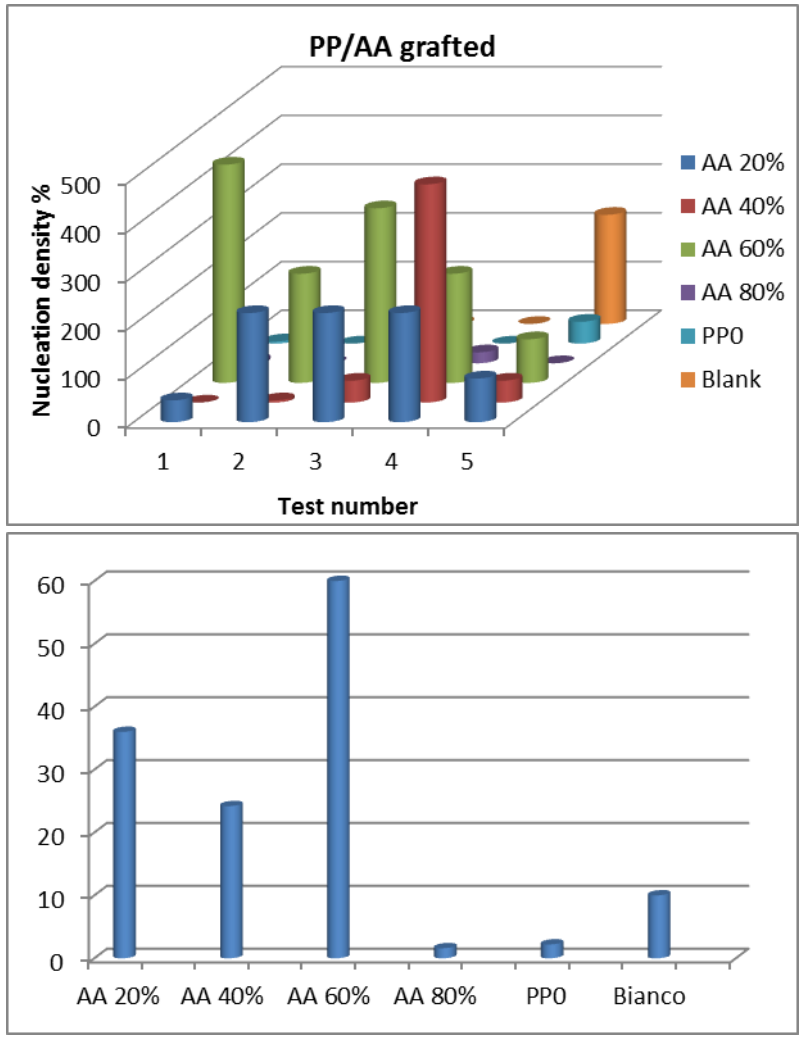

Figure 12. Nucleation density % for INA S=1.79 when tested PP fibers (PP0) and grafted PP at different initial monomer percentage (AA 20%, 40%, 60%, 80%): a) ND% for all experiments series ; b) ND% calcultated as average of 5 samples.

Increasing the INA concentration, the maximum ND% was for AA 60% following AA 20% and AA 40%, while PP0 and AA 80% gave a ND% lower than

the blank experiments, meaning that polypropylene does not affect the nucleation or would inhibit the nucleation of INA.
To explain the low ND% value given by AA 80%, the real grafting degree of the fibers was calculated (with the formula in paragraph 1.1) and shown in following table:

Monomer %	GD%
AA 20%	59,94
AA 40%	41,64
AA 60%	39,75
AA 80%	42,27

The grafting degree calculated with the gravimetric method, does not seems to have a direct correlation with the monomer percentage used while grafting as well as no correlation with the nucleation density is shown, thus, the DG% calculation method probably is not reliable.
The crystals nucleated on the fibers were also characterized from a qualitative point of view by FT-IR spectra in order to study the ability of the AA grafted fibers to discriminate between different INA polymorphs. All vials at 1.42 supersaturation gave rise to the formation of the same crystal form, while when using 1.79 supersaturation, all vials nucleated the same crystal form except for a blank vials which nucleated a different polymorph. Figure 13 shows the spectra of these two different crystalline stuctures.
Although the blank vials (without fiber) nucleated a diffent INA polymoph, no difference were found between the spectra of AA grafted fibers and no grafted polypropylene, demonstrating that the AA molecules on the fibers' surface were not active in discriminating different INA crystals forms.

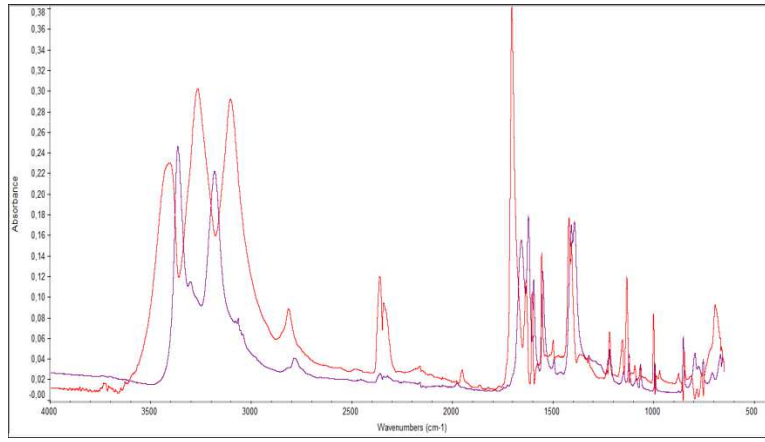

Figure 13. Spectra of two different INA crystal polymorphs nucleated at 1.79 supersaturation value.

5.4 Conclusions

All membranes surfaces tested were found to reduce the induction times compared to the experiments in absence of the membranes, and thus resulted active in inducing heterogeneous nucleation. The reason of these results can be in principle related to their porous nature which provides cavities where solute molecules can physically entrap leading to high local supersaturation values suitable for nucleation. Membrane crystallization tests revealed the ability of different membrane surfaces to differently affect the crystal nucleation leading the basis for further investigations. For the PVDF MMMs, the different chemical compositions were not seen to affect the nucleation density, while the surface texture was seen to deeply affect the nucleation density. Indeed, higher ND% were shown when using MMMs with high roughness value. Moreover, membranes of different materials, showing a different surface chemistry, can differently affect the crystals nucleation thorough preferential solute-membrane interactions. Moreover, the nonspecific chemical interaction between the membrane and the solute molecules can, lead to molecular orientation in some cases and hence facilitate the nucleation of specific polymorphs or crystal morphologies. For MMMs membranes no effects on polymorphism were observed, while for the grafted membranes the effect on polymorphism was observable. When using an high concentration of INA, the grafted membranes showed the capability to divert the normal course of crystallization inducing the preferential formation of a different INA polymorph. Finally we can conclude that this study led the basis for further investigations on the manufacturing of membranes acting as templates especially designed for membrane crystallization processes.

5.5 References

1. G. Di Profio, C. Stabile, A. Caridi, E. Curcio, E. Drioli. 12, Antisolvent Membrane Crystallization of pharmaceutical compounds, s.l. : J. pharm. Sci., 2009, Vol. 98.

2. A. Caridi, G. Di Profio, R. Caliandro,A. Guagliardi, E. Curcio, E. Drioli, Selecting the Desired Solid Form by Membrane Crystallizers: Crystals or Co-crystals. 4349-4356, s.l. : Cryst. Growth Des., 2012, Vol. 12.

3. G. Di Profio, E. Curcio, E. Drioli. Ind. Eng. Chem. Res., 49, 2010.

4. A. Alkhudhiria, N. Darwishb, N. Hila, Desalination, 287, 2012.

5. The use of polymer heteronuclei for crystalline polymorph selection. Lang M., Grzesiak A.L., Matzer A.J. 14834-14835, s.l. : J. Am. Chem. Soc, 2002, Vol. 124.

6. On the mechanism of crystalline polymorph selection by polymer heteronuclei. Lopez-Mejias V., Knight J.L., Brooks C. L., Matzger A. J. 7575-7579, s.l. : Langmuir, 2011, Vol. 27.

7. Isonicotinamide self-association: the link between solvent and polymorph nucleation, S. A. Kulkarni, E. S. McGarrity, H. Meekes, J. H. ter Horst, (2012)

8. Template-Induced Nucleation of Isonicotinamide Polymorphs, A. Caridi, S. A. Kulkarni, G. Di Profio, E. Curcio, J. H. ter Horst (2014).

Conclusions

As conclusions of this research project we can observe that lots of progress has been made in membrane crystallization. The add value of this study was the expansion of the knowledge on heterogeneous nucleation mechanism induced by the membrane and the successful application to the pharmaceutical cocrystallization field.

By studyng the heterogeneous particles it was demonstrated that all templates reduced the induction times compared to the experiments in absence of the templates. For both zeolites and titanium dioxide rutile templates form II was obtained and thus no effects on polymorphism were observed, while in the crystallization experiments in ethanol with high supersaturation, for the anatase form of titanium dioxide instead of form II the metastable form I was obtained. The effectiveness of the template anatase to induce a change in polymorph crystallization behavior suggested the occurrence of preferential interactions between the template surface and INA molecules leading to oriented arrangement of the growing crystalline structure. The same trend was not reliable when the anatase fillers where embedded into the PVDF membranes. The second study revealed the ability of the membrane-based technique of providing specific routes in the solubility phase diagram of CBZ-SAC system when opportunely choosing the initial solution conditions. The membrane had the specific role of limiting the maximum level of supersaturation reached in solution by controlling the solvent evaporation thorough its micropores. Furthermore, it was demonstrated the influence of trans-membrane flux on the polymorphic composition of the precipitates examining how as increasing the rate of supersaturation generation an increasing of the higher energetic polymorph occurred.

The design of membrane especially thought for MCr led to the preparation of sets of membranes made with the same material PVDF but different the chemical composition and structural features. These membranes were seen to differently affect the nucleation density. In the surface modification of the

commercial membranes through the chemical grafting, the crystallization tests provided about the effect of the functional groups on nucleation. This part of the study would definitely define the role of the grafted membrane for MCr process.

Acknowledgements

I would like to express my gratitude to my advisors, Prof. Enrico Drioli and Dr. Gianluca Di Profio, for having me as a part of their research group at ITM-CNR, for their guidance, caring and patience during these years and for giving me the possibility of having interesting collaborations abroad.

I wish to thank Prof. Joop ter Horst for guiding my research at TU Delft, helping me in developing my background in the crystallization field and for being always willing to give me his best suggestions. I am also thankful to his research group for supporting me during my stay in The Netherlands and making me to catch the best of Dutch life.

I would like to thank Prof. Pierre Aimar for offering me his continuous encouragement throughout the course of my experience at Universitè Paul Sabatier in Toulouse and giving me the absolute access at Laboratoire de Gènie Chimique. I benefited a lot of working with him and his research group in my understanding on membrane science.

I would also like to extend my gratitude to other members of the ITM-CNR research group, Dr. Efrem Curcio and Dr. Enrica Fontananova for their contribute on my work.

Finally, I wish to acknowledge the European Commission (European Social Fund, FSE) and Regione Calabria for the financial support of my Ph.D. fellowship.